Hard-core dipolar bosons in optical lattices

Mathias May*

Diploma thesis

August 13, 2013

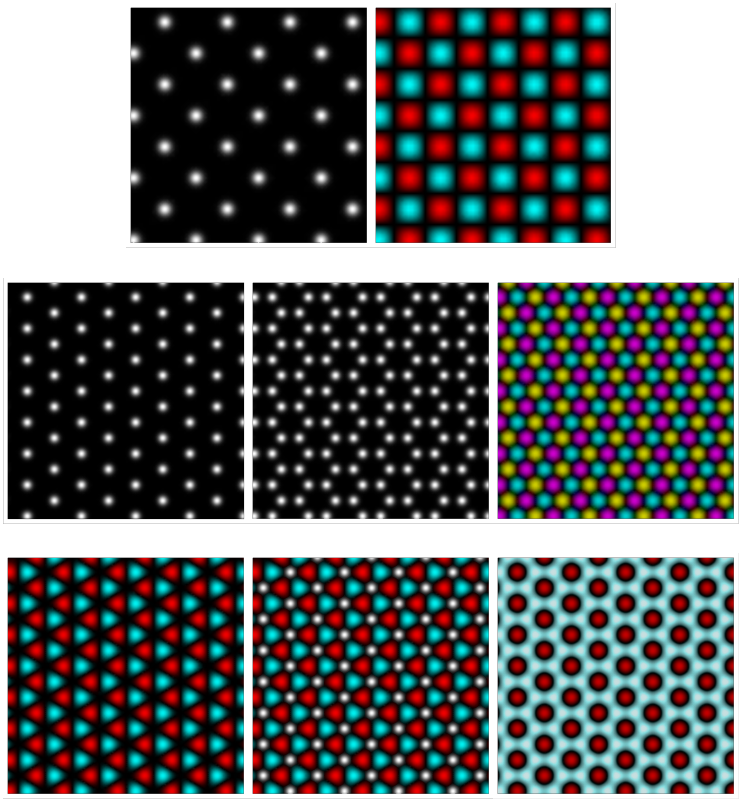

Supervisor: Priv.-Doz. Dr. Axel Pelster

Freie Universität Berlin

*mathias.may@fu-berlin.de

Title images*:* Spatial distributions of bosons in an optical lattice for different phases under the condition of negative hopping. *First row*: quadratic lattice, *second and third row*: triangular lattice. *White dots*: localized bosons, *colored*: superfluid.

Abstract

Focused on a deep mathematical understanding we investigate the different phases of bosons with a long-range interaction in an optical lattice at zero temperature. These many-body quantum systems form spatial patterns due to the long-range interaction between different lattice sites. Depending on the experimental conditions, bosons can be localized at lattice sites or be part of a superfluid. In particular, we investigate the unusual situation of negative hopping, which experimentalists are able to create by periodically shaking the lattice. For this condition there are major problems for Monte Carlo simulations, so we use the the mean-field approximation applied to the extended Bose-Hubbard model in the hard-core limit as an analytical ansatz. With this we derive a general calculation method, continue then to more special cases if necessary and end up with the phase diagrams for non-frustrated and frustrated lattices for positive and negative hopping. Negative hopping provides an interesting variety of phases especially in frustrated lattices like the triangular one including inhomogeneous superfluids and mixtures of localized and superfluid bosons (see title images). As we will see the superfluids at negative hopping tend to have unequal complex phases, which yields phase differences of 180° or 120° between the condensate densities of different sites.

Contents

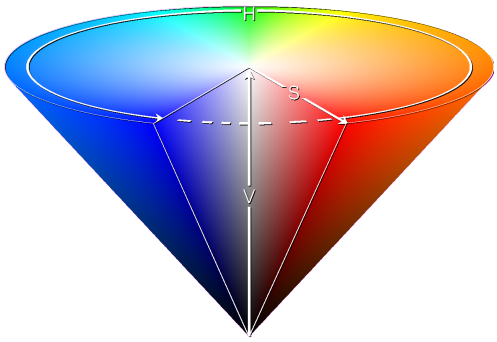

Figure 1: HSV color space. "V" stands for "value" meaning "brightness", "S" for "saturation" and "H" for "hue" [1].

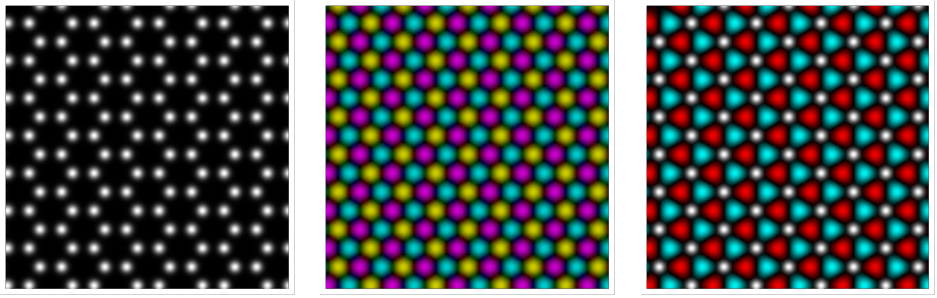

(a) solid (b) superfluid (c) mixture

Figure 2: Visualization examples: **(a)** localized particles (*white*) and empty spaces in between (*black*), **(b)** condensate density of delocalized particles (*colored*) with varying complex phases (*hue*), **(c)** mixture of localized and delocalized particles.

0.1 Visualization

We will use the HSV color space to visualize our results, hence it is shortly introduced here. The HSV color space parameterizes all colors with the variables "V" for "value", "S" for "saturation" and "H" for "hue" (see Fig. 1). The value V regulates the brightness, the saturation S regulates, how strongly the color can be perceived, and the circular variable H provides everywhere on the full circle a continuous transition between all hues. For $S = 0$ the circular hue is not defined, which corresponds exactly to a complex variable in polar coordinates, where the phase is not defined, when the absolute value is zero, and where the phase is a circular variable. So we use S and H to visualize the complex value "condensate density". The other important value we visualize in the same picture is a density between 0 and 1. Since it is a real value, we can use the brightness V for it. So all important values can be sensefully coded in the 3 dimensional HSV color space.

Fig. 2a shows a visualization example for localized particles arranged in a honeycomb pattern on the triangular lattice. "Black" stands for unoccupied lattice sites and "white" for the density 1 both without superfluid behavior, i.e. $S = 0$. Fig. 2b shows an example for $S \neq 0$, $V \neq 0$ (superfluid) with different hues (complex phases). Fig. 2c is an example, how we visualize a combination of localized and superfluid particles.

Since our calculations take place in the "discrete space" of lattice sites and not in the continuous space, we can just visualize results at the actual lattice sites, hence the color values between the lattice sites not necessarily correspond to real physical values. We just visualize in the discrete space.

Part I
Introduction

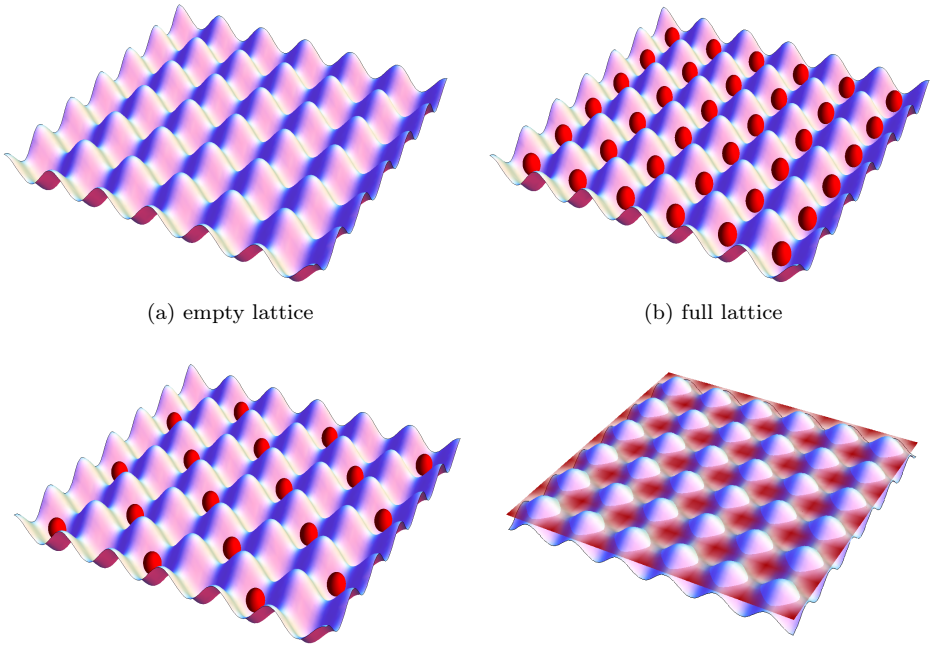

(a) empty lattice (b) full lattice

(c) 1/2 filled, checkerboard (d) homogeneous superfluid

Figure 3: Simplified visualization of ultracold atoms in optical lattices. **(a)** Mott insulator (MI) "empty lattice", **(b)** Mott insulator (MI) "full lattice", **(c)** density wave (DW) "checkerboard solid", **(d)** homogeneous superfluid (SF).

1 First glimpse

In this thesis we will investigate the topic of ultracold atoms in optical lattices, which are highly controllable and accurately observable many-body quantum systems at $T \approx 0$ temperature. Figure 3 can serve as a first simplified visualization of one of the systems, we will analyze later. Valleys in a periodic potential are occupied with in our case at most one boson. In addition the bosons can be delocalized over the whole lattice as is illustrated in Fig. 3d. In other systems in this field of research the occupation numbers can be higher, the periodic potential can be more complicated, the external influences can be different as well as the interactions between particles.

Experimentally some properties of these systems are tunable. That makes it possible to set up various conditions, under which localized bosons or superfluid bosons arrange in different spatial symmetries with different properties. Later we will also find conditions, under which both localized and superfluid bosons coexist at the same time. The different symmetries and properties classify the possible states of the system into so called "phases". For each experimental condition the system takes a certain phase. All conditions (J, μ, V) and the corresponding phase are illustrated in a phase diagram as in Fig. 4 and 5 showing different phases in different colors. These two figures show parts of phase diagrams, which have already been determined (right part) [2, 3, 4], and the part we analyze in this thesis, i.e. the unusual experimental condition of "negative hopping" (left part).

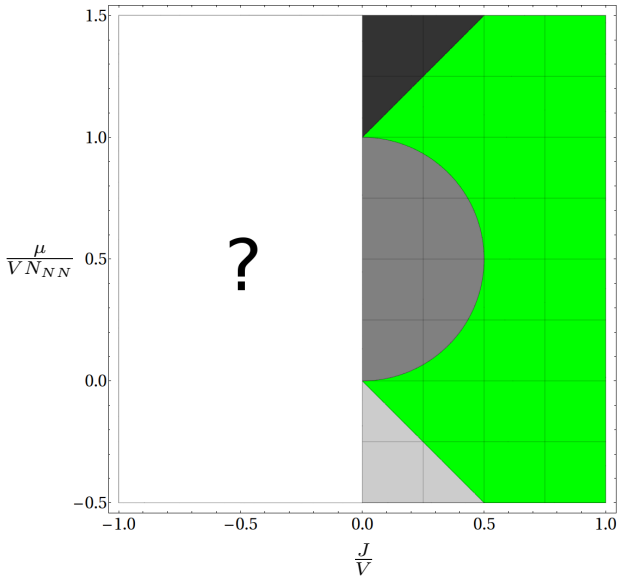

Figure 4: Phase diagram in the mean-field approximation for non-frustrated lattices like the quadratic lattice. *Right*: already determined [2, 4], *left*: issue of this thesis. *Light gray*: Mott insulator (MI) "empty lattice", *medium gray*: density wave (DW) "checkerboard solid", *dark gray*: Mott insulator (MI) "full lattice", *green*: homogeneous superfluid (SF).

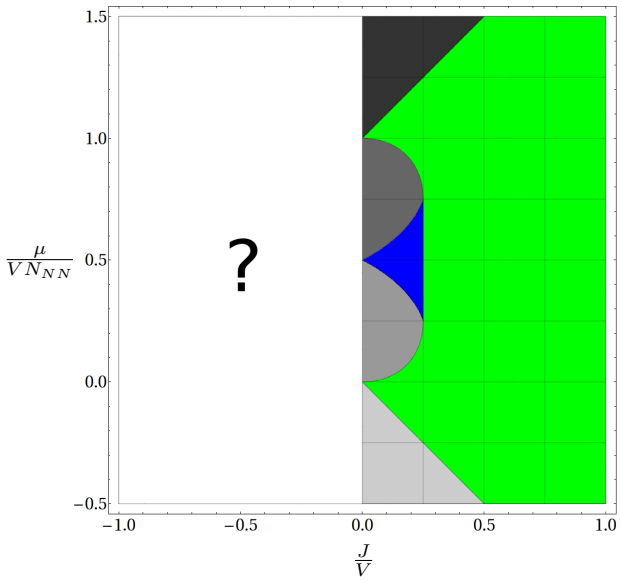

Figure 5: Phase diagram in the mean-field approximation for frustrated lattices like the triangular lattice. *Right*: already determined [3], *left*: issue of this thesis. *Lightest gray*: Mott insulator (MI) "empty lattice", *medium light gray*: density wave (DW) "1/3 filled solid", *medium dark gray*: density wave (DW) "2/3 filled solid", *dark gray*: Mott insulator (MI) "full lattice", *green*: homogeneous superfluid (SF), *blue*: inhomogeneous superfluid (SS).

2 Motivation

One important application is to use ultracold atoms in optical lattices as **quantum simulators** (see e.g. Ref. [5]), i.e. their properties are analyzed experimentally with the intention to understand less observable systems, which are supposed to behave similar. In this sense one physical situation is simulating another one. This can also have the effect, that some phenomena are observed in the quantum simulator, which have not already been included or predicted in the theoretical descriptions. And it could produce more accurate results than current numerical calculations. These lattice systems are very similar to lattice structures in solid states. So one of the interesting hopes is to find new principles to understand e.g. high temperature superconductivity [6]. Another application is the field of **quantum computing**, in which small, controllable systems are needed [7].

In different phases the particle density and condensate density can have different spatial symmetries and different superfluid properties. This way in some of these phases the translational symmetry of the lattice is broken as well as the $U(1)$ symmetry in the complex phase of the condensate density.

The systems we analyze in this thesis are systems of hard-core bosons with next neighbor interaction. Besides the simple homogeneous phases - empty lattice (Fig. 3a, 6a, 9a), full lattice (Fig. 3b, 6b, 9b) and homogeneous superfluid (Fig. 3d, 6c, 9c) - other more interesting phenomena were already predicted for these systems. Examples for non-superfluid phases are the **inhomogeneous solids** like the checkerboard solid (Fig. 3c, 7) in the quadratic lattice [2, 4] and two different solids (Fig. 8a, 8b) in the triangular lattice with the spatial symmetry of a honeycomb pattern [3]. But most interesting is an **inhomogeneous superfluid** (Fig. 10), part of a class of phases called "**supersolid**"[1], which appears in the triangular lattice under intermediate conditions (experimental parameters) between the honeycomb solids and the homogeneous superfluid [8]. Here the particle densities are distributed in a honeycomb pattern like in the neighboring solids, but all lattice sites take part in the condensate density like in the neighboring homogeneous superfluid, so all bosons are delocalized inhomogeneously in a honeycomb pattern.

The class of phenomena called **supersolidity** also includes a phase of **helium** (without optical lattice), which was predicted theoretically and tried to be found experimentally. But these experiments turned out to be not successful (Ref. [9, 10, 11]). So now it is a hope to find a supersolid phase in optical lattices as e.g. proposed in Ref. [8].

One of the experimentally tunable condition is the probability for bosons to tunnel to other lattice sites, in our approximation the next neighbor sites. This so called "hopping" appears in the mathematics as the hopping strength J. Usually in contributions to our topic it is considered to be positive, since this describes the normal behavior of our systems. But experimentalists managed to create situations, that correspond to **negative hopping** [12, 13, 14], i.e. the quantum simulator was extended to a wider range of conditions, which always has the potential for new interesting kinds of phases. For positive hopping, Monte Carlo simulations exist based on the extended Bose-Hubbard model [8], which our work is based on, too. But extending the **Monte Carlo simulations** to **negative hopping** turned out to be a **major problem** [8]. This means, we need to find other methods for this purpose. So finding such a method and describing phases for negative hopping is the main issue of this work.

We will develop a partially general calculation method for certain classes of lattices using the mean-field approximation, which, although it doesn't give very accurate quantitative results, is able to predict a few new phases for negative hopping. And it shows some properties of the mathematical structure, which can be helpful to understand the principles of these systems.

[1] The word "supersolid" is normally used for inhomogeneous superfluids (e.g. Ref. [8]) as well as a mixture of localized and superfluid particles (e.g. Ref. [9]), which we will later define as different classes of phases.

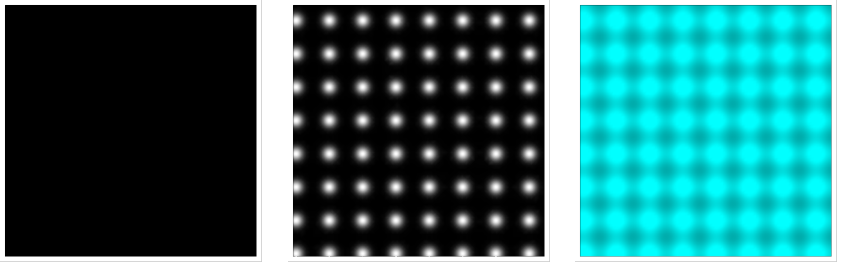

(a) empty lattice (b) full lattice (c) homogeneous SF

Figure 6: All homogeneous phases in the quadratic lattice for positive hopping.

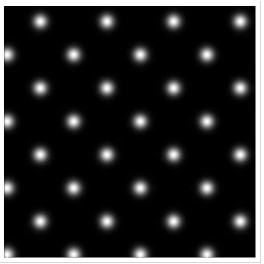

(a) 1/2 filled, checkerboard

Figure 7: Inhomogeneous solid in the quadratic lattice.

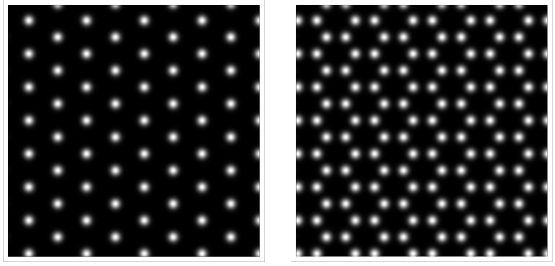

(a) 1/3 filled (b) 2/3 filled

Figure 8: Inhomogeneous solids in the triangular lattice.

(a) empty lattice (b) full lattice (c) homogeneous SF

Figure 9: All homogeneous phases in the triangular lattice for positive hopping.

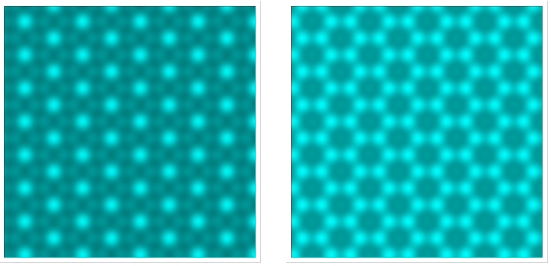

(a) inhomogeneous SF (b) inhomogeneous SF

Figure 10: Inhomogeneous superfluid phases in the triangular lattice for positive hopping. **(a)** close to the 1/3 filled solid, **(b)** close to the 2/3 filled solid.

3 Physical situation

Independent of the experimental realization (section 4) the principle physical situation can be described as follows.

We will investigate bosons at zero temperature in a **periodic potential** (the lattice, see Fig. 11), in which they can **tunnel between the valleys** (hopping). And as mentioned before the influence of the hopping can experimentally be replaced by an opposite influence (**negative hopping**). As an approximation the continuous lattice potential is reduced to a discrete space (Fig. 12a, 12b) consisting of nodes and connections, standing for lattice sites and physical relations, i.e. next neighbor hopping and next neighbor interaction.

Furthermore the particles underlie a very strong, approximately infinite (**hard-core** limit), repulsive contact interaction, which causes the bosons never to be at the same site at the same time.

Additionally there is a long range attractive or repulsive interaction, meaning, that bosons at different lattice sites influence each other. In our case we are approximately considering just **next neighbor interactions**.

In experiment the depth of the lattice potential, the strength of the next neighbor interaction and the chemical potential can easily be tuned. In the competition between the forces and the hopping tendency, the bosons arrange in different patterns depending on the relations between these parameters. This **self-organisation** occurs **in the** spatial magnitude of the **next neighbor region**, since we consider next neighbor interaction and hopping.

We will see, that the variety of phases depend on the lattice geometry, which can be e.g. in two dimensions a quadratic or triangular lattice (Fig. 11, 12) or in three dimensions a cubic lattice . Most important is a property called "**frustration**". A non-frustrated lattice geometrically allows a pattern of alternating features (Fig. 13a), e.g. an alternating occupation number of zero or one as in the checkerboard pattern (Fig. 7), whereas a frustrated lattice doesn't, because e.g. in the triangular or kagome lattice, the next neighbor sites form a triangle, which doesn't allow an alternating distribution of features (Fig. 13b). We will see, that homogeneous or alternating patterns appear in the phase diagram of our systems, unless the alternating one is geometrically forbidden, and thus allows patterns of higher energy to appear in the ground state, which, as we will see, are much more interesting and diverse.

Since the bosons self organize due to next neighbor effects, the next neighbor interaction is very important for the behavior of the system. Without it the inhomogeneous superfluid phase in the triangular lattice would not appear. We will use the so called "extended Bose-Hubbard model", which is including the interaction between different sites.

This thesis is based on the idea of bosons in optical lattices, but there are other systems with the same or similar behavior, which can serve as quantum simulators, too. One example is a spin $\frac{1}{2}$ system in two dimensions interacting with an external magnetic field [3]. It can mathematically be mapped to our hard-core boson system [15] and thus has mappable results, i.e. the three components of the spin can be translated to the real valued particle density and the complex valued condensate density.

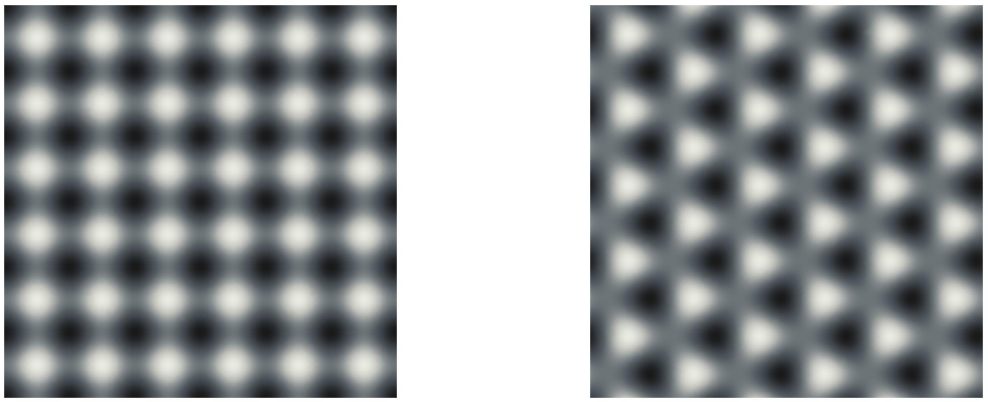

(a) quadratic (b) triangular

Figure 11: The periodic potential.

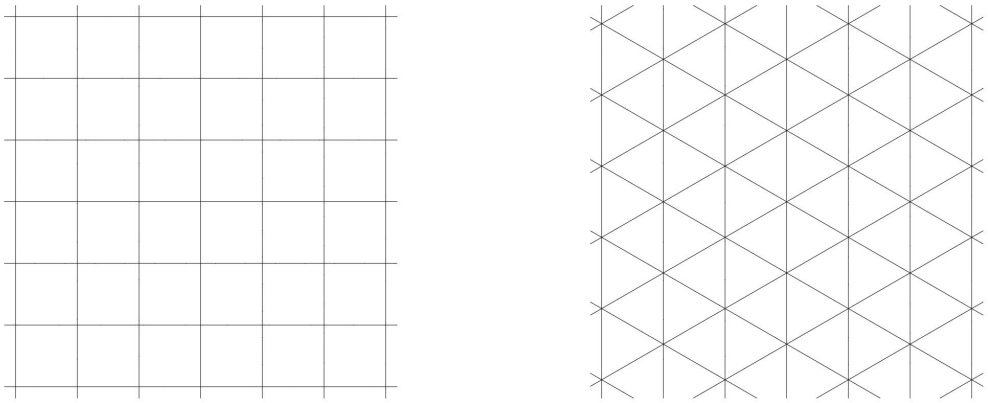

(a) quadratic (b) triangular

Figure 12: The "discrete space", which the lattice is reduced to in the mathematical description. Valleys in the potential are mapped to nodes and next neighbor relations to connections.

(a) non-frustrated (b) frustrated

Figure 13: Comparison between **(a)** non-frustrated and **(b)** frustrated lattices.

4 Experimental realization

To realize the periodic potential usually **electromagnetic standing waves** are generated by **counterpropagating lasers** or a laser, which is mirrored back to superpose with itself (Fig. 14). A few of these standing waves are arranged in a certain angle to each other modeling a periodic potential (Fig. 15) with valleys in the magnitude of the wavelength. E.g. three standing waves perpendicular to each other (Fig. 14) form a cubic lattice. The examples, which this thesis is based on, but not restricted to, are two-dimensional lattices, especially the quadratic lattice and the triangular lattice. Since the experiments take place in a three dimensional world, for these systems a potential has to be modeled [16], which behaves like a two dimensional lattice, i.e. in the mathematics two dimensions can be assumed. To model the lattice geometry it is also possible to create potentials with **more than one laser frequency** (see e.g. Ref [17]), for instance two frequencies at a ratio of $1 : 2$ as in Fig. 16. In this system different geometries can be modeled by varying phase differences (Fig. 17). Assuming, that particles just occupy the deepest valleys, lattices like the kagome lattice can be realized this way (Fig. 16). Allowing particles in higher valleys yield a more complex system with more tunable parameters, which we don't investigate in this thesis. The **atoms**, which are electromagnetically neutral at first, are able to interact with the laser field due to a **polarization** induced by it.

The **contact interaction** is tuned with an external magnetic field, which can effect the scattering length of bosons over several orders of magnitude (see Fig. 19). Close to a **Feshbach resonance** (see Ref. [18]) the contact interaction becomes very strong and, thus, we assume it to be infinite, allowing at most one boson at one lattice site at the same time (**hard-core limit**).

The origin of the **next neighbor interaction** is a dipolar one, either magnetic atomic or electric molecular. It can be attractive or repulsive (Fig. 18).

As mentioned before experimentalists managed to create situations corresponding to **negative hopping** in the mathematics. This is obtained by a **fast lattice oscillation** (see Ref. [12, 13, 14]).

In Ref. [19] another kind of systems was proposed, in which **nuclear spins** on a diamond surface interact at **room temperature**. The intention in this paper is to use it as a quantum simulator.

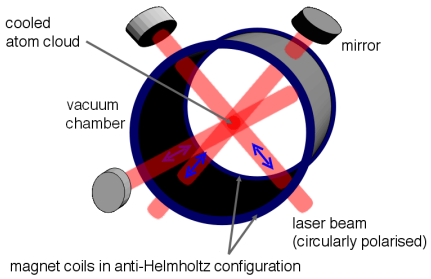

Figure 14: Schematic experimental setting [20].

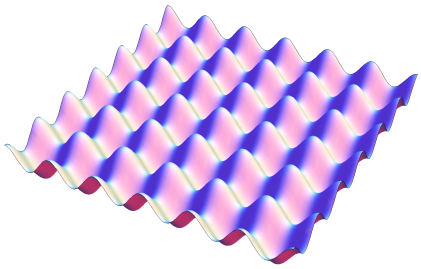

Figure 15: The periodic potential of a quadratic lattice.

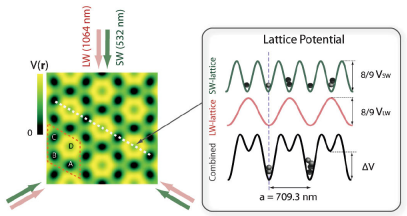

Figure 16: Kagome lattice implemented with two laser frequencies [17].

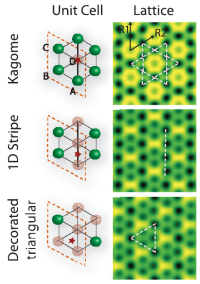

Figure 17: Other possible lattice geometries implemented with two laser frequencies [17].

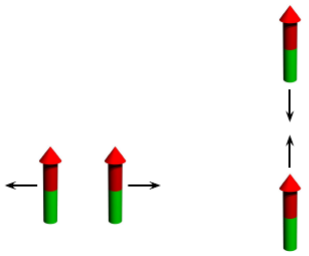

Figure 18: Principle of dipolar interaction.

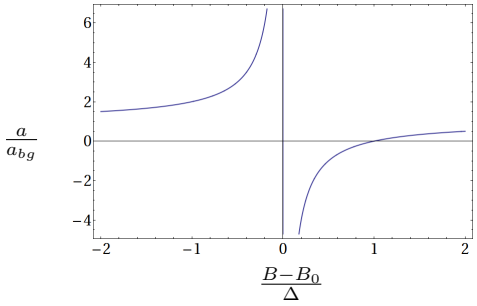

Figure 19: The scattering length a depending on the external magnetic field B with a Feshbach resonance at B_0.

5 Outline

Part II "Preparative mathematics"

In part II we describe some mathematical basics for the actual calculations in part III.

In **section 6 "Mathematical approach"** we first derive the basic model for our system from quantum field theory, the so called "extended Bose-Hubbard model". Afterwards its simplified due to the hard-core limit. And last we apply a mean-field approximation leading to a Hamiltonian, whose summands just contain operators, which act on single lattice sites. This simplified Hamiltonian can be investigated analytically for periodic patterns, which is the main issue in Part III "Main part".

In **section 7 "Periodic patterns"** we recall, how a periodic pattern is described by a unit cell and translational symmetry, and introduce how we reduce its properties to a matrix, containing just the properties we need in our further calculation.

Part III "Main part"

In part III we derive our general calculation method and end up with the final phase diagrams for both positive and negative hopping.

In **section 8 "General derivations in the mean-field approximation"** we use the symmetry of spatial periodic patterns to obtain a mean-field Hamiltonian for one unit cell, i.e. a finite number of lattice sites. After determining the matrix representation on the occupation number basis for one and two sites in the unit cell we will find the energy eigenvalues for both cases and a regularity in the expressions for the energy will become guessable leading to a general formula. With this general formula for the energy we will try to find the values of the mean-field parameters by extremizing it leading to a set of coupled equations, which will be basic to the further calculations for more special cases.

In **section 9 "Classification of phases and phase boundaries"** we mention the common classification of phases and introduce a new one and new symbols representing more appropriately the variety of phases, we will find later.

In **section 10 "Mathematics for special classes of patterns"** we will calculate the energies, densities and condensate densities for two cases of patterns. One is the homogeneous pattern, where the ansatz demands all properties to be the same at all sites leading to the well known empty lattice, full lattice and homogeneous superfluid. These solutions can be expressed independently of the lattice geometry. The other case is a whole class of patterns described by a quite general matrix with arbitrary size at first. It will serve for all lattices and patterns, we will analyze, and we will find almost all solutions, we need later, except for the case of the inhomogeneous superfluid in the frustrated lattices, where we have to consider a 3×3 matrix in a separate section. But for all other cases using the more general matrix we will proceed from a general derivation to special cases.

In **section 11 "Non-frustrated lattices"** we will describe the solutions for non-frustrated lattices, combine them to the phase diagram and find expressions for the phase boundaries. All the formulas will have a relatively simple form in the mean-field approximation.

In **section 12 "Frustrated lattices"** we do the same for frustrated lattices leading to a variety of interesting phases and a non trivial phase diagram especially for negative hopping including an inhomogeneous superfluid and a phase, in which solid sites appear together with superfluid sites.

Part II
Preparative mathematics

6 Mathematical approach

In this chapter we will derive the extended Bose-Hubbard Hamiltonian and simplify it to the hard-core case. Afterwards we apply the mean-field approximation to it.

6.1 Derivation of the extended Bose-Hubbard model

The Hamiltonian for a many-body system of bosons at $T = 0$ in the d-dimensional space representation including one- and two-particle energies is described by

$$\begin{aligned}\hat{H} &= \int d^d x\, \hat{\psi}^\dagger(\mathbf{x})\, \hat{H}_{\text{one}} \hat{\psi}(\mathbf{x}) \\ &\quad + \frac{1}{2} \int d^d x \int d^d x' \hat{\psi}^\dagger(\mathbf{x})\, \hat{\psi}^\dagger(\mathbf{x}')\, V_{\text{two}}(\mathbf{x}, \mathbf{x}')\, \hat{\psi}(\mathbf{x})\, \hat{\psi}(\mathbf{x}') \ , \end{aligned} \tag{1}$$

where $\hat{\psi}(\mathbf{x})$ denotes the bosonic field operator fulfilling the commutator relations

$$\left[\hat{\psi}(\mathbf{x}), \hat{\psi}^\dagger(\mathbf{x}')\right] = \delta(\mathbf{x} - \mathbf{x}'), \qquad \left[\hat{\psi}^\dagger(\mathbf{x}), \hat{\psi}^\dagger(\mathbf{x}')\right] = 0, \qquad \left[\hat{\psi}(\mathbf{x}), \hat{\psi}(\mathbf{x}')\right] = 0 \ , \tag{2}$$

$V_{\text{two}}(\mathbf{x}_1, \mathbf{x}_2)$ stands for the two particle interaction energy and $\hat{H}_{\text{one}}$ for the single-particle Hamiltonian

$$\hat{H}_{\text{one}} = -\frac{\hbar^2}{2m} \triangle + V_{\text{one}}(\mathbf{x}) - \mu' \ , \tag{3}$$

where $V_{\text{one}}(\mathbf{x})$ describes a potential energy involving one particle, in our case the influence of the lattice potential, and μ' the chemical potential due to a grand-canonical description.

Now we transform the Hamiltonian (1) to a polynomial of bosonic ladder operators $\hat{a}_i$, $\hat{a}_i^\dagger$ acting on single lattice sites denoted by the index of the operator. This can be done by writing the field operator $\hat{\psi}(\mathbf{x})$ as

$$\hat{\psi}(\mathbf{x}) = \sum_i \hat{a}_i w(\mathbf{x} - \mathbf{x}_i) \tag{4}$$

$$\hat{\psi}^\dagger(\mathbf{x}) = \sum_i \hat{a}_i^\dagger w^*(\mathbf{x} - \mathbf{x}_i) \ , \tag{5}$$

where $\hat{a}_i$ and $\hat{a}_i^\dagger$ are the bosonic ladder operators acting on lattice site i and fulfilling

$$\left[\hat{a}_i, \hat{a}_j^\dagger\right] = \delta_{ij}, \qquad \left[\hat{a}_i^\dagger, \hat{a}_j^\dagger\right] = 0, \qquad [\hat{a}_i, \hat{a}_j] = 0 \tag{6}$$

and $w(\mathbf{x} - \mathbf{x}_i)$ are the Wannier functions, which are defined as a complete orthonormal function basis

$$\int d^d x\, w^*(\mathbf{x} - \mathbf{x}_i)\, w(\mathbf{x} - \mathbf{x}_j) = \delta_{ij} \tag{7}$$

$$\sum_i w^*(\mathbf{x} - \mathbf{x}_i)\, w(\mathbf{x}' - \mathbf{x}_i) = \delta(\mathbf{x} - \mathbf{x}') \ , \tag{8}$$

and are localized at lattice sites.

In a spatially periodic system different energy bands exist, so there are Wannier functions for every band. In our systems the temperature is approximately zero, so we can consider all bosons to be in the lowest band. Otherwise we had to distinguish between different bands here.

Inserting the representation of the field operator (4) and (5) into the Hamiltonian (1) yields

$$\hat{H} = -\sum_{i,j} J_{i,j} \hat{a}_i^\dagger \hat{a}_j + \frac{1}{2} \sum_{i,j,k,l} V_{i,j,k,l}\, \hat{a}_i^\dagger \hat{a}_j^\dagger \hat{a}_k \hat{a}_l - \mu' \sum_i \hat{n}_i \tag{9}$$

with the abbreviations

$$J_{i,j} := -\int d^d x\; w^*\left(\mathbf{x}-\mathbf{x}_i\right)\left(-\frac{\hbar^2}{2m}\triangle + V_{\text{one}}\left(\mathbf{x}\right)\right) w\left(\mathbf{x}-\mathbf{x}_j\right) \tag{10}$$

and

$$V_{i,j,k,l} := \int d^d x\; w^*\left(\mathbf{x}-\mathbf{x}_i\right) w\left(\mathbf{x}-\mathbf{x}_k\right)\left[\int d^d x'\; w^*\left(\mathbf{x}'-\mathbf{x}_j\right) V_{\text{two}}\left(\mathbf{x},\mathbf{x}'\right) w\left(\mathbf{x}'-\mathbf{x}_l\right)\right] . \tag{11}$$

As an approximation we neglect products of Wannier functions localized at different lattice sites due to a small overlap. These products appear in (11) regarding the two index combinations i,k and j,l. So we just have to take the matrix elements $V_{i,j,k,l}$ into account, which fulfill either $i=k$ or $j=l$, yielding a simplification of the Hamiltonian (9), i.e.

$$\hat{H} = -\sum_{i,j} J_{i,j}\hat{a}_i^\dagger\hat{a}_j + \frac{1}{2}\sum_{i,j} V_{i,j}\;\hat{a}_i^\dagger\hat{a}_j^\dagger\hat{a}_i\hat{a}_j - \mu'\sum_i \hat{n}_i \tag{12}$$

with the abbreviation

$$V_{i,j} := V_{i,j,i,j} = \int d^d x\;\left|w\left(\mathbf{x}-\mathbf{x}_i\right)\right|^2\left[\int d^d x'\;\left|w\left(\mathbf{x}'-\mathbf{x}_j\right)\right|^2 V_{\text{two}}\left(\mathbf{x},\mathbf{x}'\right)\right] . \tag{13}$$

For the systems, we investigate, we consider a simple on-site interaction V_{site} and a next neighbor interaction V_{NN}

$$V_{\text{two}}\left(\mathbf{x},\mathbf{x}'\right) = V_{\text{site}}\left(\mathbf{x},\mathbf{x}'\right) + V_{\text{NN}}\left(\mathbf{x},\mathbf{x}'\right) , \tag{14}$$

and divide the interaction term of (12) into two parts

$$V_{i,j} = V_{i,j}^{\text{site}} + V_{i,j}^{\text{NN}} \tag{15}$$

with the corresponding matrix elements

$$V_{i,j}^{\text{site}} := \int d^d x\;\left|w\left(\mathbf{x}-\mathbf{x}_i\right)\right|^2\left[\int d^d x'\;\left|w\left(\mathbf{x}'-\mathbf{x}_j\right)\right|^2 V_{\text{site}}\left(\mathbf{x},\mathbf{x}'\right)\right] \tag{16}$$

$$V_{i,j}^{\text{NN}} := \int d^d x\;\left|w\left(\mathbf{x}-\mathbf{x}_i\right)\right|^2\left[\int d^d x'\;\left|w\left(\mathbf{x}'-\mathbf{x}_j\right)\right|^2 V_{\text{NN}}\left(\mathbf{x},\mathbf{x}'\right)\right] . \tag{17}$$

Then the interaction term from (12) reads

$$\frac{1}{2}\sum_{i,j} V_{i,j}\;\hat{a}_i^\dagger\hat{a}_j^\dagger\hat{a}_i\hat{a}_j = \frac{1}{2}\sum_{i,j} V_{i,j}^{\text{site}}\;\hat{a}_i^\dagger\hat{a}_j^\dagger\hat{a}_i\hat{a}_j + \frac{1}{2}\sum_{i,j} V_{i,j}^{\text{NN}}\;\hat{a}_i^\dagger\hat{a}_j^\dagger\hat{a}_i\hat{a}_j . \tag{18}$$

6.1.1 On-site interaction

Using the simple contact interaction

$$V_{\text{site}}\left(\mathbf{x},\mathbf{x}'\right) = V_{0,\text{site}}\delta\left(\mathbf{x}-\mathbf{x}'\right) \tag{19}$$

the matrix element (16) becomes

$$V_{i,j}^{\text{site}} = V_{0,\text{site}}\int d^d x\;\left|w\left(\mathbf{x}-\mathbf{x}_i\right)\right|^2\left|w\left(\mathbf{x}-\mathbf{x}_j\right)\right|^2 . \tag{20}$$

And again we can neglect products of Wannier functions for different lattice sites i and j due to a small overlap. So the on-site term in (18) simplifies to

$$\frac{1}{2}\sum_{i,j} V_{i,j}^{\text{site}}\ \hat{a}_i^\dagger \hat{a}_j^\dagger \hat{a}_i \hat{a}_j \quad = \quad \frac{1}{2}\sum_i V_{i,i}^{\text{site}} \hat{a}_i^\dagger \hat{a}_i^\dagger \hat{a}_i \hat{a}_i \tag{21}$$

with

$$V_{i,i}^{\text{site}} \quad = \quad V_{0,\text{site}} \int d^d x\ \left|w\left(\mathbf{x}-\mathbf{x}_i\right)\right|^4\ . \tag{22}$$

Since the integral (22) over the whole space is always the same independent on a shift by $\mathbf{x}_i$, all matrix elements $V_{i,i}^{\text{site}}$ have to have the same value. Then (22) becomes

$$U \quad := V_{i,i}^{\text{site}} = \quad V_{0,\text{site}} \int d^d x\ \left|w\left(\mathbf{x}\right)\right|^4 \tag{23}$$

and (21) yields the on-site term

$$\frac{1}{2}\sum_{i,j} V_{i,j}^{\text{site}}\ \hat{a}_i^\dagger \hat{a}_j^\dagger \hat{a}_i \hat{a}_j \quad = \quad \frac{U}{2}\sum_i \hat{a}_i^\dagger \hat{a}_i^\dagger \hat{a}_i \hat{a}_i\ . \tag{24}$$

Using the number operator

$$\hat{n}_i \quad = \quad \hat{a}_i^\dagger \hat{a}_i \tag{25}$$

and the operator relation

$$\hat{n}_i\left(\hat{n}_i - 1\right) \quad = \quad \hat{a}_i^\dagger \hat{a}_i^\dagger \hat{a}_i \hat{a}_i \tag{26}$$

valid for bosons, the on-site interaction (24) reads

$$\frac{1}{2}\sum_{i,j} V_{i,j}^{\text{site}}\ \hat{a}_i^\dagger \hat{a}_j^\dagger \hat{a}_i \hat{a}_j \quad = \quad \frac{U}{2}\sum_i \hat{n}_i\left(\hat{n}_i - 1\right)\ , \tag{27}$$

which is our final expression for the on-site interaction.

6.1.2 Next neighbor interaction

The sum in the next neighbor interaction term in (18) has to involve just next neighbor combinations of indices i and j, which we denote as $\langle i,j\rangle$. Since the indices are always different in these combinations, we can interchange ladder operators due to (6), and use the number operator (25) to express the next neighbor interaction term in (18) as

$$\frac{1}{2}\sum_{i,j} V_{i,j}^{\text{NN}}\ \hat{a}_i^\dagger \hat{a}_j^\dagger \hat{a}_i \hat{a}_j \quad = \quad \frac{1}{2}\sum_{\langle i,j\rangle} V_{i,j}^{\text{NN}}\ \hat{n}_i \hat{n}_j\ . \tag{28}$$

We consider the simple case, in which the next neighbor interaction is independent of the lattice sites, i.e. isotropic next neighbor interaction $V_{i,j} = V\ \forall i,j$, yielding our final expression for the next neighbor interaction

$$\frac{1}{2}\sum_{i,j} V_{i,j}^{\text{NN}}\ \hat{a}_i^\dagger \hat{a}_j^\dagger \hat{a}_i \hat{a}_j \quad = \quad \frac{V}{2}\sum_{\langle i,j\rangle} \hat{n}_i \hat{n}_j\ . \tag{29}$$

In particular, this is the case, when the lattice sites have the same distance in each direction as in the lattices, we investigate.

6.1.3 Single particle energy

The single particle term in (10) contains V_{one}, which in our systems is the interaction with the periodic potential. Due to the periodicity of the lattice potential, we can consider an isotropic next neighbor hopping $J_{i,j} = J \; \forall \langle i,j \rangle$ and a self energy $J_{i,i} = -\epsilon \; \forall i$. Dividing the sum into next neighbor combinations of indices $\langle i,,j \rangle$ and equal indices we obtain

$$-\sum_{i,j} J_{i,j} \hat{a}_i^\dagger \hat{a}_j \quad = \quad -J \sum_{\langle i,j \rangle} \hat{a}_i^\dagger \hat{a}_j + \epsilon \sum_i \hat{n}_i \tag{30}$$

using the number operator (25). The first term describes the influence on the energy due to the tunneling to next neighbor sites and the second term describes an energy a particle has independent of other sites. This last term has the form of the chemical potential term in the Hamiltonian (12) and thus can mathematically be included in an effective chemical potential

$$\mu \quad = \quad \mu' - \epsilon \; . \tag{31}$$

6.1.4 Extended Bose-Hubbard Hamiltonian for isotropic next neighbor relations

So the complete Hamiltonian of the extended Bose-Hubbard model including just next neighbor relations denotes

$$\hat{H} \quad = \quad -J \sum_{\langle i,j \rangle} \hat{a}_i^\dagger \hat{a}_j + \frac{U}{2} \sum_i \hat{n}_i \left(\hat{n}_i - 1 \right) + \frac{V}{2} \sum_{\langle i,j \rangle} \hat{n}_i \hat{n}_j - \mu \sum_i \hat{n}_i \; , \tag{32}$$

where we have inserted (27), (29) and (30) into (12) using (15) and (31).

6.2 Hard-core limit

As mentioned before, the on-site interaction U can experimentally be tuned over several orders of magnitude via tuning the scattering length of particles with an external magnetic field. If the on-site interaction is a very strong repulsive one, i.e. in optical lattices close to a Feshbach resonance, we can assume, that there is at most one particle at one lattice site at the same time, i.e. either the operator $\hat{n}$ or $\hat{n} - 1$ produces the eigenvalue zero, hence the operator $\hat{n} \left(\hat{n} - 1 \right)$ has no influence and the on-site interaction term in the Hamiltonian (27) disappears due to this so called "hard-core limit", yielding the "hard-core extended Bose-Hubbard model"

$$\hat{H} \quad = \quad -J \sum_{\langle i,j \rangle} \hat{a}_i^\dagger \hat{a}_j + \frac{V}{2} \sum_{\langle i,j \rangle} \hat{n}_i \hat{n}_j - \mu \sum_i \hat{n}_i \; , \tag{33}$$

which is the Hamiltonian, we will investigate, in this thesis.

6.3 Mean-field approximation

Since the operator sums over all next neighbors are quadratic in the operators and depend on different sites of the whole lattice, we simplify the Hamiltonian (33) with the mean-field approximation and will obtain a local Hamiltonian describing the energy of one lattice site [21].

In the mean-field approximation the operators $\hat{a}_i$, $\hat{a}_i^\dagger$, $\hat{n}_i$ are considered to be their mean-values $\langle \hat{a}_i \rangle$, $\left\langle \hat{a}_i^\dagger \right\rangle$, $\langle \hat{n}_i \rangle$ plus a "small" operator $\delta\hat{a}_i$, $\delta\hat{a}_i^\dagger$, $\delta\hat{n}_i$, where "small" means, that its square is approximately zero. So with the definitions

$$\hat{a}_i \quad = \quad \langle \hat{a}_i \rangle + \delta\hat{a}_i \tag{34}$$

$$\hat{a}_i^\dagger \quad = \quad \left\langle \hat{a}_i^\dagger \right\rangle + \delta\hat{a}_i^\dagger \tag{35}$$

$$\hat{n}_i \quad = \quad \langle \hat{n}_i \rangle + \delta\hat{n}_i \tag{36}$$

we approximate the operators according to

$$0 \approx \delta\hat{a}_i^\dagger \delta\hat{a}_j = \hat{a}_i^\dagger \hat{a}_j - \left\langle \hat{a}_i^\dagger \right\rangle \hat{a}_j - \langle \hat{a}_j \rangle \hat{a}_i^\dagger + \left\langle \hat{a}_i^\dagger \right\rangle \langle \hat{a}_j \rangle \tag{37}$$

$$0 \approx \delta\hat{n}_i \delta\hat{n}_j = \hat{n}_i \hat{n}_j - \langle \hat{n}_i \rangle \hat{n}_j - \langle \hat{n}_j \rangle \hat{n}_i + \langle \hat{n}_i \rangle \langle \hat{n}_j \rangle \tag{38}$$

and find

$$\hat{a}_i^\dagger \hat{a}_j \approx \left\langle \hat{a}_i^\dagger \right\rangle \hat{a}_j + \langle \hat{a}_j \rangle \hat{a}_i^\dagger - \left\langle \hat{a}_i^\dagger \right\rangle \langle \hat{a}_j \rangle \tag{39}$$

$$= \psi_i^* \hat{a}_j + \psi_j \hat{a}_i^\dagger - \psi_i^* \psi_j \tag{40}$$

$$\hat{n}_i \hat{n}_j \approx \langle \hat{n}_i \rangle \hat{n}_j + \langle \hat{n}_j \rangle \hat{n}_i - \langle \hat{n}_i \rangle \langle \hat{n}_j \rangle \tag{41}$$

$$= \varrho_i \hat{n}_j + \varrho_j \hat{n}_i - \varrho_i \varrho_j \tag{42}$$

with the definitions of the so called mean-field parameters

$$\psi_i = \langle \hat{a}_i \rangle \tag{43}$$

$$\varrho_i = \langle \hat{n}_i \rangle \ . \tag{44}$$

The parameter ϱ_i is the particle density at lattice site i, since it is the expectation value of the number operator $\hat{n}_i$, and the parameter ψ_i is called "condensate density", whose meaning will become clearer later. Now the Hamiltonian (33) can be approximated yielding the mean-field Hamiltonian

$$\hat{H} \approx \hat{H}^{\mathrm{MF}} = -J \sum_{<i,j>} \left(\psi_i^* \hat{a}_j + \psi_j \hat{a}_i^\dagger - \psi_i^* \psi_j \right) + \frac{V}{2} \sum_{<i,j>} \left(\varrho_i \hat{n}_j + \varrho_j \hat{n}_i - \varrho_i \varrho_j \right) - \mu \sum_i \hat{n}_i \ . \tag{45}$$

The sums can be rewritten as

$$\begin{aligned} \hat{H}^{\mathrm{MF}} = & -J \left(\sum_i \hat{a}_i \sum_{j \in NN_i} \psi_j^* + \sum_i \hat{a}_i^\dagger \sum_{j \in NN_i} \psi_j - \sum_i \psi_i^* \sum_{j \in NN_i} \psi_j \right) \\ & + \frac{V}{2} \left(\sum_i \hat{n}_i \sum_{j \in NN_i} \varrho_j + \sum_i \hat{n}_i \sum_{j \in NN_i} \varrho_j - \sum_i \varrho_i \sum_{j \in NN_i} \varrho_j \right) \\ & - \mu \sum_i \hat{n}_i \ , \end{aligned} \tag{46}$$

where NN_i is the set of indices belonging to the next neighbors of site i. In the next step using the definitions

$$\Psi_i := \sum_{j \in NN_i} \psi_j \quad , \qquad R_i := \sum_{j \in NN_i} \varrho_j \ , \tag{47}$$

we obtain a sum over local Hamiltonians

$$\hat{H}^{\mathrm{MF}} = \sum_i \hat{h}_i^{\mathrm{MF}} \tag{48}$$

with

$$\hat{h}_i^{\mathrm{MF}} := -J \left(\hat{a}_i \Psi_i^* + \hat{a}_i^\dagger \Psi_i - \psi_i^* \Psi_i \right) + \frac{V}{2} \left(2 \hat{n}_i R_i - \varrho_i R_i \right) - \mu \hat{n}_i \ . \tag{49}$$

So we have found a Hamiltonian $\hat{H}^{\mathrm{MF}}$, in which the operators $\hat{a}_i$, $\hat{a}_i^\dagger$, n_i in the summands $\hat{h}_i^{\mathrm{MF}}$ depend on just the indices of single lattice sites i, i.e. we got rid of combinations of operators, which act on different sites. The summands $\hat{h}_i^{\mathrm{MF}}$ describe the energy of one lattice site i and the influence of next neighbor sites is now contained in the scalar mean-field values R_i and Ψ_i. This simplification is basic for all calculations in this thesis.

7 Periodic patterns

7.1 Motivation for periodic patterns

As mentioned before there are already Monte Carlo simulations for positive hopping, e.g. see Ref. [8]. The results show, that periodic patterns appear with e.g. two or three lattice sites in a unit cell, which makes sense, since we are just considering next neighbor relations. These patterns appear in ϱ_i and ψ_i for different lattice sites. Hence we use this spatial symmetry to reduce our Hamiltonian to a simpler one. This has already been done in the mean-field approximation in e.g. Ref. [21] and is capable to describe negative hopping, too, as we will see below.

7.2 Describing periodic patterns

A periodic pattern is described by a translational symmetry and a unit cell. The translational symmetry describes, how far the pattern has to be moved until it looks the same. The unit cell contains everything, that repeats in that symmetry, i.e. in our cases the properties of one, two or three lattice sites. One example is the two-dimensional checkerboard pattern in Fig. 22, which is described by two sites in the unit cell and the translation vectors

$$\begin{pmatrix} 2 \\ 0 \end{pmatrix} \quad , \quad \begin{pmatrix} 1 \\ 1 \end{pmatrix} \tag{50}$$

in units of next neighbor lattice site distances. But we will not need these translational vectors.

In section 6 we reduced the mathematical description such, that all operators act on the lattice sites, i.e. our mathematics take place in a discrete space described by nodes and connections, see Fig. (20), (21). For our calculations, it is not necessary to know the spatial symmetry or number of dimensions (1D, 2D, 3D). It is just necessary to know which connections between sites are considered in the Hamiltonian, i.e. the next neighbor connections in our approximation. The way these connections appear in our mathematical description is the so called adjacency matrix $\mathcal{N}$ containing the numbers of connections between different types of sites. The checkerboard pattern this described by:

$$\mathcal{N} \;=\; \begin{pmatrix} 0 & 4 \\ 4 & 0 \end{pmatrix} . \tag{51}$$

There are two kinds of sites, i.e. the matrix has the size 2×2. The first row and first column stand for one type of site the second row and column for the second one and so on. The first row describes the next neighbors of one type, i.e. non of the same type and four of the other type. Analogously the second row describes the next neighbors of the second type.

For a pattern of 3 sites the matrix becomes a 3×3 matrix, which we need e.g. for the triangular lattice. According to Monte Carlo simulations we have to consider the 3 site pattern shown in Fig. 23 for this lattice. This pattern is described by

$$\mathcal{N} \;=\; \begin{pmatrix} 0 & 3 & 3 \\ 3 & 0 & 3 \\ 3 & 3 & 0 \end{pmatrix} . \tag{52}$$

When we divide these matrixes by the number of next neighbors N_{NN}, which is the same for all lattice sites in the cases, we will investigate, then we find normalized matrixes

$$\frac{\mathcal{N}}{N_{NN}} \;=\; \frac{1}{4}\begin{pmatrix} 0 & 4 \\ 4 & 0 \end{pmatrix} = \begin{pmatrix} 0 & 1 \\ 1 & 0 \end{pmatrix} \tag{53}$$

or

$$\frac{\mathcal{N}}{N_{NN}} \;=\; \frac{1}{6}\begin{pmatrix} 0 & 3 & 3 \\ 3 & 0 & 3 \\ 3 & 3 & 0 \end{pmatrix} = \begin{pmatrix} 0 & \frac{1}{2} & \frac{1}{2} \\ \frac{1}{2} & 0 & \frac{1}{2} \\ \frac{1}{2} & \frac{1}{2} & 0 \end{pmatrix} \tag{54}$$

respectively, which will turn out to contain the relevant information characterizing the systems in the mean-field approximation.

These normalized matrixes also have the advantage, that they describe different lattices in different numbers of dimensions. E.g. the normalized matrix

$$\frac{\mathcal{N}}{N_{NN}} = \begin{pmatrix} 0 & 1 \\ 1 & 0 \end{pmatrix} \tag{55}$$

can be used for a 1D lattice ($N_{NN} = 2$), quadratic lattice ($N_{NN} = 4$), cubic lattice ($N_{NN} = 6$) and honeycomb lattice ($N_{NN} = 3$), since all of them allow geometrically an alternating pattern, which is exactly what the matrix describes: The next neighbors are never of the same kind and always of the other kind. Lattices allowing this matrix/pattern are called "non-frustrated" lattices.

The other example

$$\frac{\mathcal{N}}{N_{NN}} = \begin{pmatrix} 0 & \frac{1}{2} & \frac{1}{2} \\ \frac{1}{2} & 0 & \frac{1}{2} \\ \frac{1}{2} & \frac{1}{2} & 0 \end{pmatrix} \tag{56}$$

can be used for the triangular ($N_{NN} = 6$) and kagome ($N_{NN} = 4$) lattice, called "frustrated lattices", where the alternating pattern is geometrically forbidden, and thus another pattern has to appear, which is described by this matrix as we will see later.

7.3 Symmetry of the adjacency matrix

In all cases we analyze the adjacency matrix $\mathcal{N} = (N_{ij})$ is symmetric. So we will use

$$N_{ij} = N_{ji} \tag{57}$$

in our further calculations without mentioning it every time. The matrix is not necessarily symmetric for all patterns. E.g. if two sites of the three site pattern (56) have the same values, it yields a honeycomb pattern as in Fig. 24, which could be described by

$$\mathcal{N} = \begin{pmatrix} 3 & 3 \\ 6 & 0 \end{pmatrix}, \tag{58}$$

but since it is not a symmetric matrix, the mathematics would be more complicated and so we will use matrix (56) and afterwards find out, that some solutions have the honeycomb symmetry.

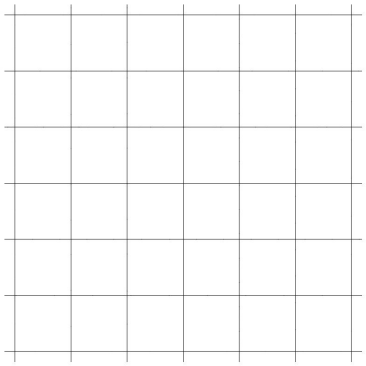

Figure 20: Discrete space for the quadratic lattice considering just next neighbor relations.

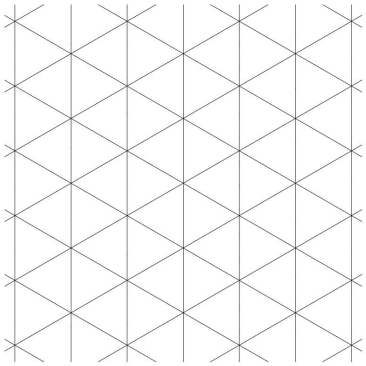

Figure 21: Discrete space for the triangular lattice considering just next neighbor relations.

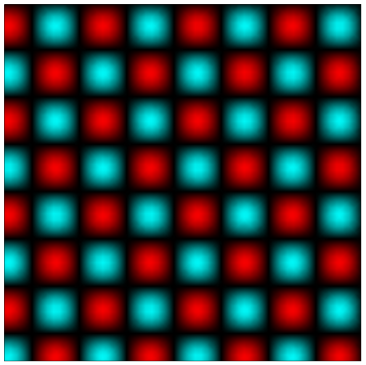

Figure 22: The checkerboard pattern for the quadratic lattice as a two dimensional example for the alternating pattern.

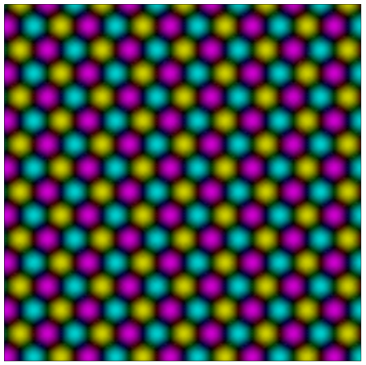

Figure 23: The three site pattern used for the triangular lattice.

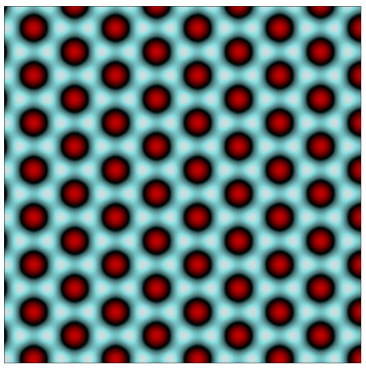

Figure 24: The honeycomb pattern on the triangular lattice. One kind of sites: honeycomb, the second kind: sites inside the honeycomb hexagons.

Part III
Main part

8 General derivations in the mean-field approximation

In **section 8.1 "Mean-field-Hamiltonian for a unit cell of a periodical pattern"** we will first derive a mean-field Hamiltonian for spatially periodic patterns describing the energy of one unit cell.

In **section 8.2 "Matrix representation and energies"** we explicitly write down its matrix representation in the occupation number basis, which is possible, since it is acting in a state space with a finite number of dimensions, and find the energy eigenvalues, which we will do for one and two sites in the unit cell. The formulas for the energies show a certain regularity yielding a general formula for an arbitrary number of sites in the unit cell.

In **section 8.3 "Finding the mean-field parameters"** we are looking for the mean-field parameters, which the energy formula still depends on. The idea to find their values is to minimize the energy with respect to them. But due to a problem in the mathematics, the second derivative can not be used to distinguish between minima and maxima. So we can just extremize the energy, i.e. we set the first derivative equal to zero. After analyzing some details of this calculation, we come to a set of equations coupled by the new introduced variables η_X.

In **section 8.4 "Rewriting the energy"** we separate the expression for the energy into a part for solid sites, a part for superfluid sites and a part, in which both solid and superfluid sites are involved. The solid part will involve just solid densities $\varrho_X^S \in \{0,1\}$, the superfluid part just the η_X and the mixed part both. We define new "normalized" energy functions, which just differ to the previous functions by a factor of $N_{NN}N_{UCsites}$, yielding expressions depending amongst others on the normalized adjacent matrix $\frac{\mathcal{N}}{N_{NN}}$ and the "normalized" chemical potential $\frac{\mu}{N_{NN}}$. This notation will show, that different lattices have the same phase diagram if $\frac{\mathcal{N}}{N_{NN}}$ is the same and μ is scaled by N_{NN}.

8.1 Mean-field-Hamiltonian for a unit cell of a periodical pattern

Until now the mean-fields ϱ_i and ψ_i can be different for every lattice site i, i.e. a sum over all $\hat{h}_i^{\mathrm{MF}}$ for every site i can describe every pattern, random or periodic or anything else. As motivated in section 7.1 we will derive the method to describe periodic patterns now.

We name the sites in the unit cell with capital letters A, B, C, ... and use X, Y, Z as placeholders for the names A, B, C, ..., e.g. in sums. The index i of the general local Hamiltonian is replaced by the names of the sites in the unit cell. To describe the energy of the whole unit cell we have to add up all local Hamiltonians for the sites of one unit cell (UC):

$$\hat{h}_{\mathrm{UC}}^{\mathrm{MF}} = \sum_X \left[-J\left(\hat{a}_X \Psi_X^* + \hat{a}_X^\dagger \Psi_X - \psi_X^* \Psi_X\right) + \frac{V}{2}\left(2\hat{n}_X R_X - \varrho_X R_X\right) - \mu \hat{n}_X \right] . \tag{59}$$

Via the replacement of the indices i, j by the names of the unit cell sites X, Y the abbreviations Ψ_X and R_X in eq. (59) are not any more directly a sum over all next neighbors, but a sum over all types of next neighbors weighted by the number of a certain type. This number is a component N_{XY} of the adjacency matrix $\mathcal{N}$ as defined in section 7.2. So Ψ_X and R_X are now defined as

$$\Psi_X = \sum_Y N_{XY}\psi_Y \quad , \qquad R_X = \sum_Y N_{XY}\varrho_Y \ . \tag{60}$$

And with the additional abbreviations

$$\Psi = \sum_X \psi_X^* \Psi_X \quad , \qquad R = \sum_X \varrho_X R_X \tag{61}$$

we can express the Hamiltonian (59) for a unit cell as

$$\hat{h}_{\mathrm{UC}}^{\mathrm{MF}} = \left(J\Psi - \frac{V}{2}R\right) - J\sum_X \left(\hat{a}_X \Psi_X^* + \hat{a}_X^\dagger \Psi_X\right) + 2\sum_X \hat{n}_X \left(\frac{V}{2}R_X - \frac{\mu}{2}\right) . \tag{62}$$

8.2 Matrix representation and energies

For the matrix representation of the Hamiltonian we use the basis vectors $|n_A, n_B, \ldots\rangle$ describing the state of the unit cell with the occupation numbers $n_A, n_B, \ldots$ of the different sites in the unit cell. The set of occupation numbers $n_A, n_B, \ldots$ can be any combination of 0 and 1 for hard-core bosons. So the dimension of the state space and the size of the matrix is 2^m, where m is the number of sites in the unit cell. The order of basis vectors we use can be described recursively vice $\mathcal{B}_{m+1} = \left\{\mathcal{B}_m \times |0\rangle_{m+1}, \mathcal{B}_m \times |1\rangle_{m+1}\right\}$, $\mathcal{B}_1 = \{|0\rangle_1, |1\rangle_1\}$, where "$\times$" denotes the Cartesian product yielding every combination of elements from two sets and the index of the one-site vectors denotes the type of lattice site in an arbitrary numbering.

$$\begin{aligned}
\mathcal{B}_1 &= \{|0\rangle_1, |1\rangle_1\} = \{|0\rangle, |1\rangle\} && (63)\\
\mathcal{B}_2 &= \{\mathcal{B}_1 \times |0\rangle_2, \mathcal{B}_1 \times |1\rangle_2\} && (64)\\
&= \{\{|0\rangle_1, |1\rangle_1\} \times |0\rangle_2, \{|0\rangle_1, |1\rangle_1\} \times |1\rangle_2\} && (65)\\
&= \{|0,0\rangle, |1,0\rangle, |0,1\rangle, |1,1\rangle\} && (66)\\
\mathcal{B}_3 &= \{|0,0,0\rangle, |1,0,0\rangle, |0,1,0\rangle, |1,1,0\rangle, |0,0,1\rangle, |1,0,1\rangle, |0,1,1\rangle, |1,1,1\rangle\} && (67)\\
&\vdots
\end{aligned}$$

This certain order of the basis vectors will be responsible for a regularity in the matrix representation of the Hamiltonian, but it is not important for our further calculations.

8.2.1 One site in the unit cell

For one site A in the unit cell, the Hamiltonian (62) becomes

$$\hat{h}_{\mathrm{UC}}^{\mathrm{MF}} = \left(J\Psi - \frac{V}{2}R\right) - J\left(\hat{a}_A\Psi_A^* + \hat{a}_A^\dagger\Psi_A\right) + 2\hat{n}_A\left(\frac{V}{2}R_A - \frac{\mu}{2}\right) \tag{68}$$

and in the basis

$$\mathcal{B} = \{|0\rangle, |1\rangle\} \tag{69}$$

the matrix representation reads

$$\begin{aligned}
&\begin{pmatrix} \langle 0|\,\hat{h}_{\mathrm{UC}}^{\mathrm{MF}}\,|0\rangle & \langle 0|\,\hat{h}_{\mathrm{UC}}^{\mathrm{MF}}\,|1\rangle \\ \langle 1|\,\hat{h}_{\mathrm{UC}}^{\mathrm{MF}}\,|0\rangle & \langle 1|\,\hat{h}_{\mathrm{UC}}^{\mathrm{MF}}\,|1\rangle \end{pmatrix} && (70)\\
= &-J\begin{pmatrix} -\Psi & \Psi_A^* \\ \Psi_A & -\Psi \end{pmatrix} + \frac{V}{2}\begin{pmatrix} -R & 0 \\ 0 & 2R_A - R \end{pmatrix} + -2\frac{\mu}{2}\begin{pmatrix} 0 & 0 \\ 0 & 1 \end{pmatrix} && (71)\\
= &\begin{pmatrix} \left(J\Psi - \frac{V}{2}R\right) & -J\Psi_A^* \\ -J\Psi_A & \left(J\Psi - \frac{V}{2}R\right) + 2\left(\frac{V}{2}R_A - \frac{\mu}{2}\right) \end{pmatrix}. && (72)
\end{aligned}$$

For this 2×2 matrix the energy eigenvalues can be determined easily, since just the roots of a quadratic polynomial have to be found:

$$E = \left(J\Psi - \frac{V}{2}R\right) + \left(\frac{V}{2}R_A - \frac{\mu}{2}\right) \pm \sqrt{\left(\frac{V}{2}R_A - \frac{\mu}{2}\right)^2 + \left(J\,|\Psi_A|\right)^2}\,. \tag{73}$$

8.2.2 Two sites in the unit cell

For two sites A, B in the unit cell, the Hamiltonian (62) becomes more complicated

$$\hat{h}_{\mathrm{UC}}^{\mathrm{MF}} = \left(J\Psi - \frac{V}{2}R\right) - J\sum_{X\in\{A,B\}}\left(\hat{a}_X\Psi_X^* + \hat{a}_X^\dagger\Psi_X\right) + 2\sum_{X\in\{A,B\}}\hat{n}_X\left(\frac{V}{2}R_X - \frac{\mu}{2}\right). \tag{74}$$

And since it is now acting in the four dimensional space

$$\mathcal{B} = \{|0,0\rangle, |1,0\rangle, |0,1\rangle, |1,1\rangle\} , \tag{75}$$

the matrix representation of the Hamiltonian is a 4×4 matrix

$$\begin{aligned}
&\begin{pmatrix}
\langle 0,0|\,\hat{h}^{\mathrm{MF}}_{\mathrm{UC}}\,|0,0\rangle & \langle 0,0|\,\hat{h}^{\mathrm{MF}}_{\mathrm{UC}}\,|1,0\rangle & \langle 0,0|\,\hat{h}^{\mathrm{MF}}_{\mathrm{UC}}\,|0,1\rangle & \langle 0,0|\,\hat{h}^{\mathrm{MF}}_{\mathrm{UC}}\,|1,1\rangle \\
\langle 1,0|\,\hat{h}^{\mathrm{MF}}_{\mathrm{UC}}\,|0,0\rangle & \langle 1,0|\,\hat{h}^{\mathrm{MF}}_{\mathrm{UC}}\,|1,0\rangle & \langle 1,0|\,\hat{h}^{\mathrm{MF}}_{\mathrm{UC}}\,|0,1\rangle & \langle 1,0|\,\hat{h}^{\mathrm{MF}}_{\mathrm{UC}}\,|1,1\rangle \\
\langle 0,1|\,\hat{h}^{\mathrm{MF}}_{\mathrm{UC}}\,|0,0\rangle & \langle 0,1|\,\hat{h}^{\mathrm{MF}}_{\mathrm{UC}}\,|1,0\rangle & \langle 0,1|\,\hat{h}^{\mathrm{MF}}_{\mathrm{UC}}\,|0,1\rangle & \langle 0,1|\,\hat{h}^{\mathrm{MF}}_{\mathrm{UC}}\,|1,1\rangle \\
\langle 1,1|\,\hat{h}^{\mathrm{MF}}_{\mathrm{UC}}\,|0,0\rangle & \langle 1,1|\,\hat{h}^{\mathrm{MF}}_{\mathrm{UC}}\,|1,0\rangle & \langle 1,1|\,\hat{h}^{\mathrm{MF}}_{\mathrm{UC}}\,|0,1\rangle & \langle 1,1|\,\hat{h}^{\mathrm{MF}}_{\mathrm{UC}}\,|1,1\rangle
\end{pmatrix} \\
= \;& \left(J\Psi - \frac{V}{2}R\right) \\
& -J \begin{pmatrix} 0 & \Psi_A^* & \Psi_B^* & 0 \\ \Psi_A & 0 & 0 & \Psi_B^* \\ \Psi_B & 0 & 0 & \Psi_A^* \\ 0 & \Psi_B & \Psi_A & 0 \end{pmatrix} \\
& + \begin{pmatrix} 0 & & & \\ & 2\left(\frac{V}{2}R_A - \frac{\mu}{2}\right) & & \\ & & 2\left(\frac{V}{2}R_B - \frac{\mu}{2}\right) & \\ & & & 2\left(\frac{V}{2}R_A - \frac{\mu}{2}\right) + 2\left(\frac{V}{2}R_B - \frac{\mu}{2}\right) \end{pmatrix} .
\end{aligned} \tag{76}$$

In order to find the energy eigenvalues, the roots of a fourth order polynomial have to be determined. In general they don't have a simple form, but for our Hamiltonian the energies are simply

$$\begin{aligned}
E = \;& \left(J\Psi - \frac{V}{2}R\right) \\
& + \left(\frac{V}{2}R_A - \frac{\mu}{2}\right) \pm_A \sqrt{\left(\frac{V}{2}R_A - \frac{\mu}{2}\right)^2 + \left(J\,|\Psi_A|\right)^2} \\
& + \left(\frac{V}{2}R_B - \frac{\mu}{2}\right) \pm_B \sqrt{\left(\frac{V}{2}R_B - \frac{\mu}{2}\right)^2 + \left(J\,|\Psi_B|\right)^2}
\end{aligned} \tag{77}$$

where $\pm_A$ and $\pm_B$ are independent signs allowing $2^{N_{UCsites}=2} = 4$ different energies as expected for a matrix of the size $2^{N_{UCsites}=2}$, where N_{UCsite} is the number of sites in the unit cell.

8.2.3 A general formula for the energies

The energies (73) and (77) have the form

$$E = \left(J\Psi - \frac{V}{2}R\right) + \sum_X \left(\frac{V}{2}R_X - \frac{\mu}{2}\right) + \sum_X (\pm_X) \sqrt{\left(\frac{V}{2}R_X - \frac{\mu}{2}\right)^2 + \left(J\,|\Psi_X|\right)^2} . \tag{78}$$

With the help of a computer we have also proven this formula for three sites in the unit cell. So for all cases we analyze in the final chapters 11 and 12, this formula is proven. For more than three sites in the unit cell it seems to be likely, that this formula is generally valid.

8.3 Finding the mean-field parameters

8.3.1 Derivatives of the energy with respect to mean-field parameters

To find the mean-field parameters, usually the energy is minimized with respect to them. As already mentioned, it turns out, that the second derivatives, which should be positive for minima, do not yield

reasonable results. So we just set the first derivative equal to zero and justify ignoring the second derivative with the reasonable results, we will find.

First we decompose the ψ's into the absolute value $|\psi_X|$ and the complex phase φ_X

$$\begin{aligned} \psi_X &= |\psi_X|\, e^{i\varphi_X} && (79)\\ \psi_X^* &= |\psi_X|\, e^{-i\varphi_X}\ . && (80) \end{aligned}$$

This way we can determine the derivative of the energy with respect to φ_Z

$$\begin{aligned} \partial_{\varphi_Z} E &= J\,|\psi_Z| \left(2\sum_Y N_{YZ} \sin\left(\varphi_Y - \varphi_Z\right) |\psi_Y| \right. \\ &\quad \left. + J \sum_X (\pm_X) \frac{\sum_Y N_{XY} \sin\left(\varphi_Y - \varphi_Z\right) |\psi_Y|}{\sqrt{\left(\frac{V}{2} R_X - \frac{\mu}{2}\right)^2 + \left(J\,|\Psi_X|\right)^2}} \right)\ , \end{aligned} \tag{81}$$

and with respect to the absolute value $|\psi_Z|$

$$\begin{aligned} \partial_{|\psi_Z|} E &= J \left(2\sum_X N_{ZX}\, |\psi_X| \cos\left(\varphi_X - \varphi_Z\right) \right. \\ &\quad \left. + J \sum_X (\pm_X) \frac{N_{XZ} \sum_Y N_{XY}\, |\psi_Y| \cos\left(\varphi_Y - \varphi_Z\right)}{\sqrt{\left(\frac{V}{2} R_X - \frac{\mu}{2}\right)^2 + \left(J\,|\Psi_X|\right)^2}} \right)\ . \end{aligned} \tag{82}$$

These two derivatives (81) and (82) can be combined to

$$\begin{aligned} |\psi_Z|\, \partial_{|\psi_Z|} E + i\, \partial_{\varphi_Z} E &= J\,|\psi_Z| \left(2\sum_X N_{XZ}\, |\psi_X|\, e^{i(\varphi_X - \varphi_Z)} \right. \\ &\quad \left. + J \sum_X (\pm_X) \frac{N_{XZ} \sum_Y N_{XY}\, |\psi_Y|\, e^{i(\varphi_Y - \varphi_Z)}}{\sqrt{\left(\frac{V}{2} R_X - \frac{\mu}{2}\right)^2 + \left(J\,|\Psi_X|\right)^2}} \right) \end{aligned} \tag{83}$$

and furthermore be written in a form, which will be useful later, i.e.

$$e^{i\varphi_Z} \left(|\psi_Z|\, \partial_{|\psi_Z|} E + i\, \partial_{\varphi_Z} E \right) = J\,|\psi_Z| \left(2\sum_X N_{XZ} \psi_X + J \sum_X (\pm_X) \frac{N_{XZ} \sum_Y N_{XY} \psi_Y}{\sqrt{\left(\frac{V}{2} R_X - \frac{\mu}{2}\right)^2 + \left(J\,|\Psi_X|\right)^2}} \right) \tag{84}$$

The ϱ's are real values, because they are expectation values of the number operator, and so we can use the real value derivatives to determine

$$\partial_{\varrho_Z} E = \frac{V}{2} \sum_X N_{XZ} \left(1 - 2\varrho_X\right) + \frac{V}{2} \sum_X N_{XZ} (\pm_X) \frac{\left(\frac{V}{2} R_X - \frac{\mu}{2}\right)}{\sqrt{\left(\frac{V}{2} R_X - \frac{\mu}{2}\right)^2 + \left(J\,|\Psi_X|\right)^2}}\ . \tag{85}$$

8.3.2 Setting the derivatives to zero

Since the first derivative of the energy with respect to the mean-field parameters has to vanish, we do this here in the following for the different derivatives, we determined in the last section.

To fulfill $\partial_{\varphi_Z} E = 0$ there are actually three ways

$$J = 0 \tag{86}$$

or

$$|\psi_Z| = 0 \tag{87}$$

or

$$-2\sum_Y N_{YZ}\,|\psi_Y|\sin(\varphi_Y-\varphi_Z) = J\sum_X N_{XZ}\,(\pm_X)\,\frac{\sum_Y N_{XY}\,|\psi_Y|\sin(\varphi_Y-\varphi_Z)}{\sqrt{\left(\frac{V}{2}R_X-\frac{\mu}{2}\right)^2+\left(J\,|\Psi_X|\right)^2}}\,, \tag{88}$$

but the solution $J = 0$ is not very interesting here, because it will be a special case of our final solutions. So we won't analyze it explicitly. The second condition means, that every ψ_Z can be chosen to be zero independently for different Z to satisfy $\partial_{\varphi_Z} E = 0$. This also will appear later in the mathematics again, so we will ignore it. Later we will also ignore similar conditions like $V = 0$ without mentioning it. The third condition is the important result here.

To fulfill $\partial_{|\psi_Z|} E = 0$ and (88) we can also fulfill

$$e^{i\varphi_Z}\left(|\psi_Z|\,\partial_{|\psi_Z|}E + i\,\partial_{\varphi_Z}E\right) = 0\,, \tag{89}$$

since $e^{i\varphi_Z}$ is never zero, the derivatives are real valued and 1 and i are linear independent. Using (84) we find the new equation

$$0 = J\,|\psi_Z|\left(2\sum_X N_{XZ}\psi_X + J\sum_X(\pm_X)\,\frac{N_{XZ}\sum_Y N_{XY}\psi_Y}{\sqrt{\left(\frac{V}{2}R_X-\frac{\mu}{2}\right)^2+\left(J\,|\Psi_X|\right)^2}}\right)\,, \tag{90}$$

which by excluding $J = 0$ and $|\psi_Z| = 0$, since it appears later again, is equivalent to

$$-2\sum_X N_{XZ}\psi_X = J\sum_X(\pm_X)\,\frac{N_{XZ}\sum_Y N_{XY}\psi_Y}{\sqrt{\left(\frac{V}{2}R_X-\frac{\mu}{2}\right)^2+\left(J\,|\Psi_X|\right)^2}}\,. \tag{91}$$

It can be written as a vector equation

$$\begin{aligned} &-2\begin{pmatrix} N_{ZA}, & N_{ZB} & \dots\end{pmatrix}\begin{pmatrix}\psi_A\\ \psi_B\\ \vdots\end{pmatrix}\\ &= J\begin{pmatrix} N_{ZA}, & N_{ZB} & \dots\end{pmatrix}\begin{pmatrix}(\pm_A)\,\frac{\sum_Y N_{AY}\psi_Y}{\sqrt{\left(\frac{V}{2}R_A-\frac{\mu}{2}\right)^2+\left(J|\Psi_A|\right)^2}}\\ (\pm_B)\,\frac{\sum_Y N_{BY}\psi_Y}{\sqrt{\left(\frac{V}{2}R_B-\frac{\mu}{2}\right)^2+\left(J|\Psi_B|\right)^2}}\\ \vdots\end{pmatrix} \end{aligned} \tag{92}$$

and for different Z it can be combined to a matrix equation

$$\begin{aligned} &-2\begin{pmatrix} N_{AA}, & N_{AB} & \dots\\ N_{BA}, & N_{BB} & \dots\\ \vdots & \vdots & \ddots\end{pmatrix}\begin{pmatrix}\psi_A\\ \psi_B\\ \vdots\end{pmatrix}\\ &= J\begin{pmatrix} N_{AA}, & N_{AB} & \dots\\ N_{BA}, & N_{BB} & \dots\\ \vdots & \vdots & \ddots\end{pmatrix}\begin{pmatrix}(\pm_A)\,\frac{\sum_Y N_{AY}\psi_Y}{\sqrt{\left(\frac{V}{2}R_A-\frac{\mu}{2}\right)^2+\left(J|\Psi_A|\right)^2}}\\ (\pm_B)\,\frac{\sum_Y N_{BY}\psi_Y}{\sqrt{\left(\frac{V}{2}R_B-\frac{\mu}{2}\right)^2+\left(J|\Psi_B|\right)^2}}\\ \vdots\end{pmatrix}\,. \end{aligned} \tag{93}$$

Now we can multiply with the inverse matrix (if it exists) and find

$$-2\begin{pmatrix}\psi_A\\ \psi_B\\ \vdots\end{pmatrix} = J\begin{pmatrix}(\pm_A)\frac{\sum_Y N_{AY}\psi_Y}{\sqrt{\left(\frac{V}{2}R_A-\frac{\mu}{2}\right)^2+(J|\Psi_A|)^2}}\\ (\pm_B)\frac{\sum_Y N_{BY}\psi_Y}{\sqrt{\left(\frac{V}{2}R_B-\frac{\mu}{2}\right)^2+(J|\Psi_B|)^2}}\\ \vdots\end{pmatrix}, \tag{94}$$

which reduces to

$$\psi_Z = -\frac{1}{2}(\pm_Z)\frac{J\Psi_Z}{\sqrt{\left(\frac{V}{2}R_Z-\frac{\mu}{2}\right)^2+(J|\Psi_Z|)^2}} \quad \forall Z\ . \tag{95}$$

In the cases, we analyze, the inverse of $\mathcal{N}=(N_{XY})$ always exist. The previous condition (95) can be fulfilled by two cases. In the first case ψ_Z is zero and so the other side of the equation has to vanish, too, hence Ψ_Z has to be zero. We exclude the other solution $J=0$ here. To distinguish between the two cases we divide the set of indices Z into a set $\mathbb{M}_{\psi=0}$ for case 1, i.e. solid sites, and a set $\mathbb{M}_{\psi\neq 0}$ for case 2, i.e. superfluid sites, which includes per definition all indices Z fulfilling $\psi_Z\neq 0$. In case 1

$$\psi_Z = 0 \quad \forall \mathbb{M}_{\psi=0} \tag{96}$$

$$\Psi_Z = 0 \quad \forall \mathbb{M}_{\psi=0} \tag{97}$$

we can rewrite the following square root by inserting (97)

$$(\pm_Z)\sqrt{\left(\frac{V}{2}R_Z-\frac{\mu}{2}\right)^2+(J|\Psi_Z|)^2} = (\pm_Z)\left|\frac{V}{2}R_Z-\frac{\mu}{2}\right| \quad \forall Z\in\mathbb{M}_{\psi=0}\ . \tag{98}$$

In case 2 $\psi_Z\neq 0$ we obtain the same square root from (95)

$$(\pm_Z)\sqrt{\left(\frac{V}{2}R_Z-\frac{\mu}{2}\right)^2+(J|\Psi_Z|)^2} = -\frac{1}{2}J\frac{\Psi_Z}{\psi_Z} \quad \forall Z\in\mathbb{M}_{\psi\neq 0}\ , \tag{99}$$

since it is allowed to divide by $\psi_Z\neq 0$ in this case. Now we define the new variables

$$\eta_Z := \frac{\Psi_Z}{\psi_Z} \quad \forall Z\in\mathbb{M}_{\psi\neq 0} \tag{100}$$

for indices $\in\mathbb{M}_{\psi\neq 0}$, because they will allow us to combine the extremalization conditions in a useful way and will reveal some interesting properties of the mathematical structure of our systems, so we insert 100 into (99) yielding

$$(\pm_Z)\sqrt{\left(\frac{V}{2}R_Z-\frac{\mu}{2}\right)^2+(J|\Psi_Z|)^2} = -\frac{1}{2}J\eta_Z \quad \forall Z\in\mathbb{M}_{\psi\neq 0}\ , \tag{101}$$

Now we can see, that the η_Z have to be real values, since all other expressions in (101) are real values, too. And it can not be zero, since Ψ_Z is not zero for $Z\in\mathbb{M}_{\psi\neq 0}$. Because it is a real value, the phase difference between ψ_X and Ψ_X has to be 0° or 180°. So the ψ_X of a lattice site always has the same or the opposite phase of the the sum over the next neighbor ψ_X. This is a major result, since it was derived for the general case.

The η_Z has to fulfill the definitions of Ψ_Z (60) and η_Z (100)

$$\Psi_X := \sum_Y N_{XY}\psi_Y \tag{102}$$

$$\eta_X := \frac{\Psi_X}{\psi_X} \quad \forall X\in\mathbb{M}_{\psi\neq 0} \tag{103}$$

leading to the condition

$$\sum_Y N_{XY}\psi_Y \quad = \quad \eta_X\psi_X \quad \forall X \in \mathbb{M}_{\psi\neq 0}. \tag{104}$$

For different X it yields the matrix equation

$$\begin{pmatrix} N_{X_1,X_1} & N_{X_1,X_2} & \cdots \\ N_{X_2,X_1} & N_{X_2,X_2} & \cdots \\ \vdots & \vdots & \ddots \end{pmatrix} \begin{pmatrix} \psi_{X_1} \\ \psi_{X_2} \\ \vdots \end{pmatrix} = \begin{pmatrix} \eta_{X_1} & 0 & \cdots \\ 0 & \eta_{X_2} & \cdots \\ \vdots & \vdots & \ddots \end{pmatrix} \begin{pmatrix} \psi_{X_1} \\ \psi_{X_2} \\ \vdots \end{pmatrix} \tag{105}$$

$$X_n \quad \in \quad \mathbb{M}_{\psi\neq 0}\ \forall n \tag{106}$$

and, thus, the η_X have to fulfill

$$0 \quad = \quad \det\left(\begin{pmatrix} N_{X_1,X_1} & N_{X_1,X_2} & \cdots \\ N_{X_2,X_1} & N_{X_2,X_2} & \cdots \\ \vdots & \vdots & \ddots \end{pmatrix} - \begin{pmatrix} \eta_{X_1} & 0 & \cdots \\ 0 & \eta_{X_2} & \cdots \\ \vdots & \vdots & \ddots \end{pmatrix}\right), \tag{107}$$

which is one of the important conditions, we have found in this section.

The last extremalization, we have to evaluate, is

$$\partial_{\varrho_Z} E \quad = \quad 0\,, \tag{108}$$

which yields

$$2\sum_X N_{XZ}\left(\varrho_X - \frac{1}{2}\right) \quad = \quad \sum_X N_{XZ}\,(\pm_X)\,\frac{\left(\frac{V}{2}R_X - \frac{\mu}{2}\right)}{\sqrt{\left(\frac{V}{2}R_X - \frac{\mu}{2}\right)^2 + \left(J\,|\Psi_X|\right)^2}} \tag{109}$$

and can be simplified the same way we did for (91). And we obtain

$$\left(\varrho_X - \frac{1}{2}\right) \quad = \quad \frac{1}{2}\,(\pm_X)\,\frac{\left(\frac{V}{2}R_X - \frac{\mu}{2}\right)}{\sqrt{\left(\frac{V}{2}R_X - \frac{\mu}{2}\right)^2 + \left(J\,|\Psi_X|\right)^2}}\,. \tag{110}$$

8.3.3 Combining the conditions

After having derived a few conditions in the last section we will combine them now and find a set of coupled equations as one final result of chapter 8.

We combine eq. (110) and (95) in the following way

$$\left(\varrho_X - \frac{1}{2}\right)^2 + |\psi_X|^2 \tag{111}$$

$$= \quad \frac{1}{4}\frac{\left(\frac{V}{2}R_X - \frac{\mu}{2}\right)^2}{\left(\frac{V}{2}R_X - \frac{\mu}{2}\right)^2 + \left(J\,|\Psi_X|\right)^2} + \frac{1}{4}\frac{J^2\,|\Psi_X|^2}{\left(\frac{V}{2}R_X - \frac{\mu}{2}\right)^2 + \left(J\,|\Psi_X|\right)^2} \tag{112}$$

$$= \quad \frac{1}{4}\,, \tag{113}$$

and hence have derived the important and simple relation

$$\left(\varrho_X - \frac{1}{2}\right)^2 + |\psi_X|^2 \quad = \quad \frac{1}{4}\,, \tag{114}$$

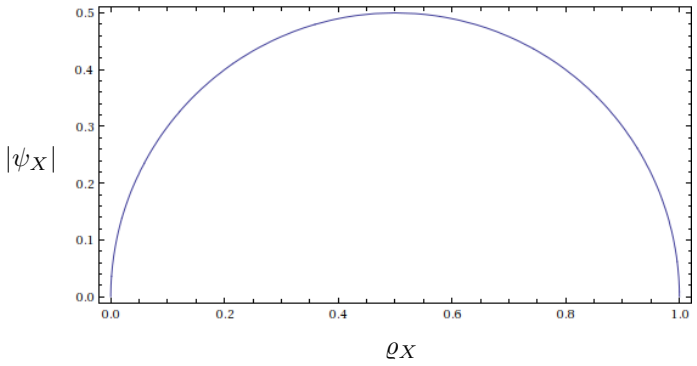

Figure 25: The simple circle relation between ϱ_X and $|\psi_X|$, which is valid for each lattice site X separately.

which is equivalent to

$$|\psi_X|^2 \quad = \quad \varrho_X \left(1 - \varrho_X\right) \ . \tag{115}$$

It describes a semicircle in the ϱ_X-$|\psi_X|$-plane, see Fig. 25. This simple equation is so important, because it describes a relation between ϱ_X and $|\psi_X|$ involving just one lattice site. It is valid for each lattice site X separately. In particular, this means, that the number of variables can be reduced from ϱ_X, $|\psi_X|$, $e^{i\varphi_X}$ for each site X in the unit cell to e.g. ϱ_X, $e^{i\varphi_X}$ for each site X in the unit cell. Later on we will use it to calculate $|\psi_X|$ after we have found ϱ_X. The relation (115) is one of the important conditions, we have found in this section.

Now we insert the square root expression (98) for the solid case $\psi_X = 0$ into the ϱ_X-extremalization equation (110), which yields

$$\left(\varrho_X - \frac{1}{2}\right) \quad = \quad \frac{1}{2}\left(\pm_X\right) \frac{\left(\frac{V}{2}R_X - \frac{\mu}{2}\right)}{\left|\frac{V}{2}R_X - \frac{\mu}{2}\right|} \quad \forall X \in \mathbb{M}_{\psi=0} \ . \tag{116}$$

Since the expression

$$\frac{\left(\frac{V}{2}R_X - \frac{\mu}{2}\right)}{\left|\frac{V}{2}R_X - \frac{\mu}{2}\right|} \quad = \quad \text{sign}\left(\frac{V}{2}R_X - \frac{\mu}{2}\right) := \left(\pm_{R\mu X}\right) \tag{117}$$

is just a sign, we denote it as $(\pm_{R\mu X})$. So (116) expresses the densities for solid sites as

$$\varrho_X \quad = \quad \frac{1}{2} + \frac{1}{2}\left(\pm_X\right)\left(\pm_{R\mu X}\right) \quad \forall X \in \mathbb{M}_{\psi=0} \ . \tag{118}$$

Thus the ϱ_X for $X \in \mathbb{M}_{\psi=0}$ can have values $\in \{0,1\}$, since (118) has the form $\frac{1}{2} \pm \frac{1}{2}$. We introduce the new symbols $(01)_X$ for $X \in \mathbb{M}_{\psi=0}$

$$(01)_X \quad = \quad \varrho_X \quad \forall X \in \mathbb{M}_{\psi=0} \ , \tag{119}$$

to express its possible values $\{0,1\}$. They depends on the combination of signs $\left(\pm_X\right)\left(\pm_{R\mu X}\right)$. The second one corresponds to a condition

$$\left(\pm_{\mu X}\right) = 1 \quad \Leftrightarrow \quad \frac{\mu}{2} < \frac{V}{2}R_X \tag{120}$$

$$\left(\pm_{\mu X}\right) = -1 \quad \Leftrightarrow \quad \frac{V}{2}R_X < \frac{\mu}{2} \ , \tag{121}$$

but these conditions are irrelevant, because for every R_X the energy eigenvalue can by the arbitrary $(\pm_X)$ be chosen such, that we get results under both conditions, which can be combined to solutions without these conditions. So in the case $X \in \mathbb{M}_{\psi=0}$ the ϱ_X can be chosen $\in \{0,1\}$ without causing any additional conditions for J, μ or V.

For the second case $\psi_X \neq 0$ we insert the square root expression (101) into the ϱ_X-extremalization equation (110) yielding

$$\left(\varrho_X - \frac{1}{2}\right) \quad = \quad \frac{1}{2}\frac{\left(\frac{V}{2}R_X - \frac{\mu}{2}\right)}{-\frac{1}{2}J\eta_Z} \quad \forall Z \in \mathbb{M}_{\psi\neq 0}\ . \tag{122}$$

Using the definition of R_X (60) the relation (122) becomes

$$J\eta_X\varrho_X + \frac{V}{2}\sum_Y N_{YX}\varrho_Y \quad = \quad \frac{1}{2}J\eta_X + \frac{\mu}{2}\ . \tag{123}$$

For the sum $\sum_Y N_{YX}\varrho_Y$ we now have to distinguish between the two cases $\psi_X = 0$ and $\psi_X \neq 0$, since different ϱ_Y appear, which can be either of the solid or superfluid case. So we divide the set of indices X into $\mathbb{M}_{\psi=0}$ and $\mathbb{M}_{\psi\neq 0}$. This way we obtain two sums

$$J\eta_X\varrho_X + \frac{V}{2}\sum_{Y\in\mathbb{M}_{\psi=0}} N_{YX}\varrho_Y + \frac{V}{2}\sum_{Y\in\mathbb{M}_{\psi\neq 0}} N_{YX}\varrho_Y \quad = \quad \frac{1}{2}J\eta_X + \frac{\mu}{2} \tag{124}$$

and after a rearrangement and expressing the ϱ_X for solid sites as $(01)_X$ we find

$$J\eta_X\varrho_X + \frac{V}{2}\sum_{Y\in\mathbb{M}_{\psi\neq 0}} N_{YX}\varrho_Y \quad = \quad \frac{1}{2}J\eta_X + \frac{\mu}{2} - \frac{V}{2}\sum_{Y\in\mathbb{M}_{\psi=0}} N_{YX}\,(01)_Y\ . \tag{125}$$

For different X it can be combined to the matrix equation

$$\left(J\begin{pmatrix}\eta_{X_1} & 0 & \cdots\\ 0 & \eta_{X_2} & \cdots\\ \vdots & \vdots & \ddots\end{pmatrix} + \frac{V}{2}\begin{pmatrix}N_{X_1,X_1} & N_{X_1,X_2} & \cdots\\ N_{X_2,X_1} & N_{X_2,X_2} & \cdots\\ \vdots & \vdots & \ddots\end{pmatrix}\right)\begin{pmatrix}\varrho_{X_1}\\ \varrho_{X_2}\\ \vdots\end{pmatrix} \tag{126}$$

$$= \quad \begin{pmatrix}\frac{1}{2}J\eta_{X_1} + \frac{\mu}{2} - \frac{V}{2}\sum_j N_{Y_jX_1}\,(01)_{Y_j}\\ \frac{1}{2}J\eta_{X_2} + \frac{\mu}{2} - \frac{V}{2}\sum_j N_{Y_jX_2}\,(01)_{Y_j}\\ \vdots\end{pmatrix} \tag{127}$$

using the indices

$$X_i \quad \in \quad \mathbb{M}_{\psi\neq 0}\ \forall i \tag{128}$$

$$Y_j \quad \in \quad \mathbb{M}_{\psi=0}\ \forall j \tag{129}$$

to distinguish between solid and superfluid sites. Inverting the matrix yields an expression for the ϱ_X

$$\begin{pmatrix}\varrho_{X_1}\\ \varrho_{X_2}\\ \vdots\end{pmatrix} \quad = \quad \left(J\begin{pmatrix}\eta_{X_1} & 0 & \cdots\\ 0 & \eta_{X_2} & \cdots\\ \vdots & \vdots & \ddots\end{pmatrix} + \frac{V}{2}\begin{pmatrix}N_{X_1,X_1} & N_{X_1,X_2} & \cdots\\ N_{X_2,X_1} & N_{X_2,X_2} & \cdots\\ \vdots & \vdots & \ddots\end{pmatrix}\right)^{-1} \tag{130}$$

$$\times\begin{pmatrix}\frac{1}{2}J\eta_{X_1} + \frac{\mu}{2} - \frac{V}{2}\sum_j N_{Y_jX_1}\,(01)_{Y_j}\\ \frac{1}{2}J\eta_{X_2} + \frac{\mu}{2} - \frac{V}{2}\sum_j N_{Y_jX_2}\,(01)_{Y_j}\\ \vdots\end{pmatrix}\ . \tag{131}$$

So now we have expressions for all ϱ_X, some of them depending on the η_X. This expression (130) for the particle densities ϱ_X is another important result of this section.

8.3.4 Vector and matrix notations

A few previous formulas included matrix operations. To write them in a more compact way, we introduce new vectors and matrices. Denoting the indices according to $X_i \in \mathbb{M}_{\psi\neq 0}\ \forall i$ and $Y_j \in \mathbb{M}_{\psi=0}\ \forall j$ they are defined as follows.

- concerning just solid sites, i.e. $\psi_X = 0$
  - Solid site densities

$$\overleftarrow{\varrho}^S = \overleftarrow{(01)} = \left(\overrightarrow{\varrho}^S\right)^T = \left(\overrightarrow{(01)}\right)^T \quad := \quad \begin{pmatrix} \varrho_{Y_1} \\ \varrho_{Y_2} \\ \vdots \end{pmatrix} = \begin{pmatrix} (01)_{Y_1} \\ (01)_{Y_2} \\ \vdots \end{pmatrix} \tag{132}$$

  - Solid site condensate densities

$$\overleftarrow{\psi}^S = \left(\overrightarrow{\psi}^S\right)^T \quad := \quad \begin{pmatrix} 0 \\ 0 \\ \vdots \end{pmatrix} \tag{133}$$

  - Connections between solid sites

$$\mathcal{N}^S \quad := \quad \begin{pmatrix} N_{Y_1,Y_1} & N_{Y_1,Y_2} & \cdots \\ N_{Y_2,Y_1} & N_{Y_2,Y_2} & \cdots \\ \vdots & \vdots & \ddots \end{pmatrix} \tag{134}$$

- concerning just superfluid sites, i.e. $\psi_X \neq 0$
  - Superfluid site densities

$$\overleftarrow{\varrho}^{SF} = \left(\overrightarrow{\varrho}^{SF}\right)^T \quad := \quad \begin{pmatrix} \varrho_{X_1} \\ \varrho_{X_2} \\ \vdots \end{pmatrix} \tag{135}$$

  - Superfluid site condensate densities

$$\overleftarrow{\psi}^{SF} = \left(\overrightarrow{\psi}^{SF}\right)^T \quad := \quad \begin{pmatrix} \psi_{X_1} \\ \psi_{X_2} \\ \vdots \end{pmatrix} \tag{136}$$

  - Connections between superfluid sites

$$\mathcal{N}^{SF} \quad := \quad \begin{pmatrix} N_{X_1,X_1} & N_{X_1,X_2} & \cdots \\ N_{X_2,X_1} & N_{X_2,X_2} & \cdots \\ \vdots & \vdots & \ddots \end{pmatrix} \tag{137}$$

  - Superfluid site η_X's as a diagonal matrix (diagonal dash "$\diagdown$")

$$\diagdown\!\!\!\!\eta \quad := \quad \begin{pmatrix} \eta_{X_1} & 0 & \cdots \\ 0 & \eta_{X_2} & \cdots \\ \vdots & \vdots & \ddots \end{pmatrix} \tag{138}$$

    and a vector

$$\overleftarrow{\eta} = \left(\overrightarrow{\eta}\right)^T \quad := \quad \begin{pmatrix} \eta_{X_1} \\ \eta_{X_2} \\ \vdots \end{pmatrix} \tag{139}$$

- concerning the interconnection between solid and superfluid sites
  - Connections between solid and superfluid sites

$$\mathcal{N}^{mix} := \begin{pmatrix} N_{Y_1,X_1} & N_{Y_1,X_2} & \cdots \\ N_{Y_2,X_1} & N_{Y_2,X_2} & \cdots \\ \vdots & \vdots & \ddots \end{pmatrix} \tag{140}$$

- miscellaneous:
  - useful vector

$$\overleftarrow{1} = \left(\overrightarrow{1}\right)^T := \begin{pmatrix} 1 \\ 1 \\ \vdots \end{pmatrix} \tag{141}$$

  - A scalar added to a matrix is meant to be the scalar multiplied by a unity matrix and then added to the matrix

$$\eta + \mathcal{N} = \eta \begin{pmatrix} 1 & 0 & \cdots \\ 0 & 1 & \cdots \\ \vdots & \vdots & \ddots \end{pmatrix} + \mathcal{N} \tag{142}$$

8.3.5 Summary

Using these vector and matrix notations, we can summarize all relevant formulas from this section in the following way:

- general relations (115)

$$|\psi_X|^2 = \varrho_X (1 - \varrho_X) \tag{143}$$

- concerning solid sites (119), (96)

$$\overrightarrow{\varrho}^S = \overrightarrow{(01)} \tag{144}$$

$$\overrightarrow{\psi}^S = 0 \tag{145}$$

- concerning superfluid sites (130), (105)

$$\overrightarrow{\varrho}^{SF} = \left(\frac{1}{2} J \overrightarrow{\eta} + \frac{\mu}{2} \overrightarrow{1} - \frac{V}{2} \overrightarrow{\varrho}^S \mathcal{N}^{mix}\right) \left(J\grave{\eta} + \frac{V}{2} \mathcal{N}^{SF}\right)^{-1} \tag{146}$$

$$\mathcal{N}^{SF} \overrightarrow{\psi}^{SF} = \grave{\eta} \overrightarrow{\psi}^{SF} \tag{147}$$

The formulas for the superfluid part still depend on undetermined variables η_X. So until now we have not found unique solutions by extremizing the energy with respect to the original mean-field parameters, which means either there is a relation, we have not found, yet, or the equation system is under-determined.

8.4 Rewriting the energy

We will now rewrite the energy using the relations, we have found so far. First we collect a few relations and combinations of them by using both cases $\mathbb{M}_{\psi=0}$ and $\mathbb{M}_{\psi\neq 0}$. The term $\frac{V}{2}R_X - \frac{\mu}{2}$ can be rewritten for the case $\mathbb{M}_{\psi\neq 0}$ according to (122)

$$\left(\frac{V}{2}R_X - \frac{\mu}{2}\right) = \begin{cases} \left(\frac{V}{2}R_X - \frac{\mu}{2}\right) & , X \in \mathbb{M}_{\psi=0} \\ -J\eta_X\left(\varrho_X - \frac{1}{2}\right) & , X \in \mathbb{M}_{\psi\neq 0} \end{cases} , \tag{148}$$

which is equivalent to

$$\frac{V}{2}R_X = \begin{cases} \frac{V}{2}R_X & , X \in \mathbb{M}_{\psi=0} \\ -J\eta_X\left(\varrho_X - \frac{1}{2}\right) + \frac{\mu}{2} & , X \in \mathbb{M}_{\psi\neq 0} \end{cases} . \tag{149}$$

This can be used to determine $R := \sum_X \varrho_X R_X$

$$\frac{V}{2}R = \frac{V}{2}\sum_{X\in\mathbb{M}_{\psi=0}} \varrho_X R_X + \sum_{X\in\mathbb{M}_{\psi\neq 0}} \left[-J\eta_X\varrho_X\left(\varrho_X - \frac{1}{2}\right) + \varrho_X\frac{\mu}{2}\right] . \tag{150}$$

Expressing Ψ_X as

$$\Psi_X = \begin{cases} 0 & , X \in \mathbb{M}_{\psi=0} \\ \eta_X\psi_X & , X \in \mathbb{M}_{\psi\neq 0} \end{cases} \tag{151}$$

and using (100) allows us to write $J\Psi$ as

$$J\Psi = J\sum_{X\in\mathbb{M}_{\psi\neq 0}} \eta_X |\psi_X|^2 . \tag{152}$$

And with the semicircle relation (143) we obtain

$$J\Psi = J\sum_{X\in\mathbb{M}_{\psi\neq 0}} \eta_X\varrho_X(1-\varrho_X) . \tag{153}$$

The other expressions, we need, are the following square root terms, which can be rewritten as

$$(\pm_X)\sqrt{\left(\frac{V}{2}R_X - \frac{\mu}{2}\right)^2 + (J|\Psi_X|)^2} = \begin{cases} (\pm_X)\left|\frac{V}{2}R_X - \frac{\mu}{2}\right| & , X \in \mathbb{M}_{\psi=0} \\ -\frac{1}{2}J\eta_X & , X \in \mathbb{M}_{\psi\neq 0} \end{cases} \tag{154}$$

and

$$\sum_X (\pm_X)\sqrt{\left(\frac{V}{2}R_X - \frac{\mu}{2}\right)^2 + (J|\Psi_X|)^2} = \sum_{X\in\mathbb{M}_{\psi=0}} (\pm_X)\left|\frac{V}{2}R_X - \frac{\mu}{2}\right| - \frac{1}{2}J\sum_{X\in\mathbb{M}_{\psi\neq 0}} \eta_X , \tag{155}$$

where we have used (98) and(101).

To rewrite the mean-field parameter dependent energies (78)

$$E = \left(J\Psi - \frac{V}{2}R\right) + \sum_X\left(\frac{V}{2}R_X - \frac{\mu}{2}\right) + \sum_X (\pm_X)\sqrt{\left(\frac{V}{2}R_X - \frac{\mu}{2}\right)^2 + (J|\Psi_X|)^2} \tag{156}$$

we first insert (153), (150), (148) and (155)

$$\begin{aligned} E &= J \sum_{X \in \mathbb{M}_{\psi \neq 0}} \eta_X \varrho_X (1 - \varrho_X) \\ &\quad - \sum_{X \in \mathbb{M}_{\psi \neq 0}} \left(-J \eta_X \varrho_X \left(\varrho_X - \frac{1}{2} \right) + \varrho_X \frac{\mu}{2} \right) - \sum_{X \in \mathbb{M}_{\psi = 0}} \frac{V}{2} \varrho_X R_X \\ &\quad + \sum_{X \in \mathbb{M}_{\psi = 0}} \left(\frac{V}{2} R_X - \frac{\mu}{2} \right) - J \sum_{X \in \mathbb{M}_{\psi \neq 0}} \eta_X \left(\varrho_X - \frac{1}{2} \right) \\ &\quad + \sum_{X \in \mathbb{M}_{\psi = 0}} (\pm_X) \left| \frac{V}{2} R_X - \frac{\mu}{2} \right| - \frac{1}{2} J \sum_{X \in \mathbb{M}_{\psi \neq 0}} \eta_X \ . \end{aligned} \tag{157}$$

After rearranging the sums

$$\begin{aligned} E &= - \sum_{X \in \mathbb{M}_{\psi = 0}} \frac{V}{2} \varrho_X R_X + \sum_{X \in \mathbb{M}_{\psi = 0}} \left(\frac{V}{2} R_X - \frac{\mu}{2} \right) + \sum_{X \in \mathbb{M}_{\psi = 0}} (\pm_X) \left| \frac{V}{2} R_X - \frac{\mu}{2} \right| \\ &\quad + J \sum_{X \in \mathbb{M}_{\psi \neq 0}} \eta_X \varrho_X (1 - \varrho_X) - \sum_{X \in \mathbb{M}_{\psi \neq 0}} \left(-J \eta_X \varrho_X \left(\varrho_X - \frac{1}{2} \right) + \varrho_X \frac{\mu}{2} \right) \\ &\quad - J \sum_{X \in \mathbb{M}_{\psi \neq 0}} \eta_X \left(\varrho_X - \frac{1}{2} \right) - \frac{1}{2} J \sum_{X \in \mathbb{M}_{\psi \neq 0}} \eta_X \end{aligned} \tag{158}$$

and combining certain sums

$$\begin{aligned} E &= - \sum_{X \in \mathbb{M}_{\psi = 0}} \frac{V}{2} \varrho_X R_X + \sum_{X \in \mathbb{M}_{\psi = 0}} \left(\frac{V}{2} R_X - \frac{\mu}{2} \right) \left(1 + (\pm_X) \frac{\left| \frac{V}{2} R_X - \frac{\mu}{2} \right|}{\left(\frac{V}{2} R_X - \frac{\mu}{2} \right)} \right) \\ &\quad + J \sum_{X \in \mathbb{M}_{\psi \neq 0}} \eta_X \varrho_X \left((1 - \varrho_X) + \left(\varrho_X - \frac{1}{2} \right) \right) - \frac{\mu}{2} \sum_{X \in \mathbb{M}_{\psi \neq 0}} \varrho_X \\ &\quad - J \sum_{X \in \mathbb{M}_{\psi \neq 0}} \eta_X \left(\varrho_X - \frac{1}{2} \right) - \frac{1}{2} J \sum_{X \in \mathbb{M}_{\psi \neq 0}} \eta_X \end{aligned} \tag{159}$$

we obtain an expression, where the term

$$1 + (\pm_X) \frac{\left| \frac{V}{2} R_X - \frac{\mu}{2} \right|}{\left(\frac{V}{2} R_X - \frac{\mu}{2} \right)} \tag{160}$$

occurs, which we already know from (116). It is twice the densities ϱ_X for $X \in \mathbb{M}_{\psi=0}$

$$1 + (\pm_X) \frac{\left| \frac{V}{2} R_X - \frac{\mu}{2} \right|}{\left(\frac{V}{2} R_X - \frac{\mu}{2} \right)} \quad = \quad 2 \varrho_X \quad \text{for } X \in \mathbb{M}_{\psi=0} \tag{161}$$

according to (119). So we replace this term in the energy and evaluate the other terms further

$$\begin{aligned} E &= - \frac{V}{2} \sum_{X \in \mathbb{M}_{\psi = 0}} \varrho_X R_X + \sum_{X \in \mathbb{M}_{\psi = 0}} \left(\frac{V}{2} R_X - \frac{\mu}{2} \right) 2 \varrho_X \\ &\quad - \frac{\mu}{2} \sum_{X \in \mathbb{M}_{\psi \neq 0}} \varrho_X - \frac{1}{2} J \sum_{X \in \mathbb{M}_{\psi \neq 0}} \eta_X \varrho_X \end{aligned} \tag{162}$$

and rewrite it again

$$\begin{aligned} E &= \frac{V}{2} \sum_{X \in \mathbb{M}_{\psi=0}} R_X \varrho_X - \mu \sum_{X \in \mathbb{M}_{\psi=0}} \varrho_X \\ &\quad - \sum_{X \in \mathbb{M}_{\psi \neq 0}} \varrho_X \left(\frac{1}{2} J \eta_X + \frac{\mu}{2} \right) . \end{aligned} \tag{163}$$

As the last step, we resolve R_X using its definition (60) and disassembling the sum into the two cases $\mathbb{M}_{\psi=0}$ and $\mathbb{M}_{\psi \neq 0}$

$$\begin{aligned} E &= \frac{V}{2} \sum_{X \in \mathbb{M}_{\psi=0}} \left(\sum_{Y \in \mathbb{M}_{\psi=0}} N_{XY} \varrho_Y + \sum_{Y \in \mathbb{M}_{\psi \neq 0}} N_{XY} \varrho_Y \right) \varrho_X - \mu \sum_{X \in \mathbb{M}_{\psi=0}} \varrho_X \\ &\quad - \sum_{X \in \mathbb{M}_{\psi \neq 0}} \varrho_X \left(\frac{1}{2} J \eta_X + \frac{\mu}{2} \right) . \end{aligned} \tag{164}$$

Now we can express the energy E as a sum consisting of three energies, E^S involving just indices $\in \mathbb{M}_{\psi=0}$, E^{SF} involving just indices $\in \mathbb{M}_{\psi \neq 0}$ and E^{mix} containing a double sum, which combines indices of both sets

$$\begin{aligned} E &= \underbrace{\frac{V}{2} \sum_{X \in \mathbb{M}_{\psi=0}} \sum_{Y \in \mathbb{M}_{\psi=0}} N_{XY} \varrho_Y \varrho_X - \mu \sum_{X \in \mathbb{M}_{\psi=0}} \varrho_X}_{=: E^S} \\ &\quad \underbrace{+ \frac{V}{2} \sum_{X \in \mathbb{M}_{\psi=0}} \sum_{Y \in \mathbb{M}_{\psi \neq 0}} N_{XY} \varrho_Y \varrho_X}_{=: E^{mix}} \\ &\quad \underbrace{- \frac{1}{2} \sum_{X \in \mathbb{M}_{\psi \neq 0}} \varrho_X \left(J \eta_X + \mu \right)}_{=: E^{SF}} \end{aligned} \tag{165}$$

$$E = E^S + E^{mix} + E^{SF} \tag{166}$$

This expression describes the energy of a unit cell and thus depends on the ansatz, which includes just one spatial symmetry. But in principle it is possible, that different patterns occur in the ground state, which need a different number of sites in the unit cell. In this situation the energies E for different patterns are not directly comparable. But they become comparable, by calculating the average energy per unit cell site, i.e. the energy E has to be divided by the number of sites in the unit cell $N_{UCsites}$. This way we will find the same formulas for the homogeneous superfluid in an ansatz with one site in the unit cell and in an ansatz with more than one site in the unit cell as one of the solutions. We also divide the energy E by the number of next neighbors N_{NN}. The reason is not so obvious here, but it turns out, that we can use the same formulas for different lattices, if we do this. It yields the "normalized" energy

$$\mathcal{E} := \frac{E}{N_{NN} N_{UCsites}} , \tag{167}$$

again separated into parts concerning solid sites ($\mathcal{E}^S$), superfluid sites ($\mathcal{E}^{SF}$) and interconnections between them ($\mathcal{E}^{mix}$)

$$\mathcal{E}^S = \frac{1}{N_{UCsites}}\left(\frac{V}{2}\sum_{X\in\mathbb{M}_{\psi=0}}\sum_{Y\in\mathbb{M}_{\psi=0}}\frac{N_{XY}}{N_{NN}}\varrho_Y\varrho_X - \frac{\mu}{N_{NN}}\sum_{X\in\mathbb{M}_{\psi=0}}\varrho_X\right) \tag{168}$$

$$\mathcal{E}^{mix} = \frac{1}{N_{UCsites}}\left(\frac{V}{2}\sum_{X\in\mathbb{M}_{\psi=0}}\sum_{Y\in\mathbb{M}_{\psi\neq 0}}\frac{N_{XY}}{N_{NN}}\varrho_Y\varrho_X\right) \tag{169}$$

$$\mathcal{E}^{SF} = \frac{1}{N_{UCsites}}\left(-\frac{1}{2}\sum_{X\in\mathbb{M}_{\psi\neq 0}}\varrho_X\left(J\frac{\eta_X}{N_{NN}}+\frac{\mu}{N_{NN}}\right)\right) \tag{170}$$

$$\mathcal{E} = \mathcal{E}^S + \mathcal{E}^{mix} + \mathcal{E}^{SF} \tag{171}$$

Using the vector and matrix notation and

$$\sum_{X\in\mathbb{M}_{\psi=0}}\varrho_X = \sum_{X\in\mathbb{M}_{\psi=0}}(01)_X = N_{\varrho=1} \tag{172}$$

yields

$$\mathcal{E}^S = \frac{1}{N_{UCsites}}\left(\frac{V}{2}\overrightarrow{\varrho}^S\frac{\mathcal{N}^S}{N_{NN}}\overleftarrow{\varrho}^S - N_{\varrho=1}\frac{\mu}{N_{NN}}\right) \tag{173}$$

$$\mathcal{E}^{mix} = \frac{1}{N_{UCsites}}\left(\frac{V}{2}\overrightarrow{\varrho}^S\frac{\mathcal{N}^{mix}}{N_{NN}}\overleftarrow{\varrho}^{SF}\right) \tag{174}$$

$$\mathcal{E}^{SF} = \frac{1}{N_{UCsites}}\left(-\frac{1}{2}\overrightarrow{\varrho}^{SF}\left(J\frac{\overleftarrow{\eta}}{N_{NN}}+\frac{\mu}{N_{NN}}\overleftarrow{1}\right)\right) \tag{175}$$

In this "normalized" energy $\mathcal{E}$ the matrix $\mathcal{N}$ now occurs in its normalized version $\frac{\mathcal{N}}{N_{NN}}$, see subsection 7.2. Furthermore η_X and μ occur as "normalized" by N_{NN}. Later we will see, that the energy $\mathcal{E}$, the particle densities ϱ_X and the condensate density ψ_X are almost independent of N_{NN} except the scaling of μ, which leads to the same phase diagram in the $\frac{\mu}{VN_{NN}}$-$\frac{J}{V}$-plane for different lattices, if the normalized matrix $\frac{\mathcal{N}}{N_{NN}}$ is the same for the patterns in the ground state.

As a last step we insert the particle densities for superfluid sites $\overrightarrow{\varrho}^{SF}$ from (146) into the energy formulas $\mathcal{E}^{mix}$ (174) and $\mathcal{E}^{SF}$ (175) and summarize including $\mathcal{E}^S$ (173)

$$\mathcal{E}^S = \frac{1}{N_{UCsites}}\left(\frac{V}{2}\overrightarrow{\varrho}^S\frac{\mathcal{N}^S}{N_{NN}}\overleftarrow{\varrho}^S - N_{\varrho=1}\frac{\mu}{N_{NN}}\right) \tag{176}$$

$$\mathcal{E}^{mix} = \frac{1}{N_{UCsites}}\left[\frac{1}{4}V\overrightarrow{\varrho}^S\frac{\mathcal{N}^{mix}}{N_{NN}}\left(J\frac{\grave{\eta}}{N_{NN}}+\frac{V}{2}\frac{\mathcal{N}^{SF}}{N_{NN}}\right)^{-1}\times\left(J\frac{\overleftarrow{\eta}}{N_{NN}}+\frac{\mu}{N_{NN}}\overleftarrow{1}-V\frac{\left(\mathcal{N}^{mix}\right)^T}{N_{NN}}\overleftarrow{\varrho}^S\right)\right] \tag{177}$$

$$\mathcal{E}^{SF} = \frac{1}{N_{UCsites}}\left[-\frac{1}{4}\left(J\frac{\overrightarrow{\eta}}{N_{NN}}+\frac{\mu}{N_{NN}}\overrightarrow{1}-V\overrightarrow{\varrho}^S\frac{\mathcal{N}^{mix}}{N_{NN}}\right)\times\left(J\frac{\grave{\eta}}{N_{NN}}+\frac{V}{2}\frac{\mathcal{N}^{SF}}{N_{NN}}\right)^{-1}\left(J\frac{\overleftarrow{\eta}}{N_{NN}}+\frac{\mu}{N_{NN}}\overleftarrow{1}\right)\right] \tag{178}$$

The energy $\mathcal{E}^S$ involves just solid sites and interconnections. Every occupied site has an influence in the amount of μ to the energy and the next neighbor interaction has an influence of $\frac{V}{2}$ for every

connection between two occupied sites. The energy $\mathcal{E}^{mix}$ consists just of the next neighbor interaction between solid and superfluid sites. Since solid sites have occupation number 0 or 1 and the densities are multiplied in the energy, effectively $\mathcal{E}^{mix}$ consists of next neighbor interactions between occupied solid and superfluid sites. The energy $\mathcal{E}^{SF}$ has a more complicated form with not so obvious terms.

The advantage of these energy formulas is, that the only undetermined values are the parameters η_X, i.e. one for each superfluid lattice site. Before the extremalization the energy depended on ϱ_X and ψ_X for all lattice sites, respectively. Although one can expect to find unique values via an extremalization, it is still a useful simplification to have less dependencies.

9 Classification of phases and phase boundaries

9.1 Phases

Usually the phases are classified in the following way:

	densities	condensate densities	
Mott insulator (MI)	$\varrho_X = \varrho \quad \forall X$	$\psi_X = 0 \quad \forall X$	homogeneous solid
Density wave (DW)	$\exists X, Y \quad \varrho_X \neq \varrho_Y$		inhomogeneous solid
Superfluid (SF)	$\varrho_X = \varrho \quad \forall X$	$\psi_X = \psi \neq 0 \quad \forall X$	homogeneous superfluid
Supersolid (SS)	$\exists X, Y \quad \varrho_X \neq \varrho_Y$	$\exists X, Y \quad \psi_X \neq \psi_Y$	everything else

These four classes are not very satisfying to describe the variety of phases we will find. So we define new classes, subclasses, phases and corresponding symbols.

Classes and subclasses			Phases	
Solids: S	$S^{\varrho:h}$		$S^{\varrho:0}$	MI, empty lattice
			$S^{\varrho:1}$	MI, full lattice
	$S^{\varrho:ih}$		$S^{\varrho:01}$	DW, 1/2 filled solid
			$S^{\varrho:001}$	DW, 1/3 filled solid
			$S^{\varrho:011}$	DW, 2/3 filled solid
			$\vdots$	$\vdots$
Superfluids: SF	$SF^{\varrho:h}$	$SF^{\varrho:h}_{pd:h}$	$SF^{\varrho:h}_{pd:0^\circ}$	homogeneous SF
			$SF^{\varrho:h}_{pd:180^\circ}$	?
			$SF^{\varrho:h}_{pd:120^\circ}$	?
			$\vdots$	$\vdots$
		$SF^{\varrho:h}_{pd:ih}$	not in our results	?
	$SF^{\varrho:ih}$	$SF^{\varrho:ih}_{pd:h}$	$SF^{\varrho:ih}_{pd:0^\circ}$	SS
			$\vdots$	$\vdots$
		$SF^{\varrho:ih}_{pd:ih}$	$SF^{\varrho:ih}_{pd:0^\circ,180^\circ}$	SS
			$\vdots$	$\vdots$
Mix: $S + SF$	$S^{\varrho:h} + SF^{\varrho:h}$	$S^{\varrho:h} + SF^{\varrho:h}_{pd:h}$	$S^{\varrho:0} + SF^{\varrho:h}_{pd:0^\circ}$	SS
			$S^{\varrho:1} + SF^{\varrho:h}_{pd:0^\circ}$	SS
			$S^{\varrho:0} + SF^{\varrho:h}_{pd:180^\circ}$	SS
			$S^{\varrho:1} + SF^{\varrho:h}_{pd:180^\circ}$	SS
		$S^{\varrho:h} + SF^{\varrho:h}_{pd:ih}$	not in our results	SS
	$S^{\varrho:h} + SF^{\varrho:ih}$	$S^{\varrho:h} + SF^{\varrho:ih}_{pd:h}$	not in our results	SS
		$S^{\varrho:h} + SF^{\varrho:ih}_{pd:ih}$	not in our results	SS
	$\vdots$	$\vdots$	$\vdots$	$\vdots$

The different parts of the symbols have the following meaning

Symbol	meaning
$\varrho : h$	homogeneous density and condensate density
$\varrho : ih$	inhomogeneous density and condensate density
$\varrho : n$	homogeneous with occupation number n
$\varrho : n_1 n_2, \ldots$	inhomogeneous with occupation numbers n_1, n_2, ...
$pd : h$	phase differences are always the same (homogeneous)
$pd : ih$	phase differences are not always the same (inhomogeneous)
$pd : \alpha$	phase differences are always α (homogeneous)
$pd : \alpha_1, \alpha_2, \ldots$	phase differences are $\alpha_1, \alpha_2, \ldots$ (inhomogeneous)

The symbols contain properties of the particle density ϱ and the phase differences pd, but not properties of the absolute value of the condensate density $|\psi|$, because it is not necessary. According to the semi-circle law (143)

$$|\psi_X|^2 \quad = \quad \varrho_X \left(1 - \varrho_X\right) \tag{179}$$

homogeneous/inhomogeneous ϱ_X yield directly homogeneous/inhomogeneous $|\psi_X|$. So we just need to denote the spatial symmetry of the ϱ_X in our symbols.

9.2 Phase diagram

For different experimental parameters the system can take a different phase, which is always the one with the lowest energy. Distinguishing between the phases in the space of parameters yields the phase diagram. In our case this space has the three dimensions J, μ and V. But all solutions can be expressed in terms of $\frac{\mu}{VN_{NN}}$ and $\frac{J}{V}$. So we have just to deal with a two dimensional space.

Phase boundaries distinguish between the phases and are classified by the order of phase transition. Phase boundaries of first kind are defined as discontinuities in properties of the system ($\varrho_X\left(J, \mu, V\right)$, $\psi_X\left(J, \mu, V\right)$) along the axes for experimental conditions (J, μ, V). Or in other words the first derivative of in our case $\varrho_X\left(J, \mu, V\right)$ and $\psi_X\left(J, \mu, V\right)$ with respect to J, μ, V is not defined at the phase boundary.

Phase boundaries of second kind have an undefined second derivative at the phase boundary, i.e. the first derivative with respect to J, μ, V has a discontinuity and $\varrho_X\left(J, \mu, V\right)$ and $\psi_X\left(J, \mu, V\right)$ show a continuous transition with a cant at the phase boundary.

10 Mathematics for special classes of patterns

In the last section we were investigating the general mathematics of our mean-field Hamiltonian, whereas in this section we have to go on with less general situations, i.e. certain classes of patterns, and exclude difficult cases, if we don't need it for the final results.

In **section 10.1 "Calculation procedure"** we first describe the principle calculation procedure, which we used in a computer calculation leading to the special cases of the following sections.

In **section 10.2 "Homogeneous pattern"** we investigate the simple homogeneous pattern, i.e. one site in unit cell, yielding formulas, which are valid for every lattice geometries included in out Hamiltonian and which are always a special case of every pattern. The results are the two homogeneous solids "empty lattice" and "full lattice" as well as the density- and phase-homogeneous superfluid.

In **section 10.3 "Other most common patterns"** we use a quite general adjacency matrix $\mathcal{N}$, whose special cases describe all patterns, we need later. We will find quite simple formulas in the case of $\eta_X = \eta \; \forall X$ including some phase boundaries. In the case of the inhomogeneous superfluid we need the help of a computer, since most of the formulas have no simple form except for the phase boundaries. The other interesting results like the densities are plotted in order to indicate the important features.

10.1 Calculation procedure

We have found a few relations between the particle densities and the condensate densities coupled via the new variables η_X (see section 8.3.5) and a new formula for the energy involving all η_X (see section 8.4). The next steps are based on calculations for certain patterns, which we can handle without computer calculations for most of the cases and with the help of a computer for the case of the inhomogeneous pure superfluid phases (see section 10.3.5). The simple cases are of cause special cases of the general computer analysis and so we can use the computer results to justify the important case $\eta_X = \eta$ (see section 10.3.2).

For the case of pure superfluids including the inhomogeneous ones, we just need the energy $\mathcal{E}^{SF}$ (178) without the $\overrightarrow{\varrho}^S$ term, since we don't have solid sites in this case. This energy just depends on the parameters η_X. The next step should be minimizing the energy again, this time with respect to the η_X, but it turns out, that we can just set the first derivative equal to zero and ignore the second derivatives in order to distinguish between minima and maxima. It is not unusual, that the same problem appears here, since the η_X are just a substitution for ϱ_X and ψ_X. The results will be senseful, so we use this method here without a reasonable explanation for this sattlepoint problem.

We let a computer find the values of the parameters η_X this way. The solutions are simple formulas for $\eta_X = \eta$ describing a lot of phases and complicated formulas for the inhomogeneous superfluids, which we don't explicitly write down here, since they are too complicated to recognize any structure in it, at least, we haven't found a simple way to express them. For $\eta_X = \eta$ we don't simply use the final computer results for the formulas, we will derive them in section 10.3.2 after replacing $\eta_X \to \eta$, which is the only step, we justify with the computer calculation.

After having determined the parameters η_X, they just have to be inserted into the formula for ϱ_X and afterwards ϱ_X can be inserted into the formula for $|\psi_X|$ (see section 8.3.5). Now we have everything except the phase factor $e^{i\varphi_X}$, which can be found via the equation system (147). This calculation procedure yields quite simple equations for $\eta_X = \eta$ and again more complicated formulas for the inhomogeneous superfluid.

10.2 Homogeneous pattern

First we make the simplest ansatz, i.e. the ansatz for a homogeneous distribution of all features of lattice sites. Or in other words we use one site in the unit cell

$$\varrho_X = \varrho \quad \forall X \quad , \qquad \psi_X = \psi \quad \forall X, \quad N_{UCsites} = 1 \; . \tag{180}$$

Although this distribution is always a special case of all other patterns, so we will find it later on anyway, we will do this calculation here, since it is valid for all lattice geometries and patterns included by our Hamiltonian, so it can also be used for lattices, we don't include in this thesis, e.g. some 3D lattices, which are more complicated than the cubic one.

Since the next neighbors in the homogeneous pattern are always of the same kind and since there are always N_{NN} of them, the adjacency matrix $\mathcal{N}$ has just one entry:

$$\mathcal{N} \quad = \quad \left(\; N_{NN} \; \right) \; . \tag{181}$$

With these basic properties of the homogeneous distribution, we can now derive expressions for the two classes of phases included in this ansatz, i.e. the homogeneous solids $S^{\varrho:h}$ and the density- and phase-homogeneous superfluid $SF^{\varrho:h}_{pd:0^\circ}$.

10.2.1 Homogeneous solids

For the homogeneous solid states the density ϱ of the only site in the unit cell can be chosen $\in \{0,1\}$ so the number of ϱ's, which have the value 1 is also

$$N_{\varrho=1} \quad \in \quad \{0,1\} \; . \tag{182}$$

The relevant connections between lattice sites are simply described by the one component matrix

$$\mathcal{N}^S = \mathcal{N} \quad = \quad \left(\; N_{NN} \; \right) \tag{183}$$

for homogeneous solids. The energy $\mathcal{E}^S$ (176) is the only one we need here for solid phases, yielding

$$\mathcal{E}\left[S^{\varrho:h}\right] N_{NN} N_{UCsites} = \mathcal{E}^S\left[S^{\varrho:h}\right] N_{NN} N_{UCsites} \quad = \quad \frac{V}{2}\varrho^2 N_{NN} - N_{\varrho=1}\mu \tag{184}$$

with the two special cases

$$\mathcal{E}\left[S^{\varrho:0}\right] \quad = \quad 0 \tag{185}$$

$$\mathcal{E}\left[S^{\varrho:1}\right] \quad = \quad \frac{V}{2} - \frac{\mu}{N_{NN}} \; , \tag{186}$$

which represent the "empty lattice" and the "full lattice", respectively.

10.2.2 Density- and phase-homogeneous superfluid

For the homogeneous superfluid we have to find one η via the matrix equation (147), which becomes a simple equation here, since $\mathcal{N} = \mathcal{N}^{SF}$ has just one component

$$N_{NN} \quad \psi^{\;SF} \quad = \quad \eta \quad \psi^{\;SF} \; . \tag{187}$$

This yields

$$\frac{\eta}{N_{NN}} \quad = \quad 1 \tag{188}$$

and by inserting it into the formula for the density (146) we find

$$\varrho^{SF} \quad = \quad \frac{J + \frac{\mu}{N_{NN}}}{2J + V} \; , \tag{189}$$

causing a restriction to the domain of J, μ and V due to the condition $0 \leq \varrho \leq 1$

$$0 \leq \quad \frac{J + \frac{\mu}{N_{NN}}}{2J+V} \quad \leq 1 \; . \tag{190}$$

The only energy, we need here for the pure superfluid case, is $\mathcal{E}^{SF}$ (178). Since the occuring vectors have just one component, the energy simplifies to

$$\mathcal{E}^{SF}\left[SF^{\varrho:h}_{pd:0^\circ}\right] N_{NN} N_{UCsites} \quad = \quad -\frac{1}{2}\frac{(J\eta+\mu)^2}{2J\eta+VN_{NN}} \; . \tag{191}$$

And inserting $\frac{\eta}{N_{NN}} = 1$ and $N_{UCsites} = 1$ yields the final energy expression

$$\mathcal{E}\left[SF^{\varrho:h}_{pd:0^\circ}\right] = \mathcal{E}^{SF}\left[SF^{\varrho:h}_{pd:0^\circ}\right] \quad = \quad -\frac{1}{2}\frac{\left(J+\frac{\mu}{N_{NN}}\right)^2}{2J+V} \tag{192}$$

for the homogeneous superfluid.

So we have found formulas for all homogeneous phases, which are valid for every lattice.

10.3 Other most common patterns

10.3.1 Basic properties

We will investigate here the patterns described by the quite general matrix

$$\mathcal{N} \quad = \quad \begin{pmatrix} A & N & N & \cdots \\ N & A & N & \\ N & N & A & \\ \vdots & & & \ddots \end{pmatrix} = (A-N) \begin{pmatrix} 1 & & & \cdots \\ & 1 & & \\ & & 1 & \\ \vdots & & & \ddots \end{pmatrix} + N \begin{pmatrix} 1 & 1 & 1 & \cdots \\ 1 & 1 & 1 & \\ 1 & 1 & 1 & \\ \vdots & & & \ddots \end{pmatrix} \; , \tag{193}$$

since it contains all special cases, we use later. The solid and superfluid part of the matrix have the same form

$$\mathcal{N}^S = \begin{pmatrix} A & N & \cdots \\ N & A & \\ \vdots & & \ddots \end{pmatrix} \quad , \qquad \mathcal{N}^{SF} = \begin{pmatrix} A & N & N & \cdots \\ N & A & N & \\ N & N & A & \\ \vdots & & & \ddots \end{pmatrix} \; , \tag{194}$$

but a different size (symbolized by the different number of components above). If we don't describe a mixture of solid and superfluid sites, one of these matrixes has of course no component. The mixed part of the matrix has just the value N as entries, since the diagonal value A of $\mathcal{N}$ is never part of it, so it is

$$\mathcal{N}^{mix} \quad = \quad \begin{pmatrix} N & N & N & \cdots \\ N & N & N & \\ \vdots & & & \ddots \end{pmatrix} = N \begin{pmatrix} 1 & 1 & 1 & \cdots \\ 1 & 1 & 1 & \\ \vdots & & & \ddots \end{pmatrix} \; . \tag{195}$$

An important relation is the following one between the components of the matrix and the number of next neighbors. The sum over all entries of a row in $\mathcal{N}$ has to yield the number of next neighbors N_{NN}

$$A + N\left(N_{UCsites} - 1\right) \quad = \quad N_{NN} \; . \tag{196}$$

So we can express N as

$$N \quad = \quad \frac{N_{NN} - A}{N_{UCsites} - 1} \; . \tag{197}$$

There will be several steps in the mathematics, where we insert this N to include the relation between N and A.

We can also simplify the energy $\mathcal{E}^S$ (176) by inserting the adjacency matrix (193)

$$\begin{aligned}
&\mathcal{E}^S N_{NN} N_{UCsites} \\
= \; & \frac{V}{2} \overrightarrow{\varrho}^S \left((A-N) \begin{pmatrix} 1 & & & \cdots \\ & 1 & & \\ & & 1 & \\ \vdots & & & \ddots \end{pmatrix} + N \begin{pmatrix} 1 & 1 & 1 & \cdots \\ 1 & 1 & 1 & \\ 1 & 1 & 1 & \\ \vdots & & & \ddots \end{pmatrix} \right) \overleftarrow{\varrho}^S - N_{\varrho=1}\mu
\end{aligned} \tag{198}$$

and then use

$$\overrightarrow{\varrho}^S \begin{pmatrix} 1 & & & \cdots \\ & 1 & & \\ & & 1 & \\ \vdots & & & \ddots \end{pmatrix} \overleftarrow{\varrho}^S = N_{\varrho=1} \tag{199}$$

$$\overrightarrow{\varrho}^S \begin{pmatrix} 1 & 1 & 1 & \cdots \\ 1 & 1 & 1 & \\ 1 & 1 & 1 & \\ \vdots & & & \ddots \end{pmatrix} \overleftarrow{\varrho}^S = (N_{\varrho=1})^2 \tag{200}$$

to obtain

$$\mathcal{E}^S N_{NN} N_{UCsites} = \frac{V}{2} N_{\varrho=1} \left(A + N \left(N_{\varrho=1} - 1 \right) \right) - N_{\varrho=1}\mu \, . \tag{201}$$

In a similar way the energy $\mathcal{E}^{mix}$ (174) can be simplified using

$$\overrightarrow{\varrho}^S \begin{pmatrix} 1 & 1 & 1 & \cdots \\ 1 & 1 & 1 & \\ \vdots & & & \ddots \end{pmatrix} \overleftarrow{\varrho}^{SF} = N_{\varrho=1} \overrightarrow{1} \overleftarrow{\varrho}^{SF} \tag{202}$$

yielding a simplified expression for the energy concerning connections between solid and superfluid sites

$$\mathcal{E}^{mix} N_{NN} N_{UCsites} = \frac{V}{2} N \; N_{\varrho=1} \overrightarrow{1} \overleftarrow{\varrho}^{SF} \, . \tag{203}$$

10.3.2 All combinations of solid phases and density-homogeneous superfluids

A lot of solutions, in fact almost all solutions for the 3×3 matrix we will use later, have the property $\eta_X = \eta \; \forall X \in \mathbb{M}_{\psi \neq 0}$. These solutions can be found by the general calculation procedure described in section 10.1, so it is justified to use it here to simplify the equations.

10.3.2.1 Unique values for η

Most important is the simplification for (147), which becomes an eigenvalue equation for $\mathcal{N}$:

$$\mathcal{N}^{SF} \overrightarrow{\psi}^{SF} = \eta \overrightarrow{\psi}^{SF} \, . \tag{204}$$

So we just have to solve

$$\det \left(\mathcal{N}^{SF} - \eta \right) = 0 \, . \tag{205}$$

The matrix $\mathcal{N}^{SF}$, describing the connections between superfluid sites,

$$\mathcal{N}^{SF} = \begin{pmatrix} A & N & N & \cdots \\ N & A & N & \\ N & N & A & \\ \vdots & & & \ddots \end{pmatrix} , \tag{206}$$

has the size $N_{\psi\neq 0} \times N_{\psi\neq 0}$. There are always just two simple eigenvalues, if the size of the matrix is at least two

$$\eta \in \{A-N,\ A+N\ (N_{\psi\neq 0}-1)\} \text{ for } 2 \leq N_{\psi\neq 0} , \tag{207}$$

where the first term is not degenerated and the second term $N_{\psi\neq 0}-1$ times. So we have found unique values for η. In the general case allowing different η_X, we would not find unique values, but one relation between all η_X. But the unique values η can be simply inserted into the other equations without any additional mathematical problems, which is a major advantage.

10.3.2.2 Particle densities of superfluid sites

For the particle densities $\overrightarrow{\varrho}^{SF}$ of the superfluid sites (146) we find the simplification due to $\eta_X = \eta \quad \forall X$

$$\overrightarrow{\varrho}^{SF} = \left(\frac{1}{2} J\eta \overrightarrow{1} + \frac{\mu}{2} \overrightarrow{1} - \frac{V}{2} \overrightarrow{\varrho}^{S} \mathcal{N}^{mix} \right) \left(J\eta + \frac{V}{2} \mathcal{N}^{SF} \right)^{-1} . \tag{208}$$

Now the matrix $J\eta + \frac{V}{2}\mathcal{N}^{SF}$ has the same entries on its diagonal and the conditions for $\overrightarrow{\varrho}^{SF}$ can be written as:

$$\begin{pmatrix} \varrho_{X_1}^{SF} \\ \varrho_{X_2}^{SF} \\ \vdots \end{pmatrix} = \begin{pmatrix} J\eta + A\frac{V}{2} & \frac{V}{2}N & \frac{V}{2}N & \cdots \\ \frac{V}{2}N & J\eta + A\frac{V}{2} & \frac{V}{2}N & \\ \frac{V}{2}N & \frac{V}{2}N & J\eta + A\frac{V}{2} & \\ \vdots & & & \ddots \end{pmatrix}^{-1} \begin{pmatrix} \frac{1}{2}J\eta + \frac{\mu}{2} - \frac{V}{2}N\ N_{\varrho=1} \\ \frac{1}{2}J\eta + \frac{\mu}{2} - \frac{V}{2}N\ N_{\varrho=1} \\ \vdots \end{pmatrix} \tag{209}$$

where again $N_{\psi\neq 0}$ is the size of the matrix and $\overrightarrow{\varrho}^{S}\mathcal{N}^{mix} = N\ N_{\varrho=1}$, since the matrix components of $\mathcal{N}^{mix}$ are always N and the solid ϱ_X, which can be zero or one, yield the factor $N_{\varrho=1}$. Because the inverse of a symmetric matrix is again a symmetric one and all components of the vector $\frac{1}{2}J\eta\overrightarrow{1} + \frac{\mu}{2}\overrightarrow{1} - \frac{V}{2}\overrightarrow{1}N\ N_{\varrho=1}$ are the same, all ϱ_X^{SF} become the same

$$\varrho_X^{SF} = \varrho^{SF}\ \forall X . \tag{210}$$

This way we can find a formula for ϱ^{SF}, since we obtain

$$\begin{pmatrix} J\eta + A\frac{V}{2} & \frac{V}{2}N & \frac{V}{2}N & \cdots \\ \frac{V}{2}N & J\eta + A\frac{V}{2} & \frac{V}{2}N & \\ \frac{V}{2}N & \frac{V}{2}N & J\eta + A\frac{V}{2} & \\ \vdots & & & \ddots \end{pmatrix} \begin{pmatrix} \varrho^{SF} \\ \varrho^{SF} \\ \vdots \end{pmatrix} = \begin{pmatrix} \frac{1}{2}J\eta + \frac{\mu}{2} - \frac{V}{2}N\ N_{\varrho=1} \\ \frac{1}{2}J\eta + \frac{\mu}{2} - \frac{V}{2}N\ N_{\varrho=1} \\ \vdots \end{pmatrix} , \tag{211}$$

which leads to the same equation for each row in the matrix

$$\left(J\eta + A\frac{V}{2} \right) \varrho^{SF} + \frac{V}{2}N\ (N_{\psi\neq 0}-1)\, \varrho^{SF} = \frac{1}{2}J\eta + \frac{\mu}{2} - \frac{V}{2}N\ N_{\varrho=1} , \tag{212}$$

and we obtain

$$\varrho^{SF} = \frac{\frac{1}{2}J\eta + \frac{\mu}{2} - \frac{V}{2}N\ N_{\varrho=1}}{J\eta + \frac{V}{2}\left(A + N\ (N_{\psi\neq 0}-1)\right)} , \tag{213}$$

where again $N_{\psi\neq 0}$ is the size of the matrix. Using eq. (197) to replace N, using $N_{\psi\neq 0} = N_{UCsites} - N_{\psi=0}$ and the new definitions

$$\nu_1 := \frac{N_{NN} - A}{N_{UCsites} - 1} N_{\varrho=1} \tag{214}$$

$$\nu_2 := N_{NN} - \frac{N_{NN} - A}{N_{UCsites} - 1} N_{\psi=0} \tag{215}$$

we find a simple expression for the densities of superfluid sites

$$\varrho^{SF} = \frac{J\frac{\eta}{N_{NN}} + \frac{\mu}{N_{NN}} - V\frac{\nu_1}{N_{NN}}}{2J\frac{\eta}{N_{NN}} + V\frac{\nu_2}{N_{NN}}} . \tag{216}$$

So ϱ^{SF} is almost determined. Just η has to be inserted at last. We could do this here, but since the formula (216) just gets more unclear without any real advantage, we won't do it. It is more useful to calculate η for a special case and afterwards inserting it into the formula for ϱ^{SF}.

10.3.2.3 Absolute value of condensate density at superfluid sites

The absolute value $|\Psi_X|$ is related to ϱ_X via the semicircle law (143). So if all ϱ_X^{SF} are the same then all $\left|\Psi_X^{SF}\right|$ have to be the same

$$\left|\psi_X^{SF}\right|^2 = \left|\psi^{SF}\right|^2 = \varrho^{SF}\left(1 - \varrho^{SF}\right) . \tag{217}$$

Inserting ϱ^{SF} (216) yields

$$\left|\psi^{SF}\right|^2 = \frac{\left(J\frac{\eta}{N_{NN}} + \frac{\mu}{N_{NN}} - V\frac{\nu_1}{N_{NN}}\right)\left(J\frac{\eta}{N_{NN}} - \frac{\mu}{N_{NN}} + V\frac{\nu_1+\nu_2}{N_{NN}}\right)}{\left(2J\frac{\eta}{N_{NN}} + V\frac{\nu_2}{N_{NN}}\right)^2} . \tag{218}$$

So we can also describe $\left|\psi^{SF}\right|$ in one expression without any complicated mathematics left. All parameters are already determined.

10.3.2.4 Complex phases of condensate density at superfluid sites

The second thing, we have to do, is finding the complex phases $e^{i\varphi_X}$ of $\psi_X = |\psi_X| e^{i\varphi_X}$. The equation, we use, is again (147). Inserting $\eta_X = \eta$ and $|\psi_X| = |\psi|$ and dividing by $|\psi|$ simplifies it to the eigenvalue equation

$$\begin{pmatrix} A & N & N & \cdots \\ N & A & N & \\ N & N & A & \\ \vdots & & & \ddots \end{pmatrix} \begin{pmatrix} e^{i\varphi_{X_1}} \\ e^{i\varphi_{X_2}} \\ e^{i\varphi_{X_3}} \\ \vdots \end{pmatrix} = \eta \begin{pmatrix} e^{i\varphi_{X_1}} \\ e^{i\varphi_{X_2}} \\ e^{i\varphi_{X_3}} \\ \vdots \end{pmatrix} \tag{219}$$

$$\begin{pmatrix} A-\eta & N & N & \cdots \\ N & A-\eta & N & \\ N & N & A-\eta & \\ \vdots & & & \ddots \end{pmatrix} \begin{pmatrix} e^{i\varphi_A} \\ e^{i\varphi_B} \\ e^{i\varphi_C} \\ \vdots \end{pmatrix} = 0 \tag{220}$$

Since the matrix has the same values on its diagonal, we get analogous equations for every row Z

$$N \sum_{\substack{n \\ X_n \neq Z}} e^{i\varphi_{X_n}} = (\eta - A)\, e^{i\varphi_Z} \qquad \forall Z \tag{221}$$

To analyze this relation further, we have to insert the two solutions for η.

In case of $\eta = A + N\ (N_{\psi\neq 0} - 1)$ we find

$$\sum_{\substack{n \\ X_n \neq Z}} e^{i\varphi_{X_n}} = (N_{\psi\neq 0} - 1)\, e^{i\varphi_Z} \tag{222}$$

with the absolute value

$$\left| \sum_{\substack{n \\ X_n \neq Z}} e^{i\varphi_{X_n}} \right| = N_{\psi\neq 0} - 1\ . \tag{223}$$

The number $N_{\psi\neq 0} - 1$ on the right side is also the number of summands on the left side, since it is a sum over all $N_{\psi\neq 0}$ indices of superfluid sites except one ($X \neq Y$). Imagining the complex phases $e^{i\varphi_{X_n}}$ as 2-dimensional arrows with length 1, the last condition means: A sum over arrows with length 1 has to have a length, which is the number of arrows. And the only solution is, that they all point in the same direction, i.e.:

$$\varphi_{X_n} = \varphi \quad \forall n\ . \tag{224}$$

So here we have found a state of our system with the same complex phase of $\psi_{X_n} = |\psi|\, e^{i\varphi_{X_n}} = |\psi|\, e^{i\varphi}$ for each lattice site.

In case of $\eta = A - N$ we find instead

$$\sum_n e^{i\varphi_{X_n}} = 0\ , \tag{225}$$

meaning, that all complex phases in the unit cell have to cancel out. For two sites in the unit cell it means, that there is a phase difference of 180° and for three sites, there is a phase difference of 120°.

10.3.2.5 Energy

The energy $\mathcal{E}^S$ (201) can not be simplified here, since it doesn't contain η, ϱ^{SF}or ψ^{SF}. But the energy $\mathcal{E}^{mix}$ (203)

$$\mathcal{E}^{mix} N_{NN} N_{UCsites} = \frac{V}{2} N\ N_{\varrho=1} \overrightarrow{1}\overleftarrow{\varrho}^{SF} \tag{226}$$

contains the densities $\overleftarrow{\varrho}^{SF}$, which are all the same as derived before and we can insert it from (216), yielding

$$\mathcal{E}^{mix} N_{NN} N_{UCsites} = \frac{V}{2} N\ N_{\varrho=1} N_{\psi\neq 0} \frac{J\eta + \mu - V\nu_1}{2J\eta + V\nu_2}\ , \tag{227}$$

where we have used

$$\overrightarrow{1}\overleftarrow{\varrho}^{SF} = N_{\psi\neq 0}\varrho^{SF}\ .$$

So now we have an expression for the mixed part $\mathcal{E}^{mix}$ of the energy, where all remaining constants are all defined by choosing a certain pattern or are already calculated before.

For the superfluid part of energy $\mathcal{E}^{SF}$ (175)

$$\mathcal{E}^{SF} N_{NN} N_{UCsites} = -\frac{1}{2} \overrightarrow{\varrho}^{SF} \left(J\overleftarrow{\eta} + \mu \overleftarrow{1} \right) \tag{228}$$

we can also insert the density ϱ^{SF} , and find

$$\mathcal{E}^{SF} N_{NN} N_{UCsites} = -\frac{1}{2} N_{\psi\neq 0} \frac{(J\eta + \mu - V\nu_1)(J\eta + \mu)}{2J\eta + V\nu_2} . \quad (229)$$

So adding up all energies $\mathcal{E}^S$ (201), $\mathcal{E}^{mix}$ (227) and $\mathcal{E}^{SF}$ (229) yields the complete final energy $\mathcal{E}$ for $\eta_X = \eta \; \forall X$:

$$\mathcal{E}\; N_{NN} N_{UCsites} = \frac{V}{2} N_{\varrho=1} (A + N(N_{\varrho=1} - 1)) - N_{\varrho=1}\mu \quad (230)$$

$$+\frac{V}{2} N\; N_{\varrho=1} N_{\psi\neq 0} \frac{J\eta + \mu - V\nu_1}{2J\eta + V\nu_2} \quad (231)$$

$$-\frac{1}{2} N_{\psi\neq 0} \frac{(J\eta + \mu - V\nu_1)(J\eta + \mu)}{2J\eta + V\nu_2} . \quad (232)$$

In this final expression which is valid for all $S + SF^{\varrho:h}$ phases, the remaining constants are all defined by choosing a certain pattern or are already calculated before, i.e. η was found in section 10.3.2.1.

10.3.2.6 Phase boundaries of second order

The second order phase transitions appear, when the formula for the particle density ϱ^{SF} leaves its allowed interval $0 \leq \varrho^{SF} \leq 1$. It has to be clipped at 0 and 1. Or in other words, when we replace ϱ^{SF} by 0 or 1 for a phase of the class $S + SF^{\varrho:h}$, we find the phase boundary to the solid phases, which are like $S + SF^{\varrho:h}$ except, that the superfluid sites are replaced by solid sites, i.e. $\varrho \in \{0, 1\}$. E.g. for $S^{\varrho:0} + SF^{\varrho:h}$ by replacing $\varrho^{SF} \to 1$ we can find a phase transition to an inhomogeneous solid, since the sites described by $S^{\varrho:0}$ stay the same and the other sites change at the phase transition from the homogeneous superfluid $SF^{\varrho:h}$ into a homogeneous solid with densities of 1 and the combination yields the inhomogeneous solid. For the phase transition we will symbolically write $\left(S_1 + SF^{\varrho:h}\right) \leftrightarrow \left(S_1 + S^{\varrho:h}\right)$, where S_1 stand for the part, which is solid before the transition. The simplest case is, that there is no S_1. Then we have the transition from a density-homogeneous superfluid to the empty of the full lattice: $SF^{\varrho:h} \leftrightarrow S^{\varrho:h}$.

So the phase transition $\left(S_1 + SF^{\varrho:h}\right) \leftrightarrow \left(S_1 + S^{\varrho:0}\right)$, which occurs, when the superfluid disappears at the boundary, is described by

$$0 = \varrho^{SF} = \frac{J\frac{\eta}{N_{NN}} + \frac{\mu}{N_{NN}} - V\frac{\nu_1}{N_{NN}}}{2J\frac{\eta}{N_{NN}} + V\frac{\nu_2}{N_{NN}}} , \quad (233)$$

which yields the phase boundary

$$J\frac{\eta}{N_{NN}} = V\frac{\nu_1}{N_{NN}} - \frac{\mu}{N_{NN}} . \quad (234)$$

And the phase transition $\left(S_1 + SF^{\varrho:h}\right) \leftrightarrow \left(S_1 + S^{\varrho:1}\right)$, which occurs, when the superfluid sites transform to occupied solid sites at the boundary, is described by

$$1 = \varrho^{SF} = \frac{J\frac{\eta}{N_{NN}} + \frac{\mu}{N_{NN}} - V\frac{\nu_1}{N_{NN}}}{2J\frac{\eta}{N_{NN}} + V\frac{\nu_2}{N_{NN}}} , \quad (235)$$

which leads to the phase boundary

$$-J\frac{\eta}{N_{NN}} = V\frac{\nu_1 + \nu_2}{N_{NN}} - \frac{\mu}{N_{NN}} . \quad (236)$$

Since η and all other parameters are independent of J, μ and V, we have found a linear function in these variables, which appears in the phase diagram on the $\frac{\mu}{VN_{NN}}$-$\frac{J}{V}$-plane as a straight line.

10.3.3 Solids

Choosing $\psi_X = 0 \; \forall X$ justified in (96) yields the non-superfluid states. The matrixes $\mathcal{N}^{mix}$ and $\mathcal{N}^{SF}$ have no entry and thus $\mathcal{E}^S$ (201) is the only energy needed here

$$\mathcal{E}^S N_{NN} N_{UCsites} = \frac{V}{2} N_{\varrho=1} \left[A + N \left(N_{\varrho=1} - 1 \right) \right] - N_{\varrho=1} \mu \; . \tag{237}$$

Inserting N (197) yields

$$\mathcal{E}^S = \frac{V}{2} N_{\varrho=1} \frac{A + \frac{N_{NN}-A}{N_{UCsites}-1} \left(N_{\varrho=1} - 1 \right)}{N_{NN} N_{UCsites}} - \frac{N_{\varrho=1}}{N_{UCsites}} \frac{\mu}{N_{NN}} \; . \tag{238}$$

The densities $\varrho_X^S = (01)_X$ can be chosen arbitrarily $\in \{0, 1\}$ for solid sites according to (144). Every combination yields a certain $N_{\varrho=1}$ and thus an energy. So all parameters are determined for a certain pattern.

10.3.3.1 Important special case: adjacency matrix diagonal elements zero

Especially important will be the case $A = 0$, i.e. the diagonal elements of $\mathcal{N}$ are zero, and the energy becomes

$$\mathcal{E}^S = \frac{V}{2} \left[\frac{N_{\varrho=1} \left(N_{\varrho=1} - 1 \right)}{N_{UCsites} \left(N_{UCsites} - 1 \right)} \right] - \frac{\mu}{N_{NN}} \left[\frac{N_{\varrho=1}}{N_{UCsites}} \right] \tag{239}$$

This energy expression describes all solid phases we will find later in the phase diagram.

10.3.4 Density-homogeneous superfluids

Choosing $\eta_X = \eta \; \forall X$ and $\psi_X = \psi \neq 0 \; \forall X$ yields the pure superfluid states with homogeneous particle density ϱ and homogeneous absolute value of the condensate density $|\psi|$ as we have shown in section 10.3.2. Due to $\psi_X = \psi \neq 0 \; \forall X$ the matrixes $\mathcal{N}^S$ and $\mathcal{N}^{mix}$ have no entry and thus $\mathcal{E}^{SF}$ (229) is the only energy needed here

$$\mathcal{E}^{SF} = -\frac{1}{2} \frac{N_{\psi \neq 0}}{N_{NN} N_{UCsites}} \frac{\left(J\eta + \mu - V\nu_1 \right) \left(J\eta + \mu \right)}{2J\eta + V\nu_2} \tag{240}$$

Since all sites are chosen to be superfluid, ϱ is never 1 due to $|\psi_X|^2 = \varrho_X \left(1 - \varrho_X \right)$ and thus $N_{\varrho=1} = 0$ and $N_{\psi=0} = 0$, which simplifies ν_1 and ν_2 as follows

$$\nu_1 = \frac{N_{NN} - A}{N_{UCsites} - 1} \, N_{\varrho=1} = 0 \tag{241}$$

$$\nu_2 = N_{NN} - \frac{N_{NN} - A}{N_{UCsites} - 1} \, N_{\psi=0} = N_{NN} \; . \tag{242}$$

With these ν_1 and ν_2 and the number of superfluid sites $N_{\psi \neq 0} = N_{UCsites}$ the energy simplifies further:

$$\mathcal{E}^{SF} = -\frac{1}{2} \frac{\left(J \frac{\eta}{N_{NN}} + \frac{\mu}{N_{NN}} \right)^2}{2J \frac{\eta}{N_{NN}} + V} \; . \tag{243}$$

At last the parameter $\frac{\eta}{N_{NN}}$ has to be determined from (207). Using $N_{\psi \neq 0} = N_{UCsites}$ (all sites in the unit cell are superfluid) and inserting N (197) we find

$$\frac{\eta}{N_{NN}} \in \left\{ \frac{A}{N_{NN}} - \frac{1 - \frac{A}{N_{NN}}}{N_{UCsites} - 1}, \quad 1 \right\} \tag{244}$$

These two cases yield the following two density-homogeneous superfluids $SF_{pd:0^\circ}^{\varrho:h}$ and $SF_{pd \neq 0^\circ}^{\varrho:h}$.

10.3.4.1 Density- and phase-homogeneous superfluid

Choosing $\frac{\eta}{N_{NN}} = 1$ leads to the energy of the density- and phase-homogeneous superfluid $SF^{\varrho:h}_{pd:0^\circ}$

$$\mathcal{E}\left[SF^{\varrho:h}_{pd:0^\circ}\right] = \mathcal{E}^{SF}\left[SF^{\varrho:h}_{pd:0^\circ}\right] = -\frac{1}{2}\frac{\left(J+\frac{\mu}{N_{NN}}\right)^2}{2J+V}\,, \tag{245}$$

the corresponding particle density

$$\varrho^{SF}\left[SF^{\varrho:h}_{pd:0^\circ}\right] = \frac{J+\frac{\mu}{N_{NN}}}{2J+V} \tag{246}$$

and the condensate density

$$|\psi|^2\left[SF^{\varrho:h}_{pd:0^\circ}\right] = \frac{\left(J+\frac{\mu}{N_{NN}}\right)\left(J-\frac{\mu}{N_{NN}}+V\right)}{(2J+V)^2}\,. \tag{247}$$

As derived before in section 10.3.2.4, the complex phases of ψ_X are all the same

$$\varphi_X = \varphi\,, \tag{248}$$

i.e. the phase differences are always 0° and thus the ψ_X are completely the same, not just the absolute value. In section 10.2.2 we have already derived this solution using one site in the unit cell. So this is a prove of concept. The complicated ansatz includes the homogeneous phase as a special case.

Since our Hamiltonian can be mapped to a spin-$\frac{1}{2}$ system (see e.g. Ref. [3]), we mention here, that this solution corresponds to parallel spin components along the two-dimensional lattice plane.

10.3.4.2 Density-homogeneous and phase-inhomogeneous superfluid

Choosing $\frac{\eta}{N_{NN}} = \frac{A}{N_{NN}} - \frac{1-\frac{A}{N_{NN}}}{N_{UCsites}-1}$ leads to the density-homogeneous superfluid $SF^{\varrho:h}_{pd\neq 0^\circ}$, which has non-zero phase differences. We don't explicitly insert η here, since the formulas become unnecessarily unclear, but we list them here as a result for this phase.

$$\mathcal{E}\left[SF^{\varrho:h}_{pd\neq 0^\circ}\right] = \mathcal{E}^{SF}\left[SF^{\varrho:h}_{pd\neq 0^\circ}\right] = -\frac{1}{2}\frac{\left(J\frac{\eta}{N_{NN}}+\frac{\mu}{N_{NN}}\right)^2}{2J\frac{\eta}{N_{NN}}+V} \tag{249}$$

$$\varrho\left[SF^{\varrho:h}_{pd\neq 0^\circ}\right] = \frac{J\frac{\eta}{N_{NN}}+\frac{\mu}{N_{NN}}}{2J\frac{\eta}{N_{NN}}+V} \tag{250}$$

$$|\psi|^2\left[SF^{\varrho:h}_{pd\neq 0^\circ}\right] = \frac{\left(J\frac{\eta}{N_{NN}}+\frac{\mu}{N_{NN}}\right)\left(J\frac{\eta}{N_{NN}}-\frac{\mu}{N_{NN}}+V\right)}{\left(2J\frac{\eta}{N_{NN}}+V\right)^2} \tag{251}$$

$$\sum_X e^{i\varphi_X} = 0 \tag{252}$$

In the spin $\frac{1}{2}$ this solution corresponds to as non-parallel as possible spin components along the two dimensional lattice plane.

10.3.5 Density-inhomogeneous superfluids

We haven't found a simple calculation method for the inhomogeneous pure superfluids $SF^{\varrho:ih}$ of the $\mathcal{N}$, we use in this section. Just for a 3×3 matrix with $A = 0$ we have done the calculation with the computer, since we need it for the triangular lattice.

10.3.5.1 Special case: 3 sites in unit cell, adjacency matrix diagonal elements zero

Here the computer calculations show, that two of the three η_X are always the same, e.g. $\eta_A = \eta_B =: \eta_{AB}$, i.e. we always find a honeycomb pattern in the triangular lattice. The equation (147) yields

$$\eta_A \eta_B \eta_C \quad = \quad \eta_A N^2 + \eta_B N^2 + \eta_C N^2 + 2N^3 \tag{253}$$

via the determinant equation

$$\det\left(\mathcal{N}^{SF} - \grave{\eta}\right) \quad = \quad 0\,. \tag{254}$$

Using this relation and $\eta_A = \eta_B =: \eta_{AB}$ the energy $\mathcal{E}^{SF}$, which is the only one, we need here, can be expressed depending just on one η_X, e.g. η_{AB}. The next step is to set the first derivative of the energy with respect to this one variable to zero. And again we do not investigate the second derivative (see section 10.1). This way the computer can find four solutions. One is simply

$$\frac{\eta_A}{N_{NN}} = \frac{\eta_B}{N_{NN}} = \frac{\eta_C}{N_{NN}} \quad = \quad 1 \tag{255}$$

describing the homogeneous superfluid with 0° phase differences, which we have already found in section 10.2.2.

The others are new solutions describing the inhomogeneous superfluids. As mentioned before the formulas for the η, ϱ_X and ψ_X are too complicated to write them down here explicitly.

Later we want to find out, which phase appears in the ground state. This means, we will determine, which phase has the lowest energy in which domain of J, μ and V. Since the formulas are complicated here, we have done this with a computer analysis, too. Not all branches of the solution for inhomogeneous superfluids appear in the ground state, so we will describe here just, what is important for the ground state.

There are three separate regions in the domain of J, μ and V. One lies between the two inhomogeneous solids and the homogeneous superfluid in the $\frac{J}{V}$-$\frac{\mu}{VN_{NN}}$ phase diagram for $0 < \frac{J}{V}$. The density distributions $\varrho_A = \varrho_B$ and ϱ_C in Fig. (28) and (29) change in $\frac{\mu}{VN_{NN}}$-direction between 0 and 1 and show a discontinuity at $\frac{\mu}{VN_{NN}} = \frac{1}{2}$. So here we have found a phase transition of first order dividing this region of the phase diagram into two phases. In the example of the triangular lattice the pattern jumps from Fig. 26a to Fig. 26b. The formulas for the densities have defined values also beyond $0 \leq \varrho_X \leq 1$, but since it is not physically allowed, we have to cut the functions there, i.e. they are restricted to a certain domain of J, μ and V. Cutting a density function due to $0 \leq \varrho_X \leq 1$ always means, we have found a transition of first order to a solid, in this case the two inhomogeneous solids. These two phase boundaries can be expressed in the two simple formulas

$$\left(2\frac{J}{V} + \frac{\mu}{VN_{NN}}\right)^2 \quad = \quad \frac{\mu}{VN_{NN}}\left(4 - 7\frac{\mu}{VN_{NN}}\right) \tag{256}$$

and

$$\left(2\frac{J}{V} - \frac{\mu}{VN_{NN}} + 1\right)^2 \quad = \quad \frac{\mu}{VN_{NN}}\left(10 - 7\frac{\mu}{VN_{NN}}\right) - 3\,. \tag{257}$$

Both form ellipses on the $\frac{J}{V}$-$\frac{\mu}{VN_{NN}}$-plane, but just a part of them appear in the phase diagram as phase boundaries, since the energy of the corresponding phase has to be the lowest in comparison to all other phases. At $\frac{J}{V} = \frac{1}{4}$ the formulas for the densities have a non-vanishing imaginary part and thus have no physical interpretation any more. So here a phase transition has to occur, which turns out to be a discontinuous transition to the homogeneous superfluid. The $|\psi_X|$ are directly connected to the ϱ_X via the semicircle law $|\psi_X|^2 = \varrho_X\,(1 - \varrho_X)$ and thus reveal nothing new. The phase differences of the ψ_X are always 0° in these two phases independent of J, μ or V, although the complete set of solutions include phase differences varying with J, μ or V, but they never appear in the ground state. After this

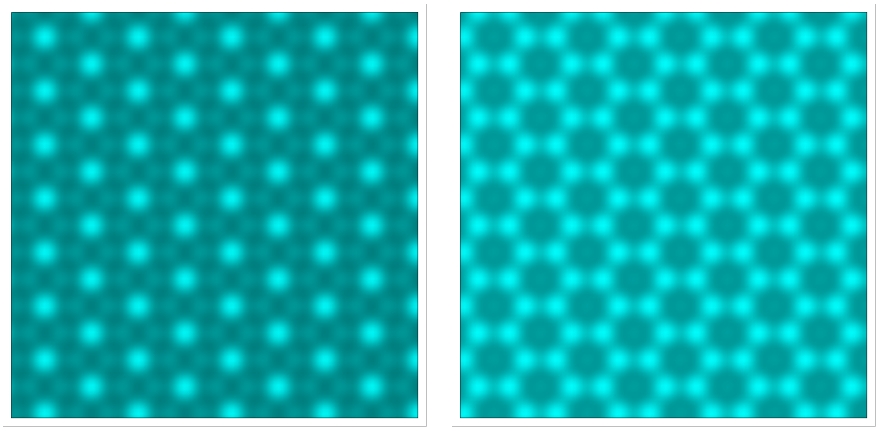

(a) $SF^{\varrho:ih}_{pd:0^\circ}$ (b) $SF^{\varrho:ih}_{pd:0^\circ}$

Figure 26: Spatial distributions of inhomogeneous superfluids in the triangular lattice for positive hopping. **(a)** close to the 1/3 filled solid, **(b)** close to the 2/3 filled solid.

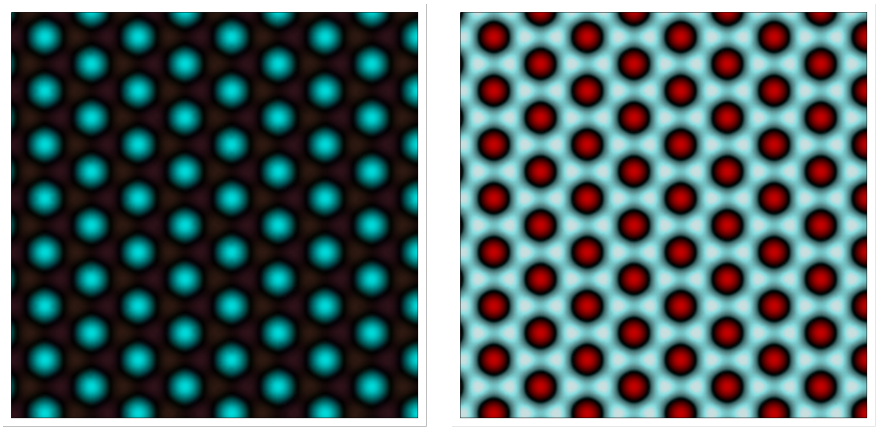

(a) $SF^{\varrho:ih}_{pd:0^\circ,180^\circ}$ (b) $SF^{\varrho:ih}_{pd:0^\circ,180^\circ}$

Figure 27: Spatial distributions of inhomogeneous superfluids in the triangular lattice for **negative hopping**. **(a)** between empty lattice and 1/3 filled solid, **(b)** between 2/3 filled solid and full lattice.

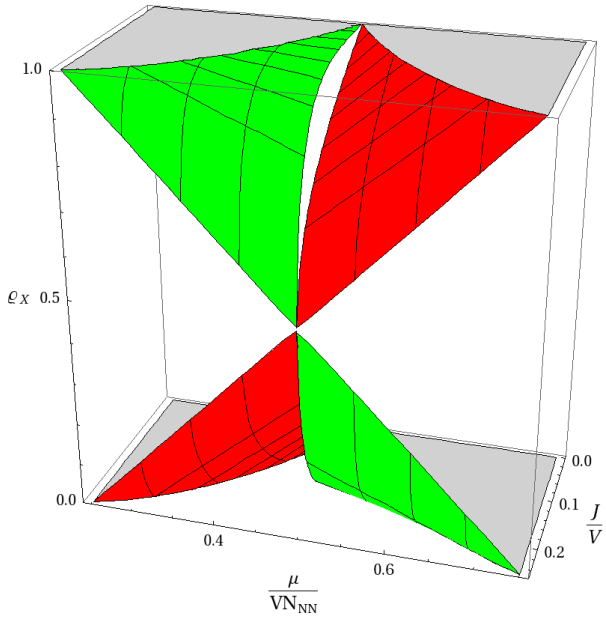

Figure 28: Densities of the inhomogeneous superfluid $SF^{\varrho:ih}_{pd:0^\circ}$ for positive hopping illustrating the discontinuous phase transition at $\frac{\mu}{VN_{NN}} = \frac{1}{2}$ and the continuous transitions to the inhomogeneous solids. *Red*: two equal densities $\varrho_A = \varrho_B$, *green*: third density $\varrho_C \neq \varrho_A, \varrho_B$, *gray*: density reached its limits $0 \leq \varrho_X \leq 1$.

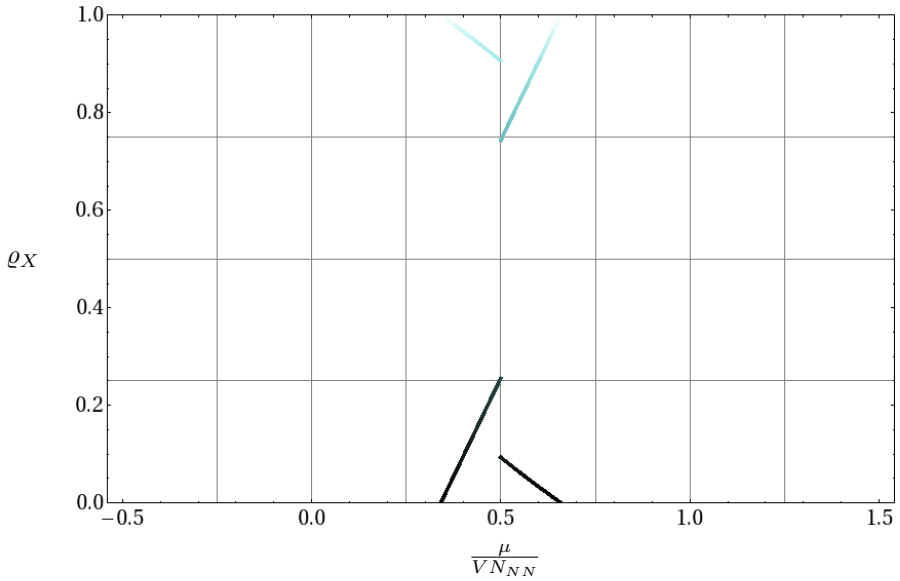

Figure 29: Densities of the inhomogeneous superfluid $SF^{\varrho:ih}_{pd:0^\circ}$ for positive hopping at $\frac{J}{V} = 0.2$ (color according to section 0.1).

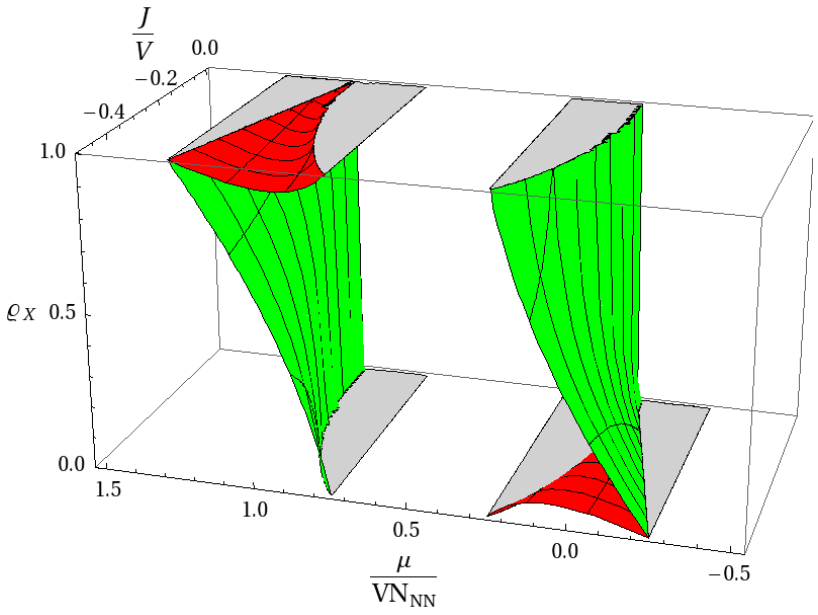

Figure 30: Densities of the inhomogeneous superfluid $SF^{\varrho:ih}_{pd:0°,180°}$ for **negative hopping** illustrating the continuous transitions to the solids. *Red*: two equal densities $\varrho_A = \varrho_B$, *green*: third density $\varrho_C \neq \varrho_A, \varrho_B$, *gray*: density reached its limits $0 \leq \varrho_X \leq 1$.

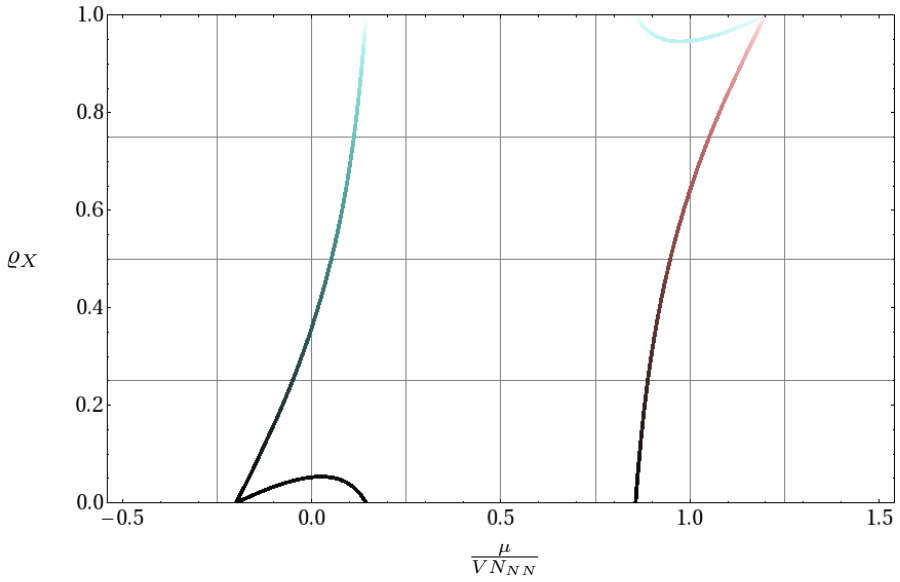

Figure 31: Densities of the inhomogeneous superfluid $SF^{\varrho:ih}_{pd:0°,180°}$ for **negative hopping** at $\frac{J}{V} = -0.4$ (color according to section 0.1).

analysis the previous two phases should be called inhomogeneous superfluids with phase differences of 0°, hence the symbol $SF^{\varrho:ih}_{pd:0^\circ}$.

The other two phases are located in the phase diagram at $\frac{J}{V} < 0$ between the homogeneous solids, the nearest inhomogeneous solid and a homogeneous superfluid with phase differences of 120°, which we will completely describe in chapter 12. We just mention it here to describe all phase boundaries.

Again in these two phases the formulas for the density leave the allowed values $0 \leq \varrho_X \leq 1$, see Fig. (30) and (31)), which gives us directly the second order phase transitions for these inhomogeneous superfluids to the corresponding solids. Again these phase boundaries can be expressed in two simple formulas, but they are the same as before, see (256) and (257). Just a different part of these two ellipses appear in the phase diagram.

The density ϱ_C changes in $\frac{\mu}{VN_{NN}}$-direction between 0 and 1, whereas the densities $\varrho_A = \varrho_B$ just change a little bit and come back to their previous value at the transition to the solid, see Fig. 30 and 31. And again the $|\psi_X|$ yield nothing new. For the triangular lattice the spatial distributions are shown in Fig. 27a and 27b.

As mentioned before varying phase differences appear in the complete solution set, but also in the phases, that appear for $\frac{J}{V} < 0$ in the ground state, the complex phase of the ψ_X is not changing with J, μ or V. In these states it is 0° or 180°. So this phase should be called inhomogeneous superfluids with phase differences of 0° and 180°, hence the symbol $SF^{\varrho:ih}_{pd:0^\circ,180^\circ}$.

11 Non-frustrated lattices

Within the mean-field approximation several different lattices lead to the same phase diagram, when μ is taken in units of the number of next neighbors N_{NN}, i.e. $\frac{\mu}{N_{NN}}$. Or in other words they only differ in a scaling of the μ-axis.

One class of lattices are the non frustrated ones, i.e. they allow a pattern with alternating properties for the next neighbor sites. These patterns with two sites in the unit cell are in the mean-field approximation all described by the normalized matrix

$$\frac{\mathcal{N}}{N_{NN}} = \begin{pmatrix} 0 & 1 \\ 1 & 0 \end{pmatrix} , \tag{258}$$

since it expresses, that the next neighbors are all of the other type. It can be used for a 1D lattice ($N_{NN} = 2$), quadratic lattice ($N_{NN} = 4$), cubic lattice ($N_{NN} = 6$) or honeycomb lattice ($N_{NN} = 3$), since all of them allow an alternating pattern. This is a special case of (193) so we can use all results from section 10.3. The alternating pattern is then determined by

$$A = 0 \quad , \qquad N = N_{NN} \tag{259}$$

and the size of the matrix

$$N_{UCsites} = 2 . \tag{260}$$

There are other patterns, which have to be considered at first, like e.g. a stripe pattern on the quadratic lattice described by

$$\mathcal{N} = \begin{pmatrix} 2 & 2 \\ 2 & 2 \end{pmatrix} , \tag{261}$$

which means

$$A = 2 \quad , \qquad N = 2 \tag{262}$$

and again

$$N_{UCsites} = 2 \tag{263}$$

or a 3 site pattern on the 1D lattice described by

$$\mathcal{N} = \begin{pmatrix} 0 & 1 & 1 \\ 1 & 0 & 1 \\ 1 & 1 & 0 \end{pmatrix} \tag{264}$$

with

$$A = 0 \quad , \qquad N = 1 \tag{265}$$

and

$$N_{UCsites} = 3 . \tag{266}$$

These patterns are all included in the calculation method and results of section 10.3, so we can simply calculate all relevant properties and find out, whether these patterns occur in the ground state. It turns out, that they don't. Just the alternating pattern is relevant for the non-frustrated lattices, so we just describe this pattern in the following sections.

Furthermore, we have not found a mixture $S + SF^{\varrho:h}$, an inhomogeneous superfluid $SF^{\varrho:ih}$ or more complicated phases in the ground state, so we will not mention them any more in the following. We just describe the phases, which appear in the ground state.

11.1 Phases

11.1.1 Solids

For pure solids, we need the energy $\mathcal{E}^S[S]$ (239) for $A = 0$ and $N_{UCsites} = 2$

$$\mathcal{E}[S] = \mathcal{E}^S[S] \quad = \quad \frac{1}{4} N_{\varrho=1} \left(N_{\varrho=1} - 1\right) \; V - \frac{1}{2} N_{\varrho=1} \frac{\mu}{N_{NN}} \; . \tag{267}$$

Since we have two sites in the unit cell, $N_{\varrho=1}$ can be chosen

$$N_{\varrho=1} \quad \in \quad \{0, 1, 2\} \tag{268}$$

yielding all properties of all solid phases

phase	$N_{\varrho=1}$	ϱ_A	ϱ_B	$\psi_A = \psi_B$	$\mathcal{E}$ [phase]	domain of J,μ,V
$S^{\varrho:0}$	0	0	0	0	0	$\mathbb{R}$
$S^{\varrho:01}$	1	0	1		$-\frac{1}{2}\frac{\mu}{N_{NN}}$	
		1	0			
$S^{\varrho:1}$	2	1	1		$\frac{V}{2} - \frac{\mu}{N_{NN}}$	

As mentioned before these results are valid for different lattices. E.g. the $S^{\varrho:01}$ appears in the 1D lattice simply as a 1D alternating pattern, in the quadratic lattice as the checkerboard pattern and in a cubic lattice as the 3D version of a checkerboard. The other phases are simply the homogeneous distribution of empty or occupied sites, respectively.

11.1.2 Density- and phase-homogeneous superfluid

For the homogeneous superfluid with 0° phase differences the results were already determined in section 10.2.2 and 10.3.4.1 by the equations (245), (246) and (247) yielding

$$\mathcal{E}\left[SF^{\varrho:h}_{pd:0^\circ}\right] \quad = \quad -\frac{1}{2} \frac{\left(J + \frac{\mu}{N_{NN}}\right)^2}{2J + V} \tag{269}$$

$$\varrho \quad = \quad \frac{J + \frac{\mu}{N_{NN}}}{2J + V} \tag{270}$$

$$|\psi|^2 \quad = \quad \frac{\left(J + \frac{\mu}{N_{NN}}\right)\left(J - \frac{\mu}{N_{NN}} + V\right)}{\left(2J + V\right)^2} \tag{271}$$

with the equal phases

$$\varphi_A \quad = \quad \varphi_B \; . \tag{272}$$

11.1.3 Density-homogeneous and phase-inhomogeneous superfluid

The density-homogeneous and phase-inhomogeneous superfluid is basically the result from section 10.3.4.2. Using

$$A = 0 \quad , \qquad N_{UCsites} = 2 \tag{273}$$

$$\frac{\eta}{N_{NN}} \quad = \quad \frac{A}{N_{NN}} - \frac{1 - \frac{A}{N_{NN}}}{N_{UCsites} - 1} = -1 \tag{274}$$

for the alternating pattern the equations (249), (250) and (251) yield

$$\mathcal{E}\left[SF^{\varrho:h}_{pd:180^\circ}\right] = -\frac{1}{2}\frac{\left(-J+\frac{\mu}{N_{NN}}\right)^2}{-2J+V} \tag{275}$$

$$\varrho = \frac{-J+\frac{\mu}{N_{NN}}}{-2J+V} \tag{276}$$

$$|\psi|^2 = \frac{\left(-J+\frac{\mu}{N_{NN}}\right)\left(-J-\frac{\mu}{N_{NN}}+V\right)}{(-2J+V)^2}\,. \tag{277}$$

And the condition (252) leads directly to phase differences of 180°

$$e^{i\varphi_A} = -e^{i\varphi_B} \tag{278}$$

$$\varphi_A - \varphi_B = 180^\circ\,. \tag{279}$$

So here we have found a density-homogeneous and phase-alternating superfluid. The alternating phases can just appear here, since the alternating pattern is per definition geometrically allowed in non-frustrated lattices.

11.1.4 Summary

In order to have an overview over all properties of the phases, we summarize them in the following table including the condition $0 \leq \varrho_X \leq 1$, which restricts J,μ and V to a certain domain. We use the abbreviations "p.d." for "phase differences" and "n.d." for "not defined".

phase	ϱ_A	ϱ_B	$\lvert\psi_A\rvert^2 = \lvert\psi_B\rvert^2$	p.d.	$\mathcal{E}$ [phase]	domain of J,μ,V
$S^{\varrho:0}$	0		0	n.d.	0	$\mathbb{R}$
$S^{\varrho:01}$	0	1			$-\frac{1}{2}\frac{\mu}{N_{NN}}$	
	1	0				
$S^{\varrho:1}$	1				$\frac{V}{2}-\frac{\mu}{N_{NN}}$	
$SF^{\varrho:h}_{pd:0^\circ}$	$\frac{J+\frac{\mu}{N_{NN}}}{2J+V}$		$\frac{\left(J+\frac{\mu}{N_{NN}}\right)\left(J-\frac{\mu}{N_{NN}}+V\right)}{(2J+V)^2}$	0°	$-\frac{1}{2}\frac{\left(J+\frac{\mu}{N_{NN}}\right)^2}{2J+V}$	$0 \leq \frac{J+\frac{\mu}{N_{NN}}}{2J+V} \leq 1$
$SF^{\varrho:h}_{pd:180^\circ}$	$\frac{-J+\frac{\mu}{N_{NN}}}{-2J+V}$		$\frac{\left(-J+\frac{\mu}{N_{NN}}\right)\left(-J-\frac{\mu}{N_{NN}}+V\right)}{(-2J+V)^2}$	180°	$-\frac{1}{2}\frac{\left(-J+\frac{\mu}{N_{NN}}\right)^2}{-2J+V}$	$0 \leq \frac{-J+\frac{\mu}{N_{NN}}}{-2J+V} \leq 1$

11.2 Phase boundaries

11.2.1 Continuous transitions

The second order transitions are all included in (234)

$$J\frac{\eta}{N_{NN}} = V\frac{\nu_1}{N_{NN}} - \frac{\mu}{N_{NN}} \tag{280}$$

and (236)

$$-J\frac{\eta}{N_{NN}} = V\frac{\nu_1+\nu_2}{N_{NN}} - \frac{\mu}{N_{NN}}\,. \tag{281}$$

Since we don't have $S+SF$ mixed phases and thus $N_{\varrho=1}=0$ and $N_{\psi=0}=0$ for the superfluid states, ν_1 in (214) and ν_2 in (215) become simply

$$\nu_1 = \frac{N_{NN}-A}{N_{UCsites}-1}\, N_{\varrho=1}=0 \tag{282}$$

$$\nu_2 = N_{NN}-\frac{N_{NN}-A}{N_{UCsites}-1}\, N_{\psi=0}=N_{NN} \tag{283}$$

So the two classes of phase boundaries simplify to

$$J\frac{\eta}{N_{NN}} = -\frac{\mu}{N_{NN}} \tag{284}$$

and

$$-J\frac{\eta}{N_{NN}} = V-\frac{\mu}{N_{NN}}\,. \tag{285}$$

Now we just have to insert $\frac{\eta}{N_{NN}}$ for the two superfluid phases yielding four phase boundaries between a superfluid and a solid respectively.

$\frac{\eta}{N_{NN}}$	SF state	solid state	transition line
1	$SF^{\varrho:h}_{pd:0^\circ}$	$S^{\varrho:0}$	$J=-\frac{\mu}{N_{NN}}$
		$S^{\varrho:1}$	$-J=V-\frac{\mu}{N_{NN}}$
-1	$SF^{\varrho:h}_{pd:180^\circ}$	$S^{\varrho:0}$	$-J=-\frac{\mu}{N_{NN}}$
		$S^{\varrho:1}$	$J=V-\frac{\mu}{N_{NN}}$

11.2.2 Discontinuous transitions

The first-order transitions occur between the two superfluid states and the inhomogeneous solid. Since this happens, when the energies are the same, we set the energies of the superfluid states equal to the energy of the inhomogeneous solid to find the phase boundaries. Both yield the same result

$$\mathcal{E}\left[SF^{\varrho:h}_{pd:0^\circ}\right]=\mathcal{E}\left[S^{\varrho:01}\right] \quad , \quad \mathcal{E}\left[SF^{\varrho:h}_{pd:180^\circ}\right]=\mathcal{E}\left[S^{\varrho:01}\right] \tag{286}$$

$$\Downarrow \tag{287}$$

$$\left(\frac{J}{V}\right)^2+\left(\frac{\mu}{VN_{NN}}-\frac{1}{2}\right)^2 = \left(\frac{1}{2}\right)^2\,, \tag{288}$$

which describes a circle in the $\frac{J}{V}$-$\frac{\mu}{VN_{NN}}$ phase diagram. Its center lies at $\left(\frac{J}{V},\,\frac{\mu}{VN_{NN}}\right)=\left(0,\frac{1}{2}\right)$ and the radius is $\frac{1}{2}$. In the ground state the phase boundaries to $SF^{\varrho:h}_{pd:0^\circ}$ and $SF^{\varrho:h}_{pd:180^\circ}$ occur for $0<\frac{J}{V}$ and $\frac{J}{V}<0$, respectively. So in summery all first-order transitions for the non-frustrated lattices are

$\frac{\eta}{N_{NN}}$	SF state	solid state	transition line
1	$SF^{\varrho:h}_{pd:0^\circ}$	$S^{\varrho:01}$	$\left(\frac{J}{V}\right)^2+\left(\frac{\mu}{VN_{NN}}-\frac{1}{2}\right)^2=\left(\frac{1}{2}\right)^2,\ 0<\frac{J}{V}$
-1	$SF^{\varrho:h}_{pd:180^\circ}$		$\left(\frac{J}{V}\right)^2+\left(\frac{\mu}{VN_{NN}}-\frac{1}{2}\right)^2=\left(\frac{1}{2}\right)^2,\ \frac{J}{V}<0$

11.3 Phase diagram

Finally, the formulas for the phase boundaries enable us to plot the phase diagram for positive and negative hopping on non-frustrated lattices, see Fig. 32 and 33, which was one of the two major goals of this thesis. The other one is the phase diagram for frustrated lattices, which we will find in the next chapter. One example of non-frustrated lattices is the quadratic one. The spatial distributions of the particle density and the condensate density in this case are illustrated in Fig. 34 and 35 using the visualization method of section 0.1.

For positive hopping our obtained phase diagram is the same as in [2, 4]. So our general calculation method works for the well-known phases. The new phase appearing at negative hopping in the non-frustrated lattices is the alternating superfluid $SF^{o:h}_{pd:180^\circ}$.

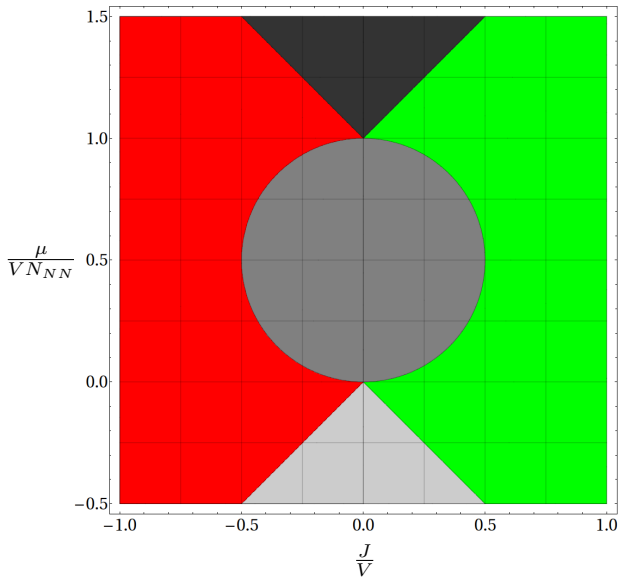

Figure 32: The final phase diagram for non-frustrated lattices. *Grayscales*: solid phases, *colored*: superfluid phases. *Light gray*: $S^{\varrho:0}$, *medium gray*: $S^{\varrho:01}$, *dark gray*: $S^{\varrho:1}$. *Green*: $SF^{\varrho:h}_{pd:0^\circ}$, *red*: $SF^{\varrho:h}_{pd:180^\circ}$.

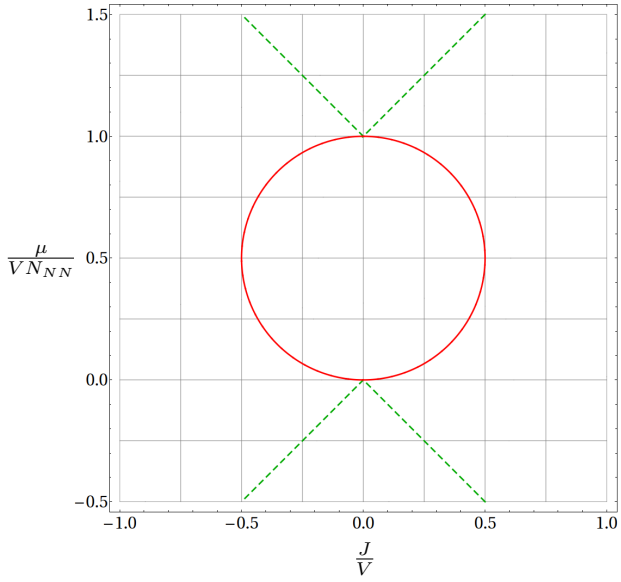

Figure 33: Phase boundaries for the non-frustrated lattices. *Green dotted*: continuous transition (second order transition), *red solid*: discontinuous transition (first order transition).

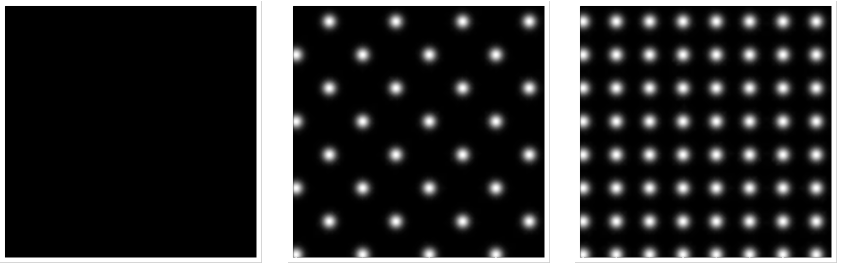

(a) $S^{\varrho:0}$ (b) $S^{\varrho:01}$ (c) $S^{\varrho:1}$

Figure 34: Spatial distributions of solids in the quadratic lattice for positive and negative hopping. **(a)** empty lattice, **(b)** checkerboard solid (alternating occupation numbers), **(c)** full lattice.

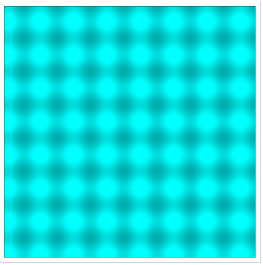

(a) $SF^{\varrho:h}_{pd:0^\circ}$

Figure 35: Spatial distribution of the only superfluid in the quadratic lattice for positive hopping. **(a)** homogeneous superfluid with 0° phase differences.

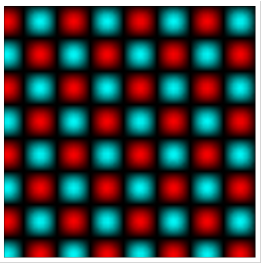

(a) $SF^{\varrho:h}_{pd:180^\circ}$

Figure 36: Spatial distribution of the only superfluid in the quadratic lattice for **negative hopping**. **(a)** density-homogeneous superfluid with 180° phase differences (alternating phases).

12 Frustrated lattices

In frustrated lattices an alternating pattern is per definition geometrically not possible, i.e. patterns with this symmetry can not appear in the ground state. These forbidden states are the half filled solid $S^{\varrho:01}$ and the alternating homogeneous superfluid $SF^{\varrho:h}_{pd:180^\circ}$ (see chapter 11). Since they are not allowed in this case, the question is, what patterns have the lowest energy now. The pattern described by

$$\frac{\mathcal{N}}{N_{NN}} = \begin{pmatrix} 0 & \frac{1}{2} & \frac{1}{2} \\ \frac{1}{2} & 0 & \frac{1}{2} \\ \frac{1}{2} & \frac{1}{2} & 0 \end{pmatrix} \tag{289}$$

is geometrically allowed on the triangular lattice ($N_{NN} = 6$) and the kagome lattice ($N_{NN} = 4$). As a special case of (193) the adjacency matrix (289) is determined by

$$A = 0 \quad , \qquad N = \frac{1}{2} N_{NN} \tag{290}$$

and the matrix size

$$N_{UCsites} = 3 \, . \tag{291}$$

Beyond the patterns described by this adjacency matrix, we have not found any other relevant one for positive or negative hopping. Another pattern we tested for the triangular lattice is a stripe pattern described by

$$\mathcal{N} = \begin{pmatrix} 2 & 4 \\ 4 & 2 \end{pmatrix} , \tag{292}$$

which means

$$A = 2 \quad , \qquad N = 4 \tag{293}$$

$$N_{UCsites} = 2 \, . \tag{294}$$

This pattern is also included in the calculation method and results of section 10.3, but doesn't appear in the ground state. So the further calculations describe just patterns included in (289).

12.1 Phases

12.1.1 Solids

As in the case of the non-frustrated lattice, we can use eq. (239) for the solid phases inserting $A = 0$ and $N_{UCsites} = 3$

$$\mathcal{E}\left[S\right] = \mathcal{E}^S\left[S\right] = \frac{1}{6} N_{\varrho=1} \left(N_{\varrho=1} - 1\right) \frac{V}{2} - \frac{1}{3} N_{\varrho=1} \frac{\mu}{N_{NN}} \, . \tag{295}$$

Since we have three sites in the unit cell, $N_{\varrho=1}$ can be chosen as

$$N_{\varrho=1} \in \{0, 1, 2, 3\} \, , \tag{296}$$

yielding all properties of all solid phases:

phase	$N_{\varrho=1}$	ϱ_A	ϱ_B	ϱ_C	$\psi_A=\psi_B=\psi_C$	$\mathcal{E}$ [phase]	domain of J,μ,V
$S^{\varrho:0}$	0	0			0	0	$\mathbb{R}$
$S^{\varrho:001}$	1	0	0	1		$-\frac{1}{3}\frac{\mu}{N_{NN}}$	
		0	1	0			
		1	0	0			
$S^{\varrho:011}$	2	1	1	0		$\frac{1}{3}\ \frac{V}{2}-\frac{2}{3}\frac{\mu}{N_{NN}}$	
		1	0	1			
		0	1	1			
$S^{\varrho:1}$	3	1				$\frac{V}{2}-\frac{\mu}{N_{NN}}$	

So here we have found four solids, the homogeneous solids, empty lattice $S^{\varrho:0}$ and full lattice $S^{\varrho:1}$, and the two inhomogeneous solids, the 1/3 filled solid $S^{\varrho:001}$ and the 2/3 solid $S^{\varrho:011}$.

12.1.2 Density- and phase-homogeneous superfluid

As mentioned before, the formulas in sections 10.2.2 and 10.3.4.1 for the density- and phase-homogeneous superfluid are the same for all lattices, i.e. (245), (246), and (247)

$$\mathcal{E}\left[SF^{\varrho:h}_{pd:0^\circ}\right] = -\frac{1}{2}\frac{\left(J+\frac{\mu}{N_{NN}}\right)^2}{2J+V}\,, \tag{297}$$

$$\varrho = \frac{J+\frac{\mu}{N_{NN}}}{2J+V}\,, \tag{298}$$

$$|\psi|^2 = \frac{\left(J+\frac{\mu}{N_{NN}}\right)\left(J+V-\frac{\mu}{N_{NN}}\right)}{(2J+V)^2}\,, \tag{299}$$

$$\varphi_A = \varphi_B = \varphi_C\,. \tag{300}$$

The only difference between two different lattices can be the number of next neighbors N_{NN}, which corresponds to a scaling of the μ axis.

12.1.3 Density-homogeneous and phase-inhomogeneous superfluid

The density-homogeneous superfluid with phase differences unequal 0° is more interesting, since it differs from the corresponding phase in the non-frustrated lattices. Here $\frac{\eta}{N_{NN}}$ is not -1, which influences the J-dependence in a way, that we don't get an energy, that is simply the energy of $SF^{\varrho:h}_{pd:0^\circ}$ mirrored in J-direction. This is the reason, why the phase diagram will not be symmetric to the $\frac{\mu}{VN_{NN}}$-axis. Using

$$A=0 \quad , \quad N_{UCsites}=3 \tag{301}$$

$$\frac{\eta}{N_{NN}} = \frac{A}{N_{NN}}-\frac{1-\frac{A}{N_{NN}}}{N_{UCsites}-1}=-\frac{1}{2}\,, \tag{302}$$

we determine the properties of this phase by the formulas (249), (250), and (251)

$$\mathcal{E}\left[SF^{\varrho:h}_{pd:120^\circ}\right] = -\frac{1}{2}\frac{\left(-\frac{1}{2}J+\frac{\mu}{N_{NN}}\right)^2}{-J+V} \tag{303}$$

$$\varrho = \frac{-\frac{1}{2}J + \frac{\mu}{N_{NN}}}{-J+V} \tag{304}$$

$$|\psi|^2 = \frac{\left(-\frac{1}{2}J + \frac{\mu}{N_{NN}}\right)\left(-\frac{1}{2}J + V - \frac{\mu}{N_{NN}}\right)}{(-J+V)^2} \,. \tag{305}$$

And the condition 252

$$e^{i\varphi_A} + e^{i\varphi_B} + e^{i\varphi_C} = 0 \tag{306}$$

can just be fulfilled by phase differences of 120°.

12.1.4 Solids coexisting with density-homogeneous superfluids

The next interesting phases are combinations of solid sites and superfluid sites. The mathematical reason, why this is possible, is that the 3×3 matrix

$$\frac{\mathcal{N}}{N_{NN}} = \begin{pmatrix} 0 & \frac{1}{2} & \frac{1}{2} \\ \frac{1}{2} & 0 & \frac{1}{2} \\ \frac{1}{2} & \frac{1}{2} & 0 \end{pmatrix} \tag{307}$$

can be divided into the matrixes

$$\frac{\mathcal{N}^S}{N_{NN}} = \begin{pmatrix} 0 \end{pmatrix} \tag{308}$$

$$\frac{\mathcal{N}^{mix}}{N_{NN}} = \begin{pmatrix} \frac{1}{2} & \frac{1}{2} \end{pmatrix} \tag{309}$$

$$\frac{\mathcal{N}^{SF}}{N_{NN}} = \begin{pmatrix} 0 & \frac{1}{2} \\ \frac{1}{2} & 0 \end{pmatrix} \tag{310}$$

by the ansatz, that one ϱ_X is $\in \{0,1\}$, i.e. it describes a solid site. The others are chosen to be superfluid in this ansatz. The only entry in $\frac{\mathcal{N}^S}{N_{NN}}$ is 0. But this does not mean, that there are no solutions. It just means, that there is no connection between solid sites, which could have an influence on the energy. The matrix $\frac{\mathcal{N}^{mix}}{N_{NN}}$ describes the connections between solid and superfluid sites and the entries are not 0 and thus have an effect on the energy. And finally the matrix $\frac{\mathcal{N}^{SF}}{N_{NN}}$ describes connections between superfluid sites. The entries are not all 0 and thus a delocalization via the corresponding lattice sites is possible within this ansatz. In the example of the triangular lattice this disassembly of the matrix divides the triangular spatial symmetry into a superfluid honeycomb part and a part for solid sites in the middle of the honeycomb hexagons.

The important formulas for the mixture of a density-homogeneous superfluid and a solid have been derived in section 10.3.2. Two different η occur for these phases. Using

$$A = 0, \qquad N_{\psi=0} = 1, \qquad N_{UCsites} = 3 \tag{311}$$

and (197) and inserting it into the expressions for η in (207) yields

$$\frac{\eta}{N_{NN}} \in \left\{-\frac{1}{2}, \frac{1}{2}\right\} \,. \tag{312}$$

According to (224) the positive η corresponds to a phase with 0° phase differences in the superfluid and according to (225) the negative η corresponds to 180°, since both solutions fulfill the matrix equation (147)

$$\begin{pmatrix} 0 & \frac{1}{2} \\ \frac{1}{2} & 0 \end{pmatrix} \begin{pmatrix} \left|\psi^{SF}\right| e^{i\varphi_{X_1}} \\ \left|\psi^{SF}\right| e^{i\varphi_{X_2}} \end{pmatrix} = \frac{\eta}{N_{NN}} \begin{pmatrix} \left|\psi^{SF}\right| e^{i\varphi_{X_1}} \\ \left|\psi^{SF}\right| e^{i\varphi_{X_2}} \end{pmatrix} \tag{313}$$

$$\begin{pmatrix} 0 & \frac{1}{2} \\ \frac{1}{2} & 0 \end{pmatrix} \begin{pmatrix} e^{i\varphi_{X_1}} \\ e^{i\varphi_{X_2}} \end{pmatrix} = \pm\frac{1}{2} \begin{pmatrix} e^{i\varphi_{X_1}} \\ e^{i\varphi_{X_2}} \end{pmatrix} \tag{314}$$

Since we have a $S + SF$ mixed phase, we have to use the complete energy formula (232)

$$\mathcal{E}\left[SF^{\varrho:h} + S\right] = \mathcal{E}^{S}\left[SF^{\varrho:h} + S\right] + \mathcal{E}^{mix}\left[SF^{\varrho:h} + S\right] + \mathcal{E}^{SF}\left[SF^{\varrho:h} + S\right] \tag{315}$$

with the respective energy contributions

$$\mathcal{E}^{S}\left[SF^{\varrho:h} + S\right] N_{NN} N_{UCsites} = \frac{V}{2} N_{\varrho=1} \left(A + N\left(N_{\varrho=1} - 1\right)\right) - N_{\varrho=1}\mu \,, \tag{316}$$

$$\mathcal{E}^{mix}\left[SF^{\varrho:h} + S\right] N_{NN} N_{UCsites} = \frac{V}{2} N \, N_{\varrho=1} N_{\psi\neq 0} \frac{J\eta + \mu - V\nu_1}{2J\eta + V\nu_2} \,, \tag{317}$$

$$\mathcal{E}^{SF}\left[SF^{\varrho:h} + S\right] N_{NN} N_{UCsites} = -\frac{1}{2} \frac{\left(J\eta + \mu - V\nu_1\right)\left(J\eta + \mu\right)}{2J\eta + V\nu_2} \,. \tag{318}$$

And using

$$A = 0, \qquad N = \tfrac{1}{2} N_{NN}, \qquad N_{UCsites} = 3$$

$$N_{\psi=0} = 1, \qquad N_{\psi\neq 0} = 2$$

$$\nu_1 = \frac{1}{2} N_{NN} N_{\varrho=1} \tag{319}$$

$$\nu_2 = \frac{N_{NN}}{2} \tag{320}$$

yields

$$\mathcal{E}^{S}\left[SF^{\varrho:h} + S\right] = \frac{1}{6}\frac{V}{2} \, N_{\varrho=1}\left(N_{\varrho=1} - 1\right) - \frac{N_{\varrho=1}}{3}\frac{\mu}{N_{NN}} \,, \tag{321}$$

$$\mathcal{E}^{mix}\left[SF^{\varrho:h} + S\right] = \frac{1}{3}\frac{V}{2} \, N_{\varrho=1} \frac{J\frac{\eta}{N_{NN}} + \frac{\mu}{N_{NN}} - \frac{1}{2}VN_{\varrho=1}}{2J\frac{\eta}{N_{NN}} + \frac{1}{2}V} \,, \tag{322}$$

$$\mathcal{E}^{SF}\left[SF^{\varrho:h} + S\right] = -\frac{1}{3} \frac{\left(J\frac{\eta}{N_{NN}} + \frac{\mu}{N_{NN}} - \frac{1}{2}VN_{\varrho=1}\right)\left(J\frac{\eta}{N_{NN}} + \frac{\mu}{N_{NN}}\right)}{2J\frac{\eta}{N_{NN}} + \frac{1}{2}V} \,. \tag{323}$$

Now we can insert $\frac{\eta}{N_{NN}} \in \left\{-\frac{1}{2}, \frac{1}{2}\right\}$ by expressing it as $\frac{\eta}{N_{NN}} = \pm\frac{1}{2}$

$$\mathcal{E}^{S}\left[SF^{\varrho:h} + S\right] = \frac{1}{6}\frac{V}{2} \, N_{\varrho=1}\left(N_{\varrho=1} - 1\right) - \frac{N_{\varrho=1}}{3}\frac{\mu}{N_{NN}} \,, \tag{324}$$

$$\mathcal{E}^{mix}\left[SF^{\varrho:h} + S\right] = \frac{1}{3}\frac{V}{2} \, N_{\varrho=1} \frac{\pm\frac{1}{2}J + \frac{\mu}{N_{NN}} - \frac{1}{2}VN_{\varrho=1}}{\pm J + \frac{1}{2}V} \,, \tag{325}$$

$$\mathcal{E}^{SF}\left[SF^{\varrho:h} + S\right] = -\frac{1}{3} \frac{\left(\pm\frac{1}{2}J + \frac{\mu}{N_{NN}} - \frac{1}{2}VN_{\varrho=1}\right)\left(\pm\frac{1}{2}J + \frac{\mu}{N_{NN}}\right)}{\pm J + \frac{1}{2}V} \,. \tag{326}$$

And in the last step we use

$$N_{\varrho=1} \quad \in \quad \{0,1\} \ , \tag{327}$$

which leads to the final energy expressions for four phases

phase	$\frac{\eta}{N_{NN}}$	$N_{\varrho=1}$	$\mathcal{E}^S$ [phase] $+\mathcal{E}^{mix}$ [phase] $+\mathcal{E}^{SF}$ [phase]
$SF^{\varrho:h}_{pd:0^\circ} + S^{\varrho:0}$	$\frac{1}{2}$	0	$-\frac{1}{3}\frac{\left(\frac{1}{2}J+\frac{\mu}{N_{NN}}\right)^2}{J+\frac{1}{2}V}$
$SF^{\varrho:h}_{pd:0^\circ} + S^{\varrho:1}$		1	$-\frac{1}{3}\frac{\mu}{N_{NN}}$ $+\frac{1}{3}\frac{V}{2}\ \frac{\frac{1}{2}J+\frac{\mu}{N_{NN}}-\frac{1}{2}V}{J+\frac{1}{2}V}$ $-\frac{1}{3}\frac{\left(\frac{1}{2}J+\frac{\mu}{N_{NN}}-\frac{1}{2}V\right)\left(\frac{1}{2}J+\frac{\mu}{N_{NN}}\right)}{J+\frac{1}{2}V}$
$SF^{\varrho:h}_{pd:180^\circ} + S^{\varrho:0}$	$-\frac{1}{2}$	0	$-\frac{1}{3}\frac{\left(-\frac{1}{2}J+\frac{\mu}{N_{NN}}\right)^2}{-J+\frac{1}{2}V}$
$SF^{\varrho:h}_{pd:180^\circ} + S^{\varrho:1}$		1	$-\frac{1}{3}\frac{\mu}{N_{NN}}$ $+\frac{1}{3}\frac{V}{2}\ \frac{-\frac{1}{2}J+\frac{\mu}{N_{NN}}-\frac{1}{2}V}{-J+\frac{1}{2}V}$ $-\frac{1}{3}\frac{\left(-\frac{1}{2}J+\frac{\mu}{N_{NN}}-\frac{1}{2}V\right)\left(-\frac{1}{2}J+\frac{\mu}{N_{NN}}\right)}{-J+\frac{1}{2}V}$

For the density ϱ^{SF} we need the formula (216)

$$\varrho^{SF} \quad = \quad \frac{J\frac{\eta}{N_{NN}}+\frac{\mu}{N_{NN}}-V\frac{\nu_1}{N_{NN}}}{2J\frac{\eta}{N_{NN}}+V\frac{\nu_2}{N_{NN}}} \tag{328}$$

and for $\left|\psi^{SF}\right|$ the formula (218)

$$\left|\psi^{SF}\right|^2 \quad = \quad \frac{\left(J\frac{\eta}{N_{NN}}+\frac{\mu}{N_{NN}}-V\frac{\nu_1}{N_{NN}}\right)\left(J\frac{\eta}{N_{NN}}-\frac{\mu}{N_{NN}}+V\frac{\nu_1+\nu_2}{N_{NN}}\right)}{\left(2J\frac{\eta}{N_{NN}}+V\frac{\nu_2}{N_{NN}}\right)^2} \ . \tag{329}$$

All parameters are already determined by now

$$\frac{\eta}{N_{NN}} \quad = \quad \pm\frac{1}{2} \tag{330}$$

$$\frac{\nu_1}{N_{NN}} \quad = \quad \frac{1}{2}N_{\varrho=1} \tag{331}$$

$$\frac{\nu_2}{N_{NN}} \quad = \quad \frac{1}{2} \tag{332}$$

and so we find

$$\varrho^{SF} \quad = \quad \frac{\pm\frac{1}{2}J+\frac{\mu}{N_{NN}}-\frac{1}{2}VN_{\varrho=1}}{\pm J+\frac{1}{2}V} \ , \tag{333}$$

$$\left|\psi^{SF}\right|^2 \quad = \quad \frac{\left(\pm\frac{1}{2}J+\frac{\mu}{N_{NN}}-\frac{1}{2}VN_{\varrho=1}\right)\left(\pm\frac{1}{2}J-\frac{\mu}{N_{NN}}+V\left(\frac{1}{2}N_{\varrho=1}+\frac{1}{2}\right)\right)}{\left(\pm J+\frac{1}{2}V\right)^2} \ . \tag{334}$$

So now we can express the final densities of the following four phases

phase	$\frac{\eta}{N_{NN}}$	$N_{\varrho=1}$	ϱ^{SF}	domain of J,μ,V
$SF^{\varrho:h}_{pd:0^\circ} + S^{\varrho:0}$	$\frac{1}{2}$	0	$\frac{\frac{1}{2}J+\frac{\mu}{N_{NN}}}{J+\frac{1}{2}V}$	$0 \leq \frac{\frac{1}{2}J+\frac{\mu}{N_{NN}}}{J+\frac{1}{2}V} \leq 1$
$SF^{\varrho:h}_{pd:0^\circ} + S^{\varrho:1}$		1	$\frac{\frac{1}{2}J+\frac{\mu}{N_{NN}}-\frac{1}{2}V}{J+\frac{1}{2}V}$	$0 \leq \frac{\frac{1}{2}J+\frac{\mu}{N_{NN}}-\frac{1}{2}V}{J+\frac{1}{2}V} \leq 1$
$SF^{\varrho:h}_{pd:180^\circ} + S^{\varrho:0}$	$-\frac{1}{2}$	0	$\frac{-\frac{1}{2}J+\frac{\mu}{N_{NN}}}{-J+\frac{1}{2}V}$	$0 \leq \frac{-\frac{1}{2}J+\frac{\mu}{N_{NN}}}{-J+\frac{1}{2}V} \leq 1$
$SF^{\varrho:h}_{pd:180^\circ} + S^{\varrho:1}$		1	$\frac{-\frac{1}{2}J+\frac{\mu}{N_{NN}}-\frac{1}{2}V}{-J+\frac{1}{2}V}$	$0 \leq \frac{-\frac{1}{2}J+\frac{\mu}{N_{NN}}-\frac{1}{2}V}{-J+\frac{1}{2}V} \leq 1$

as well as the condensate densities

phase	$\frac{\eta}{N_{NN}}$	$N_{\varrho=1}$	$\left\|\psi^{SF}\right\|^2$	domain of J,μ,V
$SF^{\varrho:h}_{pd:0^\circ} + S^{\varrho:0}$	$\frac{1}{2}$	0	$\frac{\left(\frac{1}{2}J+\frac{\mu}{N_{NN}}\right)\left(\frac{1}{2}J-\frac{\mu}{N_{NN}}+\frac{1}{2}V\right)}{\left(J+\frac{1}{2}V\right)^2}$	$0 \leq \frac{\frac{1}{2}J+\frac{\mu}{N_{NN}}}{J+\frac{1}{2}V} \leq 1$
$SF^{\varrho:h}_{pd:0^\circ} + S^{\varrho:1}$		1	$\frac{\left(\frac{1}{2}J+\frac{\mu}{N_{NN}}-\frac{1}{2}V\right)\left(\frac{1}{2}J-\frac{\mu}{N_{NN}}+V\right)}{\left(J+\frac{1}{2}V\right)^2}$	$0 \leq \frac{\frac{1}{2}J+\frac{\mu}{N_{NN}}-\frac{1}{2}V}{J+\frac{1}{2}V} \leq 1$
$SF^{\varrho:h}_{pd:180^\circ} + S^{\varrho:0}$	$-\frac{1}{2}$	0	$\frac{\left(-\frac{1}{2}J+\frac{\mu}{N_{NN}}\right)\left(-\frac{1}{2}J-\frac{\mu}{N_{NN}}+\frac{1}{2}V\right)}{\left(-J+\frac{1}{2}V\right)^2}$	$0 \leq \frac{-\frac{1}{2}J+\frac{\mu}{N_{NN}}}{-J+\frac{1}{2}V} \leq 1$
$SF^{\varrho:h}_{pd:180^\circ} + S^{\varrho:1}$		1	$\frac{\left(-\frac{1}{2}J+\frac{\mu}{N_{NN}}-\frac{1}{2}V\right)\left(-\frac{1}{2}J-\frac{\mu}{N_{NN}}+V\right)}{\left(-J+\frac{1}{2}V\right)^2}$	$0 \leq \frac{-\frac{1}{2}J+\frac{\mu}{N_{NN}}-\frac{1}{2}V}{-J+\frac{1}{2}V} \leq 1$

Although the energies for these four states can be calculated, the two $SF^{\varrho:h}_{pd:0^\circ} + S$ phases will not appear in the ground state, because other energies are lower for the whole phase diagram, as we will see later. So we will just find the $SF^{\varrho:h}_{pd:180^\circ} + S$ phases with alternating phases in the superfluid part. For the triangular lattice this is an alternating honeycomb superfluid with an empty site or one localized boson in the center of the honeycomb hexagons.

12.1.5 Density-inhomogeneous superfluids

The other interesting class of phases are those with $\exists X,Y\ \eta_X \neq \eta_Y$ yielding $\exists X,Y\ \varrho_X^{SF} \neq \varrho_Y^{SF}$ and $\exists X,Y\ \left|\psi_X^{SF}\right| \neq \left|\psi_Y^{SF}\right|$. This means, that we can't use the simplifications of section 10.3.2 any more. As already described in section 10.3.5, we have used a computer to find the solutions for the ground state, including particle densities $\varrho_A = \varrho_B$ and ϱ_C, condensate densities $\psi_A = \psi_B$ and ψ_C as well as phase boundaries. But only the functions determining the phase boundaries have a simple form. The other values can not be written down here explicitly.

12.1.6 Summary

In order to have an overview over all properties of the phases, we summarize them in table 1 not including the domain of J,μ,V due to the lack of space, but it is not necessary, since it is always determined by the condition $0 \leq \varrho_X \leq 1$.

12.2 Phase boundaries

12.2.1 Continuous transitions

The second-order phase transitions for density-homogeneous phases, i.e. $\eta_X = \eta$, are all included in (234)

$$J\frac{\eta}{N_{NN}} = V\frac{\nu_1}{N_{NN}} - \frac{\mu}{N_{NN}} \tag{335}$$

phase	$\varrho_A = \varrho_B$	ϱ_C	$\lvert\psi_A\rvert^2 = \lvert\psi_B\rvert^2$	$\lvert\psi_C\rvert^2$	$\varphi_{BC}, \varphi_{CA}$	φ_{AB}	$\mathcal{E}$ [phase]
$S^{\varrho:0}$	0		0	0	n.d.	n.d.	0
$S^{\varrho:001}$	0	1					$-\frac{1}{3}\frac{\mu}{N_{NN}}$
$S^{\varrho:011}$	1	0					$\frac{1}{3}\frac{V}{2} - \frac{2}{3}\frac{\mu}{N_{NN}}$
$S^{\varrho:1}$	1						$\frac{V}{2} - \frac{\mu}{N_{NN}}$
$SF^{\varrho:h}_{pd:0^\circ}$	$\frac{J+\frac{\mu}{N_{NN}}}{2J+V}$		$\frac{\left(J+\frac{\mu}{N_{NN}}\right)\left(J+V-\frac{\mu}{N_{NN}}\right)}{(2J+V)^2}$		0°		$-\frac{1}{2}\frac{\left(J+\frac{\mu}{N_{NN}}\right)^2}{2J+V}$
$SF^{\varrho:h}_{pd:120^\circ}$	$\frac{-\frac{1}{2}J+\frac{\mu}{N_{NN}}}{-J+V}$		$\frac{\left(-\frac{1}{2}J+\frac{\mu}{N_{NN}}\right)\left(-\frac{1}{2}J+V-\frac{\mu}{N_{NN}}\right)}{(-J+V)^2}$		120°		$-\frac{1}{2}\frac{\left(-\frac{1}{2}J+\frac{\mu}{N_{NN}}\right)^2}{-J+V}$
$SF^{\varrho:ih}_{pd:0^\circ}$	n.s.	n.s.	n.s.	n.s.	0°		n.s.
$SF^{\varrho:ih}_{pd:0^\circ,180^\circ}$	n.s.	n.s.	n.s.	n.s.	180°	0°	n.s.
$SF^{\varrho:h}_{pd:180^\circ} + S^{\varrho:0}$	$\frac{-\frac{1}{2}J+\frac{\mu}{N_{NN}}}{-J+\frac{1}{2}V}$	0	$\frac{\left(-\frac{1}{2}J+\frac{\mu}{N_{NN}}\right)\left(-\frac{1}{2}J-\frac{\mu}{N_{NN}}+\frac{1}{2}V\right)}{\left(-J+\frac{1}{2}V\right)^2}$	0	n.d.	180°	$-\frac{1}{3}\frac{\left(-\frac{1}{2}J+\frac{\mu}{N_{NN}}\right)^2}{-J+\frac{1}{2}V}$
$SF^{\varrho:h}_{pd:180^\circ} + S^{\varrho:1}$	$\frac{-\frac{1}{2}J+\frac{\mu}{N_{NN}}-\frac{1}{2}V}{-J+\frac{1}{2}V}$	1	$\frac{\left(-\frac{1}{2}J+\frac{\mu}{N_{NN}}-\frac{1}{2}V\right)\left(-\frac{1}{2}J-\frac{\mu}{N_{NN}}+V\right)}{\left(-J+\frac{1}{2}V\right)^2}$	0	n.d.	180°	$-\frac{1}{3}\frac{\mu}{N_{NN}}$ $+\frac{1}{3}\frac{V}{2}\frac{-\frac{1}{2}J+\frac{\mu}{N_{NN}}-\frac{1}{2}V}{-J+\frac{1}{2}V}$ $-\frac{1}{3}\frac{\left(-\frac{1}{2}J+\frac{\mu}{N_{NN}}-\frac{1}{2}V\right)\left(-\frac{1}{2}J+\frac{\mu}{N_{NN}}\right)}{-J+\frac{1}{2}V}$

Table 1: Summary for all phases in the frustrated lattices, φ_{XY} is the complex phase difference between lattice site X and Y. "n.d.": "not defined" (complex phase not defined due to a zero absolute value), "n.s.": "not simple" (no simple formula found).

and (236)

$$-J\frac{\eta}{N_{NN}} = V\frac{\nu_1+\nu_2}{N_{NN}} - \frac{\mu}{N_{NN}}\,, \tag{336}$$

which are the same formulas, we used for the non-frustrated lattices. But now we also have $S+SF$ mixed phases, so that ν_1 in (214) and ν_2 in (215)

$$\nu_1 = \frac{1}{2}N_{NN}\,N_{\varrho=1} \tag{337}$$

$$\nu_2 = N_{NN}\left(1-\frac{1}{2}\,N_{\psi=0}\right) \tag{338}$$

have different values for different states. This yields the following transition lines

$N_{\psi=0}$	$N_{\varrho=1}$	$\frac{\eta}{N_{NN}}$	$\frac{\nu_1}{N_{NN}}$	$\frac{\nu_2}{N_{NN}}$	SF state	solid state	transition line
0	0	1	0	1	$SF^{\varrho:h}_{pd:0^\circ}$	$S^{\varrho:0}$	$J=-\frac{\mu}{N_{NN}}$
						$S^{\varrho:1}$	$-J=V-\frac{\mu}{N_{NN}}$
		$-\frac{1}{2}$			$SF^{\varrho:h}_{pd:120^\circ}$	$S^{\varrho:0}$	$-\frac{1}{2}J=-\frac{\mu}{N_{NN}}$
						$S^{\varrho:1}$	$\frac{1}{2}J=V-\frac{\mu}{N_{NN}}$
1	0	$-\frac{1}{2}$	0	$\frac{1}{2}$	$SF^{\varrho:h}_{pd:180^\circ}+S^{\varrho:0}$	$S^{\varrho:0}$	not in ground state
						$S^{\varrho:011}$	$\frac{1}{2}J=\frac{1}{2}V-\frac{\mu}{N_{NN}}$
	1		$\frac{1}{2}$		$SF^{\varrho:h}_{pd:180^\circ}+S^{\varrho:1}$	$S^{\varrho:001}$	$-\frac{1}{2}J=\frac{1}{2}V-\frac{\mu}{N_{NN}}$
						$S^{\varrho:1}$	not in ground state

For the inhomogeneous superfluids ($\exists X,Y\ \eta_X\neq\eta_Y$) there are also continuous transitions to solid phases. We have found them with the help of a computer as described in section 10.3.5. In summary the phase boundaries are

phase	phase	transition line
$SF^{\varrho:ih}_{pd:0^\circ}$	$S^{\varrho:001}$	$\left(2\frac{J}{V}+\frac{\mu}{VN_{NN}}\right)^2=\frac{\mu}{VN_{NN}}\left(4-7\frac{\mu}{VN_{NN}}\right)$
	$S^{\varrho:011}$	$\left(2\frac{J}{V}-\frac{\mu}{VN_{NN}}+1\right)^2=\frac{\mu}{VN_{NN}}\left(10-7\frac{\mu}{VN_{NN}}\right)-3$
$SF^{\varrho:ih}_{pd:0^\circ,180^\circ}$	$S^{\varrho:0}$	$-\frac{1}{2}J=-\frac{\mu}{N_{NN}}$
	$S^{\varrho:001}$	$\left(2\frac{J}{V}+\frac{\mu}{VN_{NN}}\right)^2=\frac{\mu}{VN_{NN}}\left(4-7\frac{\mu}{VN_{NN}}\right)$
	$S^{\varrho:011}$	$\left(2\frac{J}{V}-\frac{\mu}{VN_{NN}}+1\right)^2=\frac{\mu}{VN_{NN}}\left(10-7\frac{\mu}{VN_{NN}}\right)-3$
	$S^{\varrho:1}$	$\frac{1}{2}J=V-\frac{\mu}{N_{NN}}$

12.2.2 Discontinuous transitions

The discontinuous phases were again determined by setting the energies equal or by computer calculation, see section 10.3.5 for the transitions of $SF^{\varrho:ih}_{pd:0^\circ}$. The resulting transition lines are

phase	phase	transition line
$SF^{\varrho:h}_{pd:0^\circ}$	$S^{\varrho:001}$	$\left(-3\frac{J}{V}-\frac{\mu}{VN_{NN}}\right)^2=\frac{\mu}{VN_{NN}}\left(6-8\frac{\mu}{VN_{NN}}\right)$
	$S^{\varrho:011}$	$\left(-3\frac{J}{V}+\frac{\mu}{VN_{NN}}-1\right)^2=\frac{\mu}{VN_{NN}}\left(10-8\frac{\mu}{VN_{NN}}\right)-2$
	$SF^{\varrho:ih}_{pd:0^\circ}$	$\frac{J}{V}=\frac{1}{4}$
$SF^{\varrho:h}_{pd:120^\circ}$	$SF^{\varrho:ih}_{pd:0^\circ,180^\circ}$ (both)	$\frac{J}{V}=-\frac{1}{2}$
	$S^{\varrho:1}+SF^{\varrho:h}_{pd:180^\circ}$	
	$S^{\varrho:0}+SF^{\varrho:h}_{pd:180^\circ}$	
$S^{\varrho:0}+SF^{\varrho:h}_{pd:180^\circ}$	$S^{\varrho:1}+SF^{\varrho:h}_{pd:180^\circ}$	$\frac{\mu}{VN_{NN}}=\frac{1}{2}$
$SF^{\varrho:ih}_{pd:0^\circ}$ (within the phase)		

A special case is the discontinuity within $SF^{\varrho:ih}_{pd:0^\circ}$ (see section 10.3.5). This could be a reason to define different symbols for the two parts and call them different phases, but it seems to be overdone, so we don't do it.

12.3 Phase diagram

With these formulas for the phase boundaries, we can now visualize the phase diagram for positive and negative hopping in Fig. 37 and 38, which was the second major goal of this thesis. One example of the frustrated lattices is the triangular one. The spatial distributions of the particle density and the condensate density are illustrated in Figs. (39), (40), (41), and (42) using the visualization method of section 0.1.

For positive hopping our obtained phase diagram is the same as in [3]. So our general calculation method also works for the inhomogeneous superfluid. The new phases appearing at negative hopping in the frustrated lattices consist of a whole variety phases, whereas the non-frustrated lattices offer just one new. We have found a density-homogeneous superfluid with 120° phase differences, inhomogeneous superfluids with 0° and 180° phase differences at the same time as well as solids coexisting with density-homogeneous superfluids. The latter one comes closest to the supersolid phase in helium [9, 10] and thus a similar configuration, i.e. small negative hopping relative to the next neighbor interaction, could possibly serve as a quantum simulator for helium.

Numerical results were found for positive hopping in the triangular lattice in [22] via the CMF-10 method and in [8] via Monte Carlo simulations. Figure (43) shows these two numerical results for the phase diagram overlayed with ours. In both numerical calculations the regions in the phase diagram for the inhomogeneous solids are smaller than in our results, which could be caused by the inaccuracy of the mean-field approximation due to neclegted quantum fluctuations or it could be systematic problems of the numerical methods, e.g. due to the finite lattice size in a simulation. The discontinuous transition within the inhomogeneous superfluid at $\frac{\mu}{VN_{NN}}=\frac{1}{2}$ was also found in [22], without any recognizable difference to our result. As mentioned before, extending the Monte Carlo simulations to negative hopping is a major problem, but in the mean-field approach there is no such problem. The difficulties of the calculations are almost the same for both positive and negative hopping, which is especially regarding the inhomogeneous superfluid.

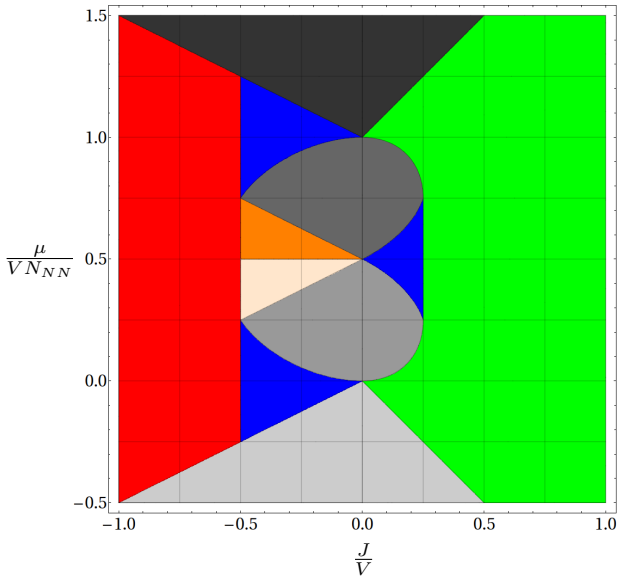

Figure 37: The final phase diagram for frustrated lattices. *Grayscales*: solid phases, *colored*: superfluid or mixed phases. *Lightest gray*: $S^{\varrho:0}$, *medium light gray*: $S^{\varrho:001}$, *medium dark gray*: $S^{\varrho:011}$, *dark gray*: $S^{\varrho:1}$. *Green*: $SF^{\varrho:h}_{pd:0°}$, *red*: $SF^{\varrho:h}_{pd:120°}$, *blue:* $SF^{\varrho:ih}_{pd:0°}$ and $SF^{\varrho:ih}_{pd:180°}$, *light orange:* $S^{\varrho:1} + SF^{\varrho:h}_{pd:180°}$, *dark orange:* $S^{\varrho:0} + SF^{\varrho:h}_{pd:180°}$.

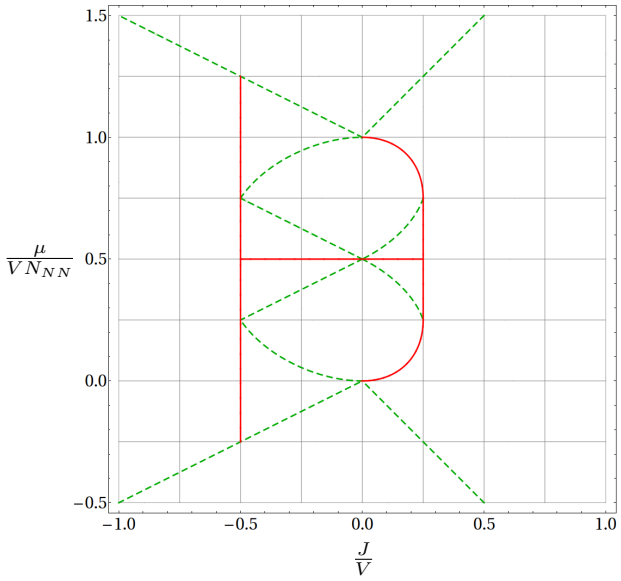

Figure 38: Phase boundaries for the frustrated lattices. *Green dotted*: continuous transition (second order transition), *red solid*: discontinuous transition (first order transition).

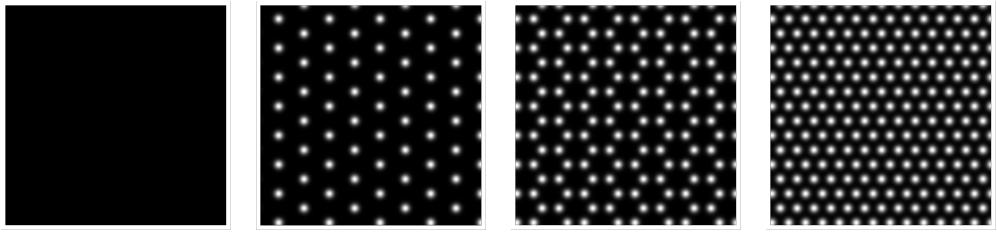

(a) $S^{\varrho:0}$ (b) $S^{\varrho:001}$ (c) $S^{\varrho:011}$ (d) $S^{\varrho:1}$

Figure 39: Spatial distributions of solids in the triangular lattice for positive and negative hopping. **(a)** empty lattice, **(b)** 1/3 filled solid, honeycomb empty sites, **(c)** 2/3 filled solid, honeycomb occupied sites, **(d)** full lattice.

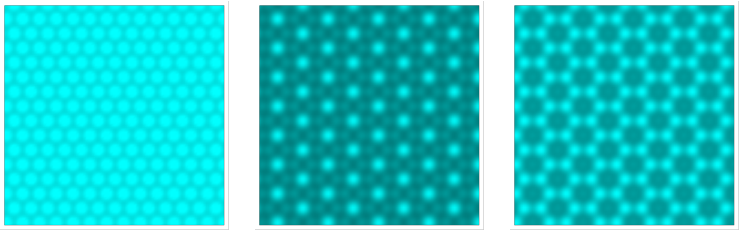

(a) $SF^{\varrho:h}_{pd:0^\circ}$ (b) $SF^{\varrho:ih}_{pd:0^\circ}$ (c) $SF^{\varrho:ih}_{pd:0^\circ}$

Figure 40: Spatial distributions of superfluids in the triangular lattice for positive hopping. **(a)** homogeneous superfluid, **(b)** inhomogeneous superfluid close to the 1/3 filled solid, **(c)** inhomogeneous superfluid close to the 2/3 filled solid.

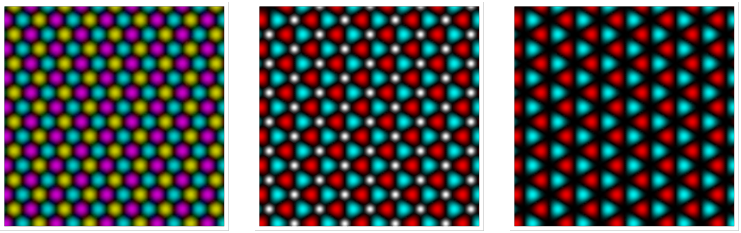

(a) $SF^{\varrho:h}_{pd:120^\circ}$ (b) $SF^{\varrho:h}_{pd:180^\circ} + S^{\varrho:1}$ (c) $SF^{\varrho:h}_{pd:180^\circ} + S^{\varrho:0}$

Figure 41: Spatial distributions of phases with density-homogeneous superfluids in the triangular lattice for **negative hopping**. **(a)** superfluid with 120° phase differences, **(b)** alternating honeycomb superfluid and occupied solid sites, **(c)** alternating honeycomb superfluid and empty sites.

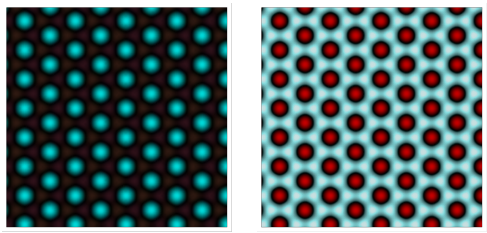

(a) $SF^{\varrho:ih}_{pd:0^\circ,180^\circ}$ (b) $SF^{\varrho:ih}_{pd:0^\circ,180^\circ}$

Figure 42: Spatial distributions of inhomogeneous superfluids in the triangular lattice for **negative hopping**. **(a)** between empty lattice and 1/3 filled lattice, **(b)** between 2/3 filled lattice and full lattice.

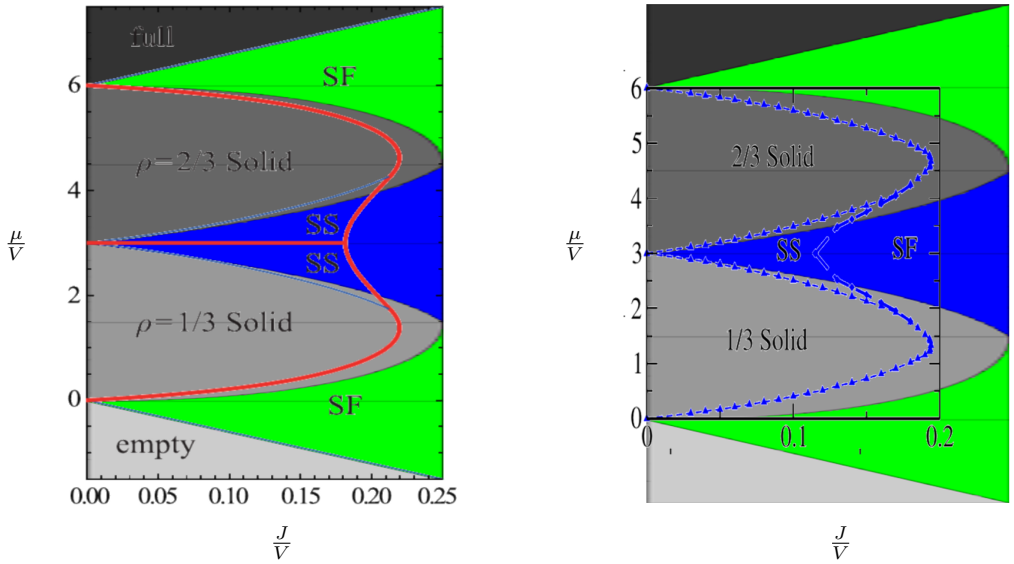

(a) CMF-10 (b) Monte Carlo

Figure 43: Phase diagram for the triangular lattice ($N_{NN} = 6$) for positive hopping from **(a)** a CMF-10 calculation [22] and **(b)** a Monte Carlo simulation [8] both overlayed with our results. *"empty", lightest gray*: $S^{\varrho:0}$, *"1/3 solid", medium light gray*: $S^{\varrho:001}$, *"2/3 solid", medium dark gray*: $S^{\varrho:011}$, *"full", dark gray*: $S^{\varrho:1}$, *"SF", green*: $SF^{\varrho:h}_{pd:0^\circ}$, *"SS", blue*: $SF^{\varrho:ih}_{pd:0^\circ}$. "SF" in (b) belongs to the $SF^{\varrho:h}_{pd:0^\circ}$ phase from the Monte Carlo calculation, not to the blue $SF^{\varrho:ih}_{pd:0^\circ}$ region from our results.

Part IV
Conclusion

13 Summary

In this thesis we developed a general calculation approach for periodic patterns within the mean-field approximation for hard-core dipolar bosons in optical lattices. Within this method we derived the particle densities and the condensate wave functions at the respective sites in the unit cell as well as the energies for all phases occurring for both positive and negative hopping. Most of the obtained expressions had a simple form except those for the inhomogeneous superfluids, where the analytically derived expressions had to be evaluated with the help of a computer due to their complex form . These results lead to the complete phase diagrams of non-frustrated and frustrated lattices for both positive and negative hopping in Figs. 32, 33 and Figs. 37, 38, respectively.

A major step was finding a general formula (78) for the energies depending on the mean-field parameters, which can easily be proven for one and two sites in the unit cell, and which we have proven for three sites with the help of a computer. For more complex patterns it should be possible to prove it with a computer, too.

Finding the mean-field parameters turned out to lead to some equations, see section 8.3.5, involving the new variables $\eta_X := \frac{\Psi_X}{\psi_X}$ (100), describing the relation between the condensate wave function ψ_X of a lattice site and the sum over the next neighboring ψ_X denoted by Ψ_X. This relation turned out to yield a real valued η_X and so the phase difference to the sum over the next neighboring ψ_X is always $0°$ or $180°$ yielding the sign of η_X. In all results for both the non-frustrated and frustrated lattices the $180°$ phase difference occurs just for negative hopping in the ground state. We haven't proven it, but it could be a general principle. Definitely related to this is the observation that η_X always occurs as a prefactor of J.

The definition of the η_X lead to the matrix equation (147), which becomes an eigenvalue equation for $\eta_X = \eta \; \forall X$ being valid for a lot of phases, see section 10.3.2. This is simplifying the mathematics significantly and especially for the quite general class of patterns, we investigated in section 10.3, it is including all patterns with $\eta_X = \eta \; \forall X$, which we needed later. Furthermore, the equations can be simplified to equations without matrix operations, which is a major advantage.

In the other cases, i.e. $\exists X, Y \; \eta_X \neq \eta_Y$, see section 10.3.5, we determined our results analytically, but with the help of a computer, yielding the inhomogeneous superfluids. Therefore, the derived energy $\mathcal{E}^{SF}$ in (178), which depends just on the parameters η_X, was combined with the determinant equation (107) and setting two η_X equal, which is justified by a computer calculation, where we have used all η_X without this simplification. Extremizing with respect to the remaining η_X was yielding all results for the inhomogeneous superfluids, which could not be expressed in a simple formula.

Another result, which is also from the general calculations, is the semi-circle law (143). It is valid for all lattice sites independently. One consequence of it is, that there is no delocalization at a lattice site, when the density is 0 or 1, i.e. $\varrho_X \in \{0, 1\}$ implies $\psi_X = 0$.

The total system energy (171) was divided into one energy concerning the solid sites (176), one concerning superfluid sites (178) and one concerning the influences between solid and superfluid sites (177). The sum of them yields the complete energy (171) and for the phases with just solid or just superfluid sites, just one of these energies have to be used, which is also a major advantage within the general derivations.

For the homogeneous pattern and the other class of patterns from section 10.3 described by the adjacency matrix (193) we have derived formulas, which are almost the final formulas for the special cases. Just a few constants have to be inserted, which are determined by considering a certain special case. This means, we have described a whole class of patterns almost completely, hence it could at least partially be applied to lattices we have not investigated in this thesis. E.g. the description of the homogeneous superfluid with $0°$ phase differences, see section 10.3, which was already derived in section 10.2, just depends on the number of next neighbors N_{NN} scaling the $\frac{\mu}{VN_{NN}}$-axis, but can within our approximations be applied to every lattice not directly dependent on the lattice geometry or number of dimensions, which is an important result due to its generality. One other example is, that for large negative hopping the complex phases of the ψ_X are at their maximum. For the non-frustrated lattices this yields phase differences of $180°$, see section 11.1.3, and for the frustrated lattices $120°$, see section

12.1.3.

To obtain the phase diagram, we compared all energies occurring for a certain pattern and determined the phase with the lowest energy for the different experimental conditions, which the phase diagram is representing. This lead to simple formulas for all phase boundaries of both kinds of considered lattices.

We have found the phase diagram for non-frustrated lattices shown in Figs. 32 and 33 or in other words for lattices, which geometrically allow an alternating pattern. This phase diagram is not directly restricted to a certain lattice geometry or number of dimensions. It is just restricted to the "not frustrated" property. E.g. a 1D, a quadratic, a cubic or a honeycomb lattice fulfill this condition and, thus, they have the same phase diagram within our approximations. The only difference would be a scaling of the $\frac{\mu}{V}$-axis by the factor N_{NN}, but we got rid of this factor by expressing everything in terms of $\frac{\mu}{VN_{NN}}$ in the phase diagram.

The phase boundaries of the non-frustrated lattices are mirror symmetrical to $\frac{J}{V} = 0$. The difference between positive and negative hopping are the phase differences in the superfluid, which are 0° for positive hopping and 180° for negative hopping corresponding to a positive and negative η, respectively, as mentioned before. The phase boundaries between the superfluid phases and the inhomogeneous solid simply form an ellipse or a circle in the right scaling of axes.

The phase boundaries of the frustrated lattices shown in Figs. 37 and 38 are not mirror symmetrical to $\frac{J}{V} = 0$. For positive hopping we have reproduced all phases and phase boundaries already determined in Ref. [3]. The most interesting phase, the inhomogeneous superfluid between the inhomogeneous solids and the homogeneous superfluid, always has 0° phase differences and consists of two parts divided by a discontinuity, i.e. a first order transition, at $\frac{\mu}{VN_{NN}} = \frac{1}{2}$. For negative hopping we have found an interesting variety of phases, which are a density-homogeneous superfluid with 120° phase differences, two inhomogeneous superfluids with 180° phase differences and a mixture of sites with localized bosons and other sites with superfluid bosons, hence a solid-superfluid mixture with 180° phase differences in the superfluid. This mixture is, what comes closest to the supersolid phase of helium [9, 11], and may be a hint or even a foundation to understand, how to construct and configure quantum simulators for helium in the supersolid phase.

In summary the general mean-field calculation, we developed, was successful. Especially the variables $\eta_X := \frac{\Psi_X}{\psi_X}$ express important properties of the phases and have an important role in the mathematical description. Furthermore, we determined the well-known results for positive hopping as well as a variety of interesting phases for negative hopping including inhomogeneous superfluids and solids coexisting with superfluids.

14 Outlook

This thesis is based on the idea to find the phase diagrams for negative hopping due to the sign problem using Monte Carlo simulations [8], so the following possible extensions are especially meant to be applied to negative hopping.

The Hamiltonian, we used, is relatively simple. It includes just next neighbor interactions, we used the hard-core limit and it is just valid, if the hopping J and the long range interaction V is the same for every connection between sites, which depends e.g. on possibly different depths of different potential valleys and different distances between the connection for next neighbors, 2nd next neighbors and so on. So the first idea for an extension, especially as far as possible in the general calculation method, is to include more than just the next neighbors, applying it for the soft-core case and using different hopping energies $J_{i,j}$ for different connections between sites i and j.

Since we just consider two-particle interactions another possible extension is to include three, four and so on particle interactions, which could presumably not be treated analytically.

Until now we have considered the temperature to be $T = 0$, so investigating the thermodynamical behavior of our systems is also a possibility.

We have investigated the non-frustrated and frustrated lattices until now. For the first one a pattern of two different types of sites is needed, for the second a pattern of 3 different types of sites. The nearby question is, if there could be a lattice, which needs 4 types of sites to describe the patterns in the next neighbor approximation. It may be possible, that this is the case in a sphere packing, since there are always four sites next to each other, which are all connected to all the other three, respectively. This geometrically forbids the 3 site pattern we had to use e.g. for the triangular lattice, since there are three sites next to each other, which are all connected to all other two, respectively. It may be possible, that this yields three inhomogeneous solids in the phase diagram.

The lattices we included in our calculation all have the same number of next neighbors for every site. Different N_{NN} for different lattice site could be included in the mathematics and experimentally realized using different laser frequencies for an optical lattice. Besides the implementation as a quantum simulator the mathematics could correspond to a physical system, which can not be observed very well, e.g. in solid states.

In Ref. [24] a variational method was used for bosons in optical lattices without long-range interaction. It has the mean-field result as a zeroth order solution and refines it in higher orders by including the impact of quantum fluctuations. This method applied to our system, i.e. including long-range interaction, is another possibility to extend our calculations.

References

[1] http://commons.wikimedia.org/wiki/File:HSV_cone.png

[2] I. Hen, M. Iskin, and M. Rigol: *Phase diagram of the hard-core Bose-Hubbard model on a checkerboard superlattice*. Phys. Rev. B **81**, 064503 (2010)

[3] G. Murthy, D. Arovas, and A. Auerbach: *Superfluids and supersolids on frustrated two-dimensional lattices*. Phys. Rev. B **55**, 3104 (1996)

[4] N. Gheeraert, S. Chester, M. May, S. Eggert, and A. Pelster: *Mean-field theory for extended Bose-Hubbard model with hard-core bosons*; in A. Pelster and G. Wunner (Editors), Proceedings of the International Symposium Selforganization in Complex Systems: The Past, Present, and Future of Synergetics; Hanse Institute of Advanced Studies, Delmenhorst (Germany), November 13 – 16, 2012; Springer (in preparation)

[5] R. Feynman: *Simulating Physics with Computers*. Int. J. Theor. Phys. **21**, 467 (1982)

[6] M. Greiner, O. Mandel, T. Esslinger, T. W. Hänsch, and I. Bloch: *Quantum phase transition from a superfluid to a Mott insulator in a gas of ultracold atoms*. Nature **415,** 39 (2002)

[7] J. K. Pachos and P. L. Knight: *Quantum Computation with a One-Dimensional Optical Lattice*. Phys. Rev. Lett. **91**, 107902 (2003)

[8] X.-F. Zhang, R. Dillenschneider, Y. Yu, and S. Eggert: *Supersolid phase transitions for hard-core bosons on a triangular lattice*. Phys. Rev. B **84**, 174515 (2011)

[9] E. Kim and M. H. W. Chan: *Probable observation of a supersolid helium phase*. Nature **427**, 225 (2004)

[10] D. Y. Kim and M. H. W. Chan: *Absence of Supersolidity in Solid Helium in Porous Vycor Glass*. Phys. Rev. Lett. **109**, 155301 (2012)

[11] X. Mi, J. D. Reppy: *In Pursuit of the Elusive Supersolid*. arXiv:1307.3805

[12] A. Eckardt, C. Weiss, and M. Holthaus: *Superfluid-Insulator Transition in a Periodically Driven Optical Lattice*. Phys. Rev. Lett. **95**, 260404 (2005)

[13] A. Eckardt, P. Hauke, P. Soltan-Panahi, C. Becker, K. Sengstock, and M. Lewenstein: *Frustrated quantum antiferromagnetism with ultracold bosons in a triangular lattice*. Eur. Phys. Lett. **89**, 10010 (2010)

[14] A. Zenesini, H. Lignier, D. Ciampini, O. Morsch, and E. Arimondo: *Coherent Control of Dressed Matter Waves*. Phys. Rev. Lett. **102**, 100403 (2009)

[15] T. Matsubara and H. Matsuda: *A Lattice Model of Liquid Helium, I*. Prog. Theor. Phys. **16**, 569 (1956)

[16] I. Bloch: *Ultracold quantum gases in optical lattices*, Nature Phys. **1**, 23 (2005)

[17] G.-B. Jo, J. Guzman, C. K. Thomas, P. Hosur, A. Vishwanath, and D. M. Stamper-Kurn: *Ultracold Atoms in a Tunable Optical Kagome Lattice.* Phys. Rev. Lett. **108**, 045305 (2012)

[18] C. Chin, R. Grimm, P. Julienne, and E. Tiesinga: *Feshbach resonances in ultracold gases*. Rev. Mod. Phys. **82**, 1225 (2010)

[19] J. Cai, A. Retzker, F. Jelezko, and M. B. Plenio: *A large-scale quantum simulator on a diamond surface at room temperature.* Nature Phys. **9**, 168 (2013)

[20] http://en.wikipedia.org/wiki/File:MOT_setup.png

[21] J. M. Kurdestany, R. V. Pai, and R. Pandit: *The inhomogeneous extended Bose-Hubbard model: Mean-Field theory.* Ann. Phys. (Berlin) **524**, 234 (2012)

[22] D. Yamamoto, I. Danshita, and C. A. R. Sá de Melo: *Dipolar bosons in triangular optical lattices: Quantum phase transitions and anomalous hysteresis.* Phys. Rev. A **85**, 021601 (2012)

[23] T. Susuki, N. Kurita, T. Tanaka, H. Nojiri, A. Matsuo, K. Kindo, and H. Tanaka: *Magnetization Process and Collective Excitations in the S=1/2 Triangular-Lattice Heisenberg Antiferromagnet* $Ba_3CoSb_2O_9$. Phys. Rev. Lett. **110**, 267201 (2013)

[24] F. E. A. dos Santos and A. Pelster: *Quantum phase diagram of bosons in optical lattices.* Phys. Rev. A **79**, 013614 (2009)

Selbstständigkeitserklärung

Hiermit versichere ich, die vorliegende Arbeit ohne unzulässige Hilfe Dritter und ohne Benutzung anderer als der angegebenen Hilfsmittel angefertigt zu haben. Die aus fremden Quellen direkt oder indirekt übernommenen Gedanken sind als solche kenntlich gemacht. Die Arbeit wurde bisher weder im In- noch im Ausland in gleicher oder ähnlicher Form einer anderen Prüfungsbehörde vorgelegt.

Berlin, 13.08.2013

Mathias May